NMR Studies of Higher-order Structures of Solid Polymers

H. KUROSU,* S. ANDO,† H. YOSHIMIZU‡ and I. ANDO*

*Department of Polymer Chemistry, Tokyo Institute of Technology, Ookayama, Meguro-ku, Tokyo, Japan
†NTT Interdisciplinary Research Laboratories, Midori-cho, Musashino-shi, Tokyo, Japan
‡Department of Materials Science and Engineering, Nagoya Institute of Technology, Gokiso-cho, Showa-ku, Nagoya, Japan

1. INTRODUCTION

Polymers are one of the most important discoveries made during the twentieth century. At present we have many kinds of polymer materials with various physical properties and chemical properties. These are due to the vitality of polymer research and development of a diversity of interests on polymer materials. In order to develop new polymer materials, polymer design has been done on the basis of advanced polymer science and technology. The properties of polymers are closely related to their structures. For this, the establishment of methods for determining the structures is very important for obtaining reliable polymer design and for developing new advanced polymers.

Since the first observation of a high-resolution ^{1}H NMR spectrum of uncured Heva rubber in CS_2 solution in 1957 by Gutowsky *et al.*,[1] high-resolution NMR spectroscopy has developed to become the most

ANNUAL REPORTS ON NMR SPECTROSCOPY
VOLUME 28 ISBN 0-12-505328-2

powerful method available for characterizing structures of polymers in the solution and solid states and for analysing dynamic aspects of their structures.[2] In this chapter, the most recent high-resolution NMR studies of solid polymers, including synthetic and natural polymers, are reviewed, with the emphasis being placed on revealing higher-order structures. The present review complements previously published reviews[2] and provides a new dimension in polymer structures and in addition is concerned with engineering plastics, high-performance polymers, liquid crystalline polymers, polymer alloys, and natural polymers.

2. ENGINEERING PLASTICS AND HIGH-PERFORMANCE POLYMERS

Engineering plastics and high-performance polymers are the most popular polymers in polymer materials. Their physical properties and functions are closely related to the structure and dynamics in the solid state. From such a situation, solid-state high-resolution NMR spectroscopy has provided the potential perspective of becoming a powerful means of determining the higher-order structure and dynamics of the polymers in the solid state, associated with physical properties and functions.

Polyethylene (PE) is one of the typical engineering plastics. The polymer takes a *trans* and two *gauche* conformations, in which the conformational energy difference is small (about 500 cal/mol) and so takes various structures under appropriate conditions. The structure of PE has been studied by several kinds of spectroscopic methods such as NMR, X-ray diffraction, electron diffraction, IR and neutron diffraction.

PE takes two kinds of crystal forms. One of them is the orthorhombic form which occurs under normal conditions; the other is the monoclinic form which occurs under high pressure or drawn conditions. In both the crystal forms the conformation takes the all-*trans* zig-zag conformation, but the chain arrangements are different from each other. The all-*trans* zig-zag planes in the orthorhombic form are perpendicular to each other, and in the monoclinic form they are parallel to each other as shown in Fig. 1.

There also exist non-crystalline and interfacial phases. Their existence strongly affects the physical properties of polymers. The fraction of these phases depends on the preparation conditions. Therefore, it is very important to analyse the detailed structure of PE in the solid state to understand the physical properties of PE. High-resolution solid-state NMR is a powerful tool for investigating these phases separately.

Figure 2 shows ^{13}C cross-polarization (CP) magic angle spinning (MAS) NMR spectra of a single crystal (SC) PE,[3] melt-quenched (MQ) PE[3] and drawn (DR) PE.[4] Only one sharp peak at 33.0 ppm appears in the SCPE spectrum. On the other hand, MQPE and DRPE have two and three peaks, respectively. This means that MQPE and DRPE have at least two or three

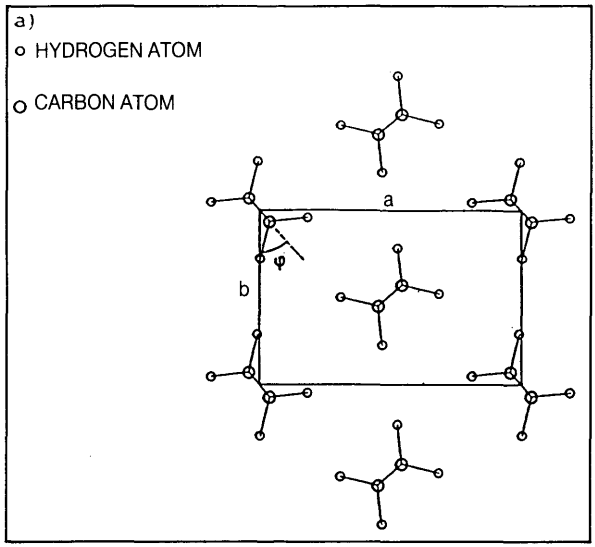

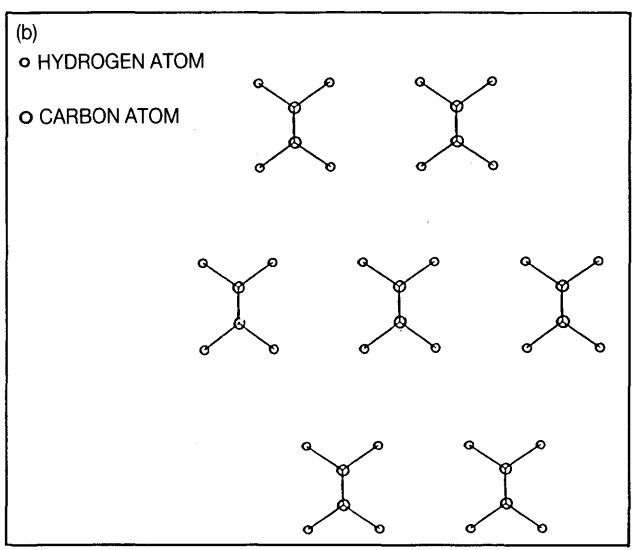

Fig. 1. Polyethylene structure model: (a) orthorhombic form and (b) monoclinic form.

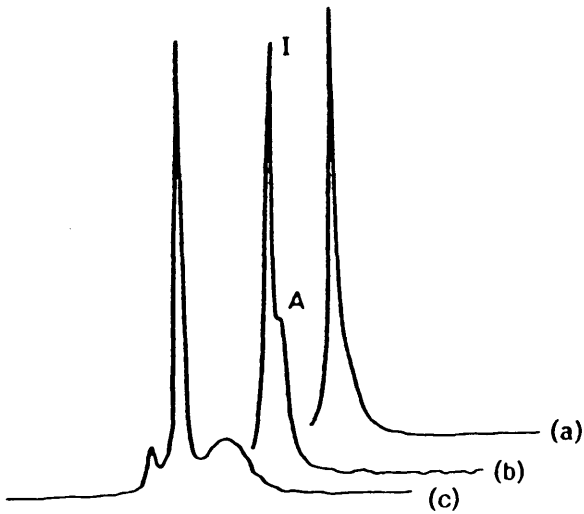

Fig. 2. ^{13}C CP MAS-NMR spectra of polyethylene. (a), SC; (b), MQ; (c), DR; PE.

kinds of magnetically inequivalent carbon atoms. VanderHart *et al.* have assigned these peaks by spin-lattice relaxation time measurements; peak A (31 ppm) comes from the amorphous region which is in a mobile state and peak I (33 ppm) comes from the crystalline region which is in an immobile state.[5] Further, the high frequency peak of DRPE (35.0 ppm) is assigned to the methylene carbons in the monoclinic crystal region. These assignments were justified by quantum chemical shielding calculations with the tight-binding (TB) sum-over-states (SOS) method.[6,7] Kitamaru *et al.* have reported that peak A comes from the amorphous region and the interfacial region which exists between the crystal and amorphous regions.[8]

The crystal structure of PE has been proposed from some models such as sharp-fold, switch-board and loose-loops models (Fig. 3).[9,10] In order to obtain detailed information on fold structure, Ando *et al.* have studied SC and MQPE by high-resolution solid-state ^{13}C NMR.[3] This study reveals that SC and MQPE take the "adjacent re-entry" type of macroconformation in addition to loose and long loops in the fold surface as shown in Fig. 4. The number of carbon atoms in the *trans* zig-zag chain from one fold to the next is estimated to be approximately 100, and thus this leads to an estimate of the stem length being about 125 Å. This magnitude is consistent with the crystal thickness (120–150 Å) measured directly for polyethylene single crystals by electron microscopy.

Nakai *et al.* have determined the orientation of the chemical shift tensor of PE by measuring the heteronuclear dipolar/chemical shift two-dimensional

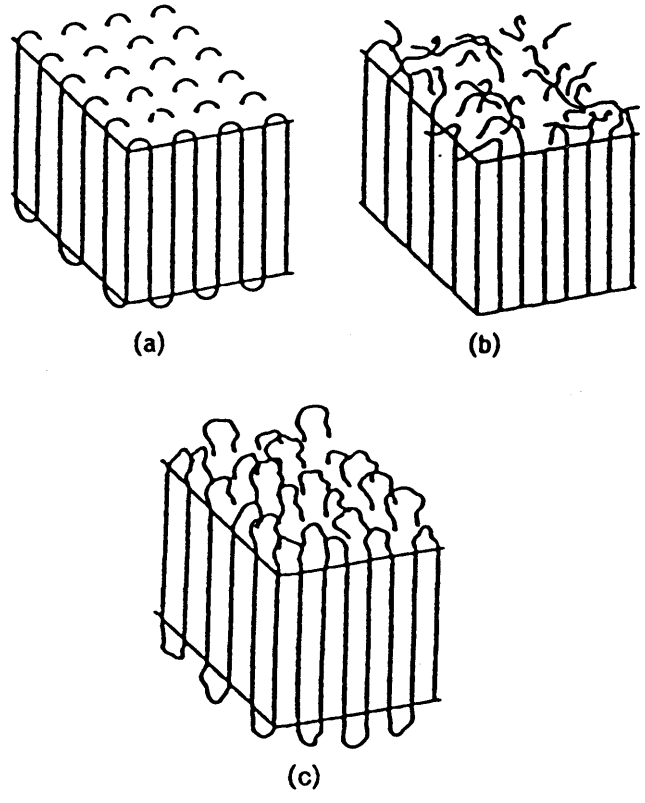

Fig. 3. Schematic drawing of the conformation models of polyethylene single crystal: (a) sharp-fold model; (b) switch-board model; (c) loose-loop model.

powder pattern.[11] Figure 5 shows experimental and theoretical ^{13}C chemical shift/^{13}C–^{1}H dipolar two-dimensional (2D) powder patterns of PE. The ω_1 and ω_2 axes represent the ^{13}C–^{1}H dipolar interaction and the ^{13}C chemical shift, respectively. We can determine the C–H distance, angle ($\angle$H–C–H) and the directions of the principal values for the chemical shift tensor from this spectrum by fitting with the observed and calculated dipolar/chemical shift 2D powder pattern. These measurements show that the directions of the principal values of the chemical shift tensor have deviations from the ideal orientation of the chemical shift tensor, and that the C–H length and $\angle$H–C–H angle have been obtained to be 1.12 ± 0.002 Å and $107° \pm 2°$, respectively.

The physical properties of polymers in the solid state are strongly affected by temperature. Variable-temperature (VT) NMR techniques should provide much useful data on the structural and dynamic aspects of polymers in

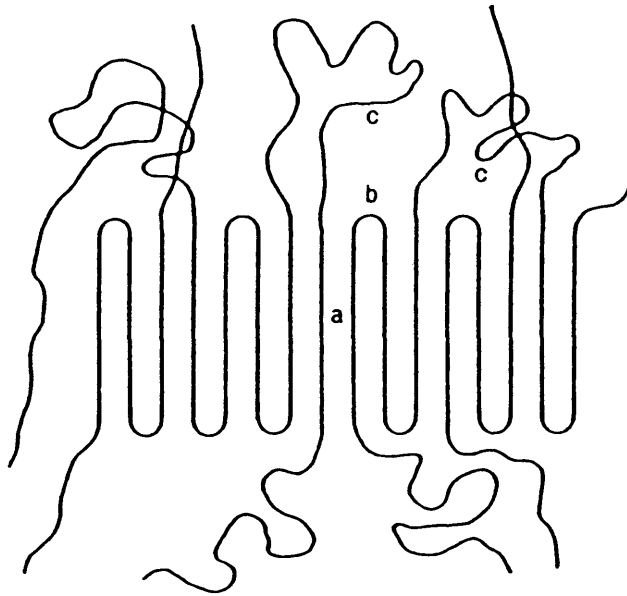

Fig. 4. A schematic illustration of the folded chain conformation for melt-quenched polyethylene: (a) *trans* zig-zag, (b) sharp fold and (c) loose and long loops.

the solid state.[12,13] The advantage of VT solid-state NMR techniques is that the temperature dependence of the conformation and molecular motion can be studied by observing the chemical shift. Akiyama *et al.* have investigated the structure of ultrahigh molecular weight (UHMW) PE in the solid state by VT ^{13}C CP MAS-NMR.[14] Figure 6 shows the ^{13}C NMR spectra of UHMW PE measured as a function of temperature, and the determined chemical shift values are listed in Table 1. The ^{13}C CP-MAS spectrum at room temperature has two peaks (the low and high frequency peaks are designated by A and I, respectively). Peak A appears to a low frequency by about 2 ppm from peak I. The ^{13}C NMR chemical shifts of peaks I and A for the UHMW PE agree with those for the melt-crystallized PE. Peaks I and A have been assigned to the crystalline component with the *trans* zig-zag conformation and to the non-crystalline component respectively. It can be seen from this figure that as the temperature is decreased, peak A shifts to low frequency but peak I shifts to high frequency. The ^{13}C chemical shift behaviour for peak A for the UHMW PE is similar to that of the melt-quenched PE.[15] At $-108°C$, the molecular motion is frozen and the chemical shift for peak A is about 32 ppm. Therefore, peak A comes from the methylene carbons in the *trans* conformation in the non-crystalline component because in the frozen state a methylene carbon in the *gauche*

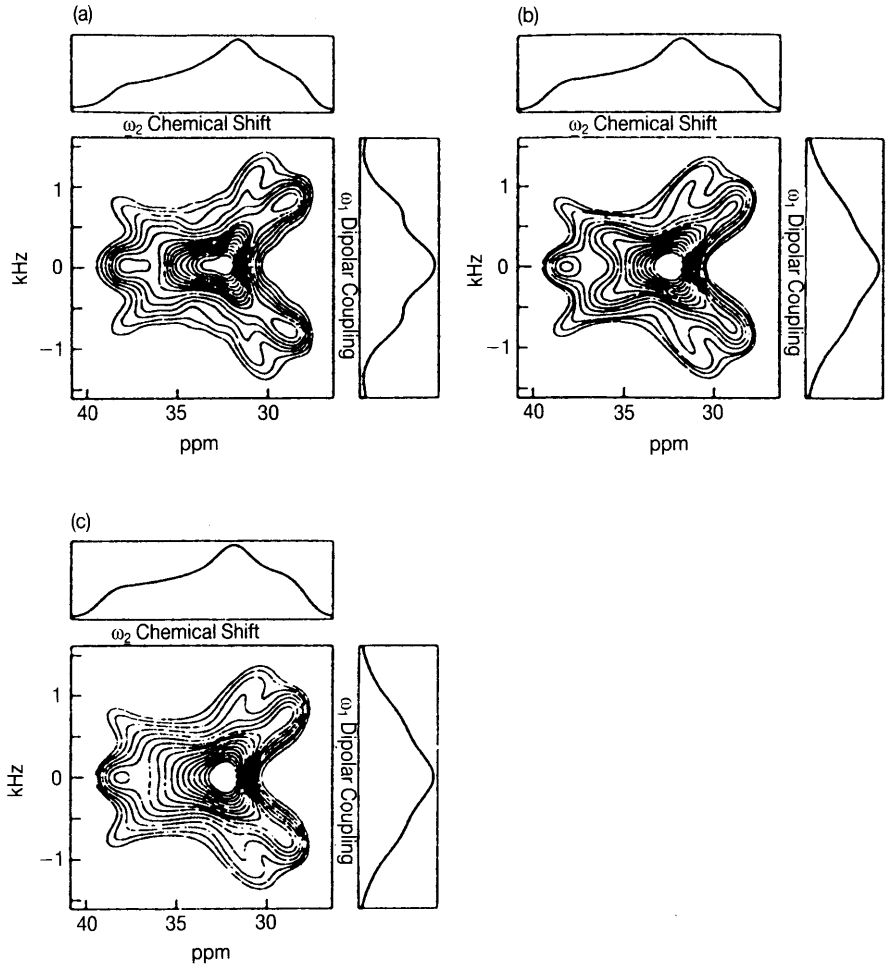

Fig. 5. ^{13}C chemical shift/^{13}C–^{1}H dipolar 2D powder patterns of polyethylene: (a) experimental; (b) and (c) calculated.

conformation should appear at about 27 ppm by the 1γ *gauche* effect. Such behaviour in the UHMW PE is very similar to that in melt-crystallized PE. Further, the temperature dependence of the ^{13}C chemical shift of peak I is considered. The low frequency shift of peak I is opposite that observed for the case of the melt-crystallized PE, where the chemical shifts are independent of temperature. At −108°C, the chemical shift is about 32 ppm, and peaks I and A coalesce. It is hard to consider that the causes for the low frequency shift of peak I is a change of structure in going from the orthorhombic form to a different crystal structure. It is known that the ^{13}C

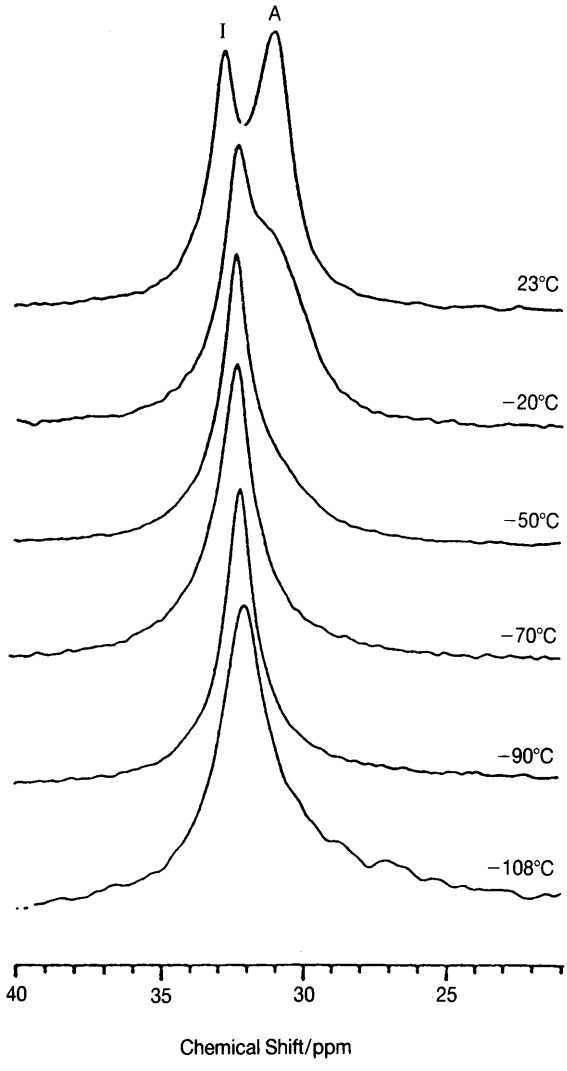

Fig. 6. ^{13}C CP MAS-NMR spectra of ultrahigh molecular weight polyethylene as a function of temperature.

chemical shifts of the methylene carbons with the *trans* zig-zag structure in orthorhombic, triclinic and monoclinic forms are about 33, 34 and 35 ppm, respectively.[16] From these results, the ^{13}C chemical shift of 32 ppm at −108°C indicates that the crystalline structure is different from that of any of the three kinds of crystal structures found at room temperature. The other possibility for the low frequency shift is the distortion of the orthorhombic form. The *a*, *b* and *c* axis lengths of UHMW PE, determined

Table 1. ^{13}C chemical shifts of UHMW and MC polyethylenes as a function of temperature.

Temperature (°C)	^{13}C chemical shift δ (ppm)[a]		$I_A/(I_A + I_I)$[b]
	Peak I	Peak A	
UHMW polyethylene[c]			
23	32.8 (1.0)[e]	31.1 (1.6)	0.67
−20	32.4 (1.1)	31.1 (2.5)	0.65
−50	32.3 (1.2)	30.9 (2.5)	0.31
−70	32.1 (1.5)	—	—
−90	32.0 (1.3)	—	—
−108	31.9 (2.0)	31.9 (2.0)	—
MC polyethylene[d]			
90	32.9 (2.5)	31.0 (1.0)	0.44
60	33.2 (0.7)	30.9 (0.9)	0.25
25	33.2 (0.5)	31.4 (1.7)	0.24
−50	33.2 (1.2)	—	—
−90	33.2 (1.2)	32.4 (1.0)	0.30
−120	33.2 (1.5)	32.1 (1.0)	0.27

[a] ±0.2 ppm from TMS.
[b] I_x: intensity of peak x.
[c] This work.
[d] Ref. 13.
[e] Values in parentheses indicate half-height width for deconvoluted peaks.

by X-ray diffraction, are listed in Table 2 together with those of the melt-crystallized PE at room temperature and −88°C.[17] The largest difference between UHMW PE and melt-crystallized PE is the change of the c axis length. The c axis length of UHMW PE changes from 2.55 Å to 2.44 Å in going from room temperature to −88°C, while that of melt-crystallized PE does not change. Therefore, it is suggested that the ^{13}C chemical shift for the UHMW PE may be influenced by a change in the c axis length. In order to elucidate the origin of the low frequency shift, quantum chemical calculations were performed. The change in c axis may come from a change in the C–C–C angle and the dihedral angle. Therefore, the ^{13}C chemical shift calculations were carried out, using n-decane, by the FPT INDO method as functions of the bond angle C–C–C and the dihedral angle. Figure 7 shows the calculated ^{13}C chemical shift contour map. It has already been reported that the dihedral angle and bond angle for the crystalline PE are 180° and 112°, respectively, as deduced from X-ray diffraction. This position is indicated by the open circle in the contour map. When the dihedral angle is varied from 180° to 150°, the methylene carbon signal shifts to low frequency with a decrease in the dihedral angle as seen from Fig. 7. This agrees with the experimental finding. From these results, it is suggested

Table 2. Lattice constants of UHMW and MC polyethylene samples as a function of temperature.

Temperature (°C)	Lattice constant (Å)		
	a	*b*	*c*
UHMW polyethylene			
20	7.43	4.95	2.55
−88	7.31	4.93	2.44
MC polyethylene			
18	7.44	4.96	2.53
−100	7.25	4.90	2.53

that a distortion of the bond angle and dihedral angle from the staggered *trans* conformation in the UHMW PE, which contains a large amount of non-crystalline component, occurs in going from room temperature to −108°C because of the influence on the crystalline structure produced by the reorientation of the non-crystalline structure through transfer from the *gauche* to the *trans* conformation and freezing of molecular motion.

The non-crystalline region of ^{13}C-labelled PEs crystallized under different conditions were studied by VT ^{13}C CP MAS-NMR.[18] The dynamics of the

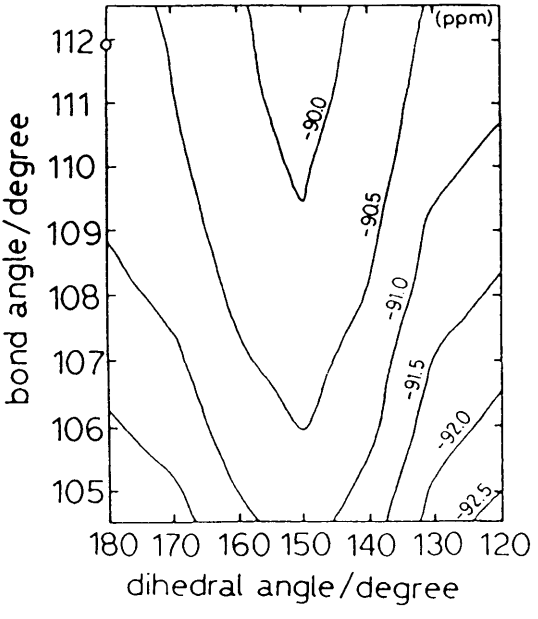

Fig. 7. ^{13}C chemical shielding contour map of polyethylene calculated by the FPT-INDO method.

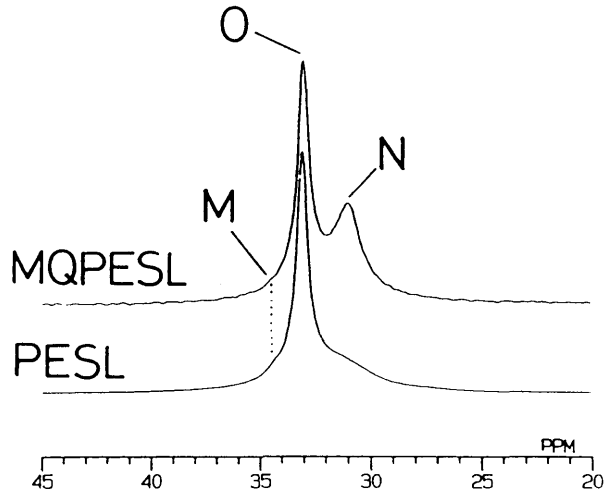

Fig. 8. Typical ^{13}C CP MAS-NMR spectra of samples of PESL and MQPESL at room temperature.

non-crystalline region were discussed by measuring ^{13}C spin-lattice relaxation times (T_1) and dipolar-dephasing relaxation times (T_{DD}) over a wide temperature range, from −120 to 44°C. Two types of ^{13}C-labelled PE samples were prepared. One is single ^{13}C-labelled (polymerized using 90% single ^{13}C-enriched ethylene) PE and the other is double labelled (polymerized using 90% double ^{13}C-enriched ethylene) PE. Typical ^{13}C CP MAS-NMR spectra of the single labelled solution-crystallized PE (PESL; the crystallinity is 95%) and single labelled melt-quenched PE (MQPESL; the crystallinity is 66%) are shown in Fig. 8. Each of these spectra consists of three peaks corresponding to an orthorhombic crystalline peak, O, at 33.0 ppm, monoclinic crystalline peak, M, at 34.4 ppm (a small shoulder on the left side of the orthorhombic peak), and a non-crystalline peak, N, which appears at 30.8–31.3 ppm. The ^{13}C T_1 data of samples of PESL and MQPESL over a wide range of temperatures, obtained using the inversion-recovery method with the PST (pulse saturation transfer) pulse sequence, are given. The PST pulse sequence enhances the intensity of mobile methylene carbons. The resulting T_1 values for samples PESL and MQPESL are plotted against the inverse of the absolute temperature ($1/T$) in Fig. 9. It had been suggested previously[19–21] that local molecular motion in the non-crystalline region of PE is independent of the degree of crystallinity, higher-order structures or morphologies. However, these suggestions are not supported by the experimental results because: (1) the T_1s of the non-crystalline region of samples PESL and MQPESL at room temperature

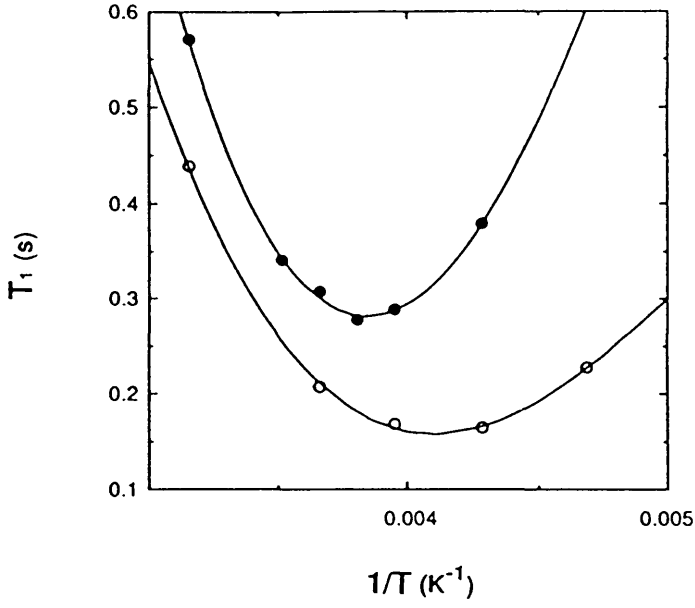

Fig. 9. Plots of non-crystalline ^{13}C spin-lattice relaxation times: T_1 of samples PESL (●) and MQPESL (○) versus the reciprocal absolute temperature.

are 570 ms and 440 ms, respectively, and the difference of 130 ms between them is beyond experimental error; and (2) the T_1 minimum values for the two samples (Fig. 9) are at different temperatures, the T_1 minimum of the sample of PESL appearing at −10.5°C and that of the sample of MQPESL at −32°C. These facts show that the local molecular motions in the non-crystalline regions of samples PESL are more constrained than that of MQPESL. In order to study whether the dynamic behaviour of the two kinds of non-crystalline region is also different on the T_2 time scale, T_{DD} values of samples of PESL and MQPESL were measured over a wide range of temperatures. The relative intensity of the non-crystalline peak obtained from the computer simulation was plotted against the delay time τ in Fig. 10. It can be clearly seen that the non-crystalline peak of the sample of PESL relaxes more quickly than that of the sample of MQPESL. The dipolar-dephasing time, T_{DD}, usually depends on molecular motion, carbon–proton dipolar interactions, MAS rate and spin diffusion.[22] Fundamentally, it can be said that the dipolar-dephasing time in the non-crystalline region becomes a measure of molecular motion because of the high mobility. Therefore, the longer T_{DD} value of the sample of MQPESL, compared with that of the sample of PESL, obviously suggests that the carbon–proton dipolar interaction is partially averaged by molecular motion on the T_2 time scale.

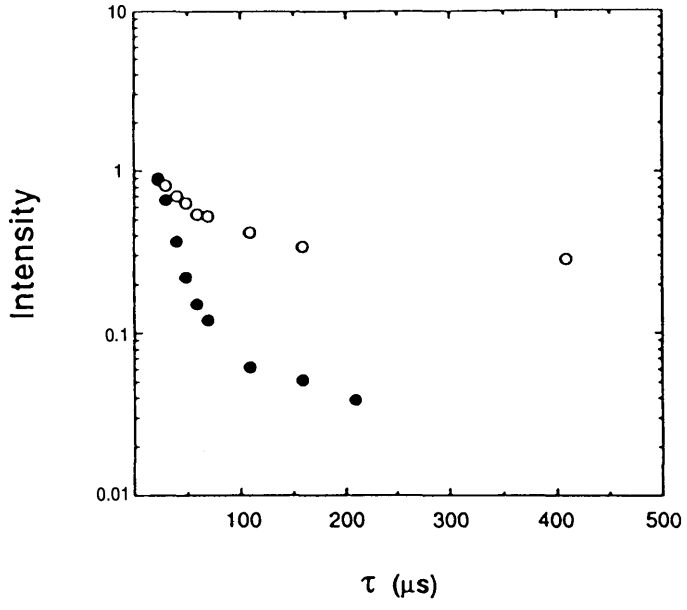

Fig. 10. Intensity of non-crystalline peaks of samples of PESL and MQPESL versus delay time τ. The peak intensity was obtained from computer simulation of the ^{13}C partially relaxed dipolar-dephasing NMR spectra.

Further, Chen *et al.*[23] have measured the ^{13}C CP MAS spectra of a ^{13}C-labelled solution crystallized PE at temperatures from -120 to 144°C. The measurements (Fig. 11) were taken in order to study changes of structure and molecular motion of the polymer with temperature variation for the crystalline and non-crystalline regions. As the crystalline and non-crystalline signals are incompletely resolved in the ^{13}C CP MAS spectrum of the PE sample, computer-fitting of the spectra is performed, and the determined ^{13}C chemical shifts of the crystalline and non-crystalline signals are shown in Fig. 12. It is shown that the ^{13}C chemical shift of the non-crystalline signal decreases with an increase in temperature, whereas the ^{13}C chemical shift of the crystalline signal does not change greatly with temperature before the melting point. This shows that an increase of the fractional population of the *trans* conformer leads to the observed high frequency shift of the non-crystalline signal with a decrease of temperature. At temperatures below -80°C the ^{13}C chemical shift of the non-crystalline signal does not change with temperature. Such a result indicates that the molecular motion in the non-crystalline region of PESL is completely frozen below -80°C on the NMR time scale. The half-height width (half width) of the crystalline and non-crystalline ^{13}C signals are plotted against temperature in Fig. 13. The half width of the non-crystalline region becomes a

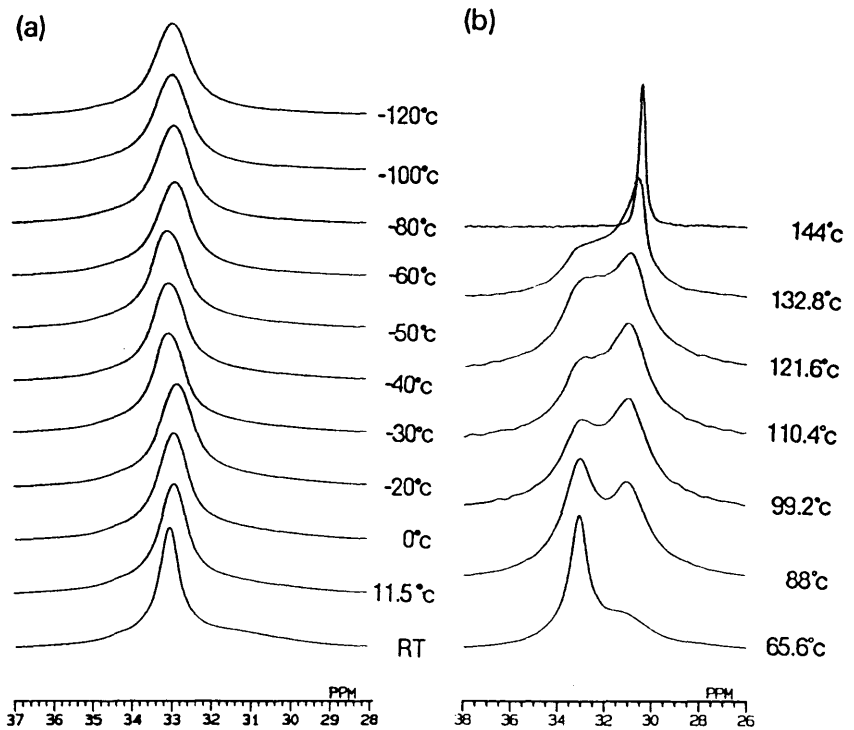

Fig. 11. ^{13}C CP MAS-NMR spectra of the PESL sample as a function of temperature: (a) −120°C to room temperature; (b) 65.6 to 144°C.

maximum at −30°C. This means that molecular motion of the non-crystalline region occurs at the frequency corresponding to the amplitude of the proton decoupling field (about 55 kHz in this case). Contrary to the results of the non-crystalline signal, the half width of the crystalline signal is almost constant at temperatures from 0 to −120°C. The half width decreases from 0.9 to 0.7 ppm as the temperature is increased from 0°C to room temperature, because of the molecular-motional narrowing effect. However, the half width of the crystalline signal increases as the temperature is increased from 65.6°C and becomes a maximum at 110.4°C. This result may suggest that there is an α-transition, T_α, in the crystalline region of PE and thus the temperature (110.4°C) at which the maximum of the half width is observed may be correlated with T_α.

Polypropylene and polystyrene are very important polymers in engineering plastics. For this, many NMR studies have been performed as reviewed in previous review articles.[1] Therefore, these polymers are not reviewed here.

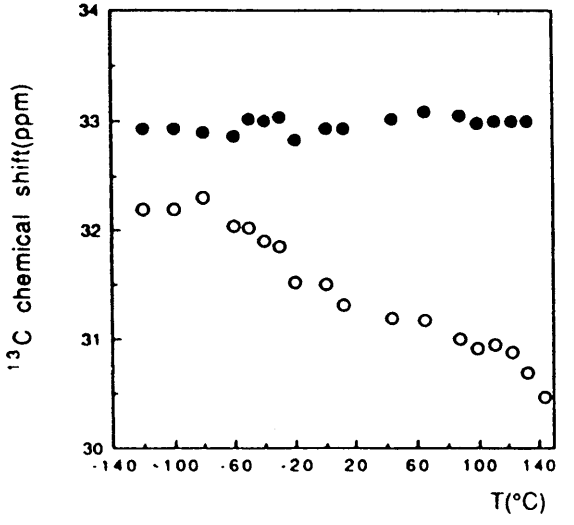

Fig. 12. Plots of the ^{13}C chemical shifts of the crystalline (●) and non-crystalline (○) signals of the PESL sample against temperature.

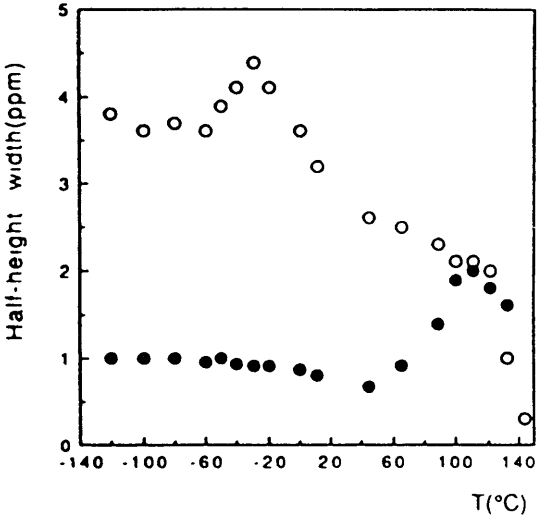

Fig. 13. Plots of the width at half the maximum peak height of the crystalline (●) and non-crystalline (○) signals of the PESL sample against temperature.

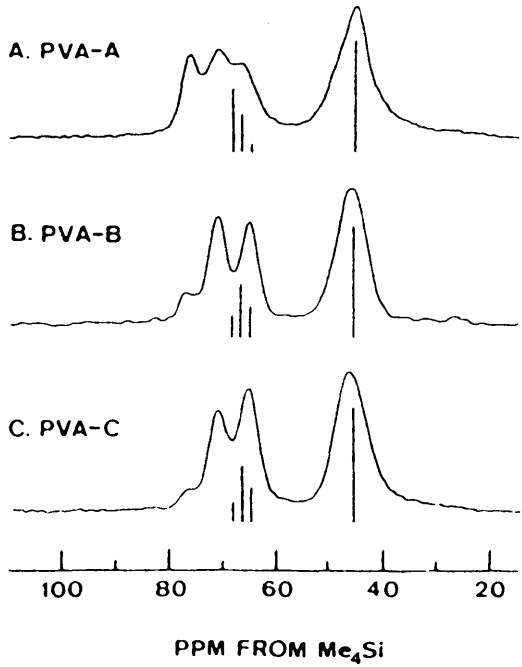

Fig. 14. ^{13}C CP MAS spectra of poly(vinyl alcohol) at room temperature: (A) PVA-A; (B) PVA-B; (C) PVA-C. Line spectra represent the ^{13}C spectra in Me_2SO_4-d_6 solution at 353 K.

One of the high performance fibres is poly(vinyl alcohol) (PVA) which has received much attention. This polymer has a high function as a barrier material against oxygen. It is important to get detailed information about the structure and molecular motion for developing and designing these materials.

The molecular structure of PVA has been investigated by high-resolution solid-state ^{13}C NMR. Terao *et al.* have measured the ^{13}C CP MAS spectra of PVA at room temperature.[24] The methine carbon resonance splits into three peaks in the CP MAS spectrum (Fig. 14). In the case of solution state NMR, the three methine carbon resonances and relative intensities correspond to the triad tacticity. However, the chemical shifts of the three methine carbons in the solid state are about 77, 71 and 65 ppm and the relative intensities are not consistent with the triad tacticity in solution. The chemical shifts of two high frequency peaks move significantly to higher frequencies in the solid state. Terao *et al.* have assigned these peaks on the basis of the formation of intramolecular hydrogen bonds as follows; the highest frequency peak of the methine carbon is assigned to the *mm* triad

Table 3. ^{13}C spin-lattice relaxation times of the respective resonance lines of different dry PVA samples, measured at room temperature.

Sample	T_{1C} (s)			
	I	II	III	CH_2
S-PVA	74.2, 13.2, n.m.	58.3, 8.7, n.m.	89.5, 12.3, n.m.	71.1, 9.2, n.m.
A-PVA	60.0, 12.1, 1.1	65.0, 14.6, 1.2	62.0, 12.3, 2.2	65.0, 14.6, 1.3
I-PVA	51.3, 10.4, n.m.	39.7, 7.3, n.m.	32.9, 4.6, n.m.	43.0, 7.8, n.m.

n.m., not measured.

with two intramolecular hydrogen bonds, the second highest frequency peak of the methine carbon is assigned to the *mm* and *mr* triads with one intramolecular hydrogen bond, and the other peak is assigned to the *mm*, *mr* and *rr* triads with no intramolecular hydrogen bonds.

The barrier properties of PVA film decreases upon the addition of water. There is a significant change in the ^{13}C CP MAS spectrum of isotactic PVA which is left in the air. The intensity of the highest frequency peak of the methine carbon increases and that of the lowest frequency peak decreases. This behaviour can be understood in terms of water molecules, which occupy positions between molecules, breaking intermolecular hydrogen bonds, and new intramolecular hydrogen bonds are formed.

PVA films with different tacticities have been studied.[25] The T_{1C} measurements, using the Tochia pulse sequence, were performed relaxation times of three CH carbons. Table 3 lists the T_{1C} values of the respective resonance lines of the CH carbons of syndiotactic (S-PVA), isotactic (I-PVA) and atactic (A-PVA) PVA samples. The ^{13}C spin-lattice relaxation time analysis has revealed that three components exist for each of the samples, which are assigned to the crystalline, less-disordered non-crystalline and amorphous regions. Using the T_{1C} difference, the spectra of the crystalline and non-crystalline components are separately recorded as shown in Fig. 15. The exact relative intensity for the crystalline component was corrected according to equation (1).

$$M_{jc}(t) = M_{jc}(0)\exp(-t/T_{1jc}) \tag{1}$$

On the other hand, the exact relative intensity for the non-crystalline component was calculated by multiplying the fraction of line j by the factor g_j, which is expressed as:

$$g_j = M_j^{CP}/(1+f_j)M_{jNC'}(t) \tag{2}$$

and then normalizing those values, where M_j^{CP} and $M_{jNC'}(t)$ are the peak intensities of line j for the spectra shown in Figs 15(a) and 15(c), and f_j is the

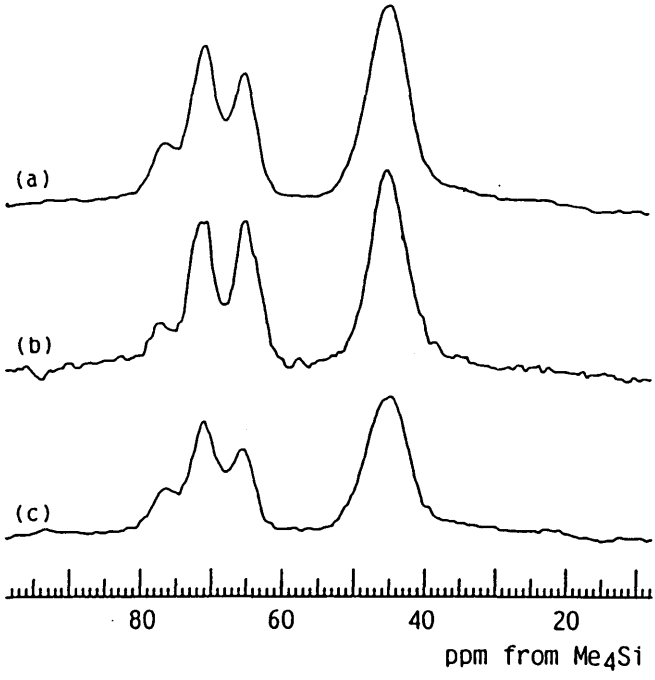

Fig. 15. ^{13}C CP MAS-NMR spectra of different components of PVA-A: (a) total; (b) crystalline; (c) non-crystalline ((a) −0.29(b)).

peak intensity ratio for the crystalline and non-crystalline components of line j, which is given by:

$$f_j = M_{jC}/M_{jNC} = M_{jC}(0)/[M_{jNK}(0) + M_{jNS}(0)]$$

The corrected relative intensities of the triplets of the CH resonance lines are not in accord with the contents of the triad sequences as listed in Table 4, suggesting the formation of intramolecular and intermolecular hydrogen bonds in the *meso* sequences of almost equal probability.

Nylon is one of the important polymers with high performance such as moderate hygroscopicity, dyeing property and high strength. Therefore, nylon is widely used as an engineering plastic and a fibre. In order to elucidate the molecular structure and dynamics of nylon in the solid state, many investigations have been done by solid-state NMR.

The ^{13}C CP MAS-NMR spectrum and assignments, of a nylon 6 single crystal, is shown in Fig. 16.[26] The PST MAS with a short pulse repetition time (5 s), which emphasizes the carbons with high mobilities, as well as the CP MAS technique, were employed for the single crystal and melt-quenched

Table 4. Integrated fractions, chemical shifts and linewidths of lines I, II and III of CH carbons for the crystalline and non-crystalline spectra of different dry PVA samples.

		Integrated fraction			Chemical shift (ppm)			Line width (Hz)		
Sample		I	II	III	I	II	III	I	II	III
Crystalline										
S-PVA	observed	0.080	0.349	0.571	76.7	71.1	64.9	193	201	156
	corrected[a]	0.064	0.350	0.586						
A-PVA	observed	0.105	0.467	0.428	77.0	71.2	64.8	156	214	197
	corrected[a]	0.109	0.457	0.434						
I-PVA	observed	0.481	0.329	0.190	75.4	69.8	64.7	141	237	211
	corrected[a]	0.386	0.351	0.263						
Non-crystalline										
A-PVA	observed	0.175	0.477	0.348	76.5	70.9	65.5	203	211	209
	corrected[b]	0.170	0.493	0.337						

[a]Corrected by equation (1).
[b]Corrected by equation (2).

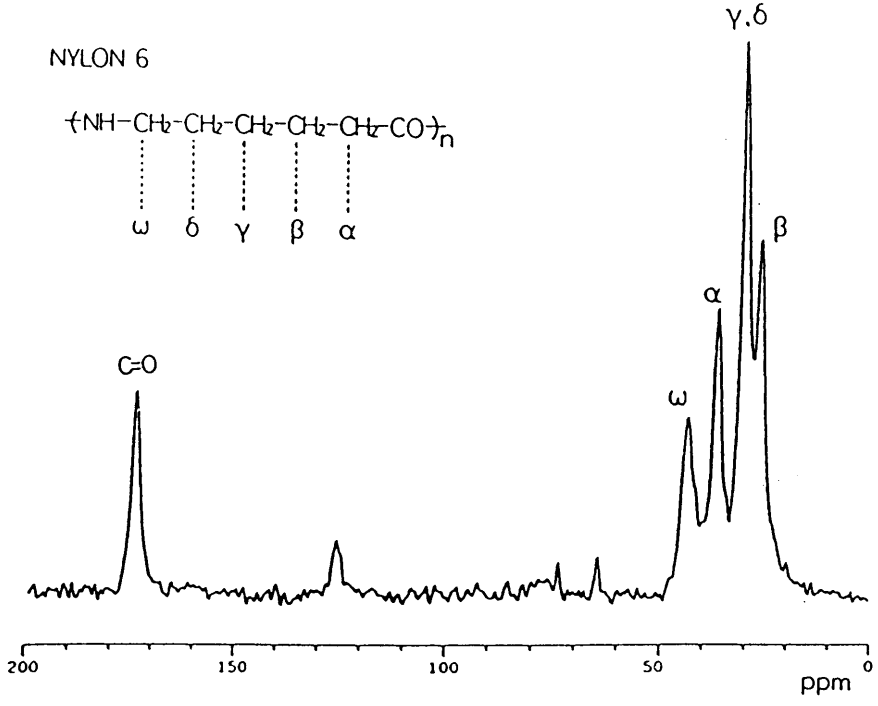

Fig. 16. Typical ^{13}C MAS-NMR spectrum of nylon 6 single crystals at room temperature.

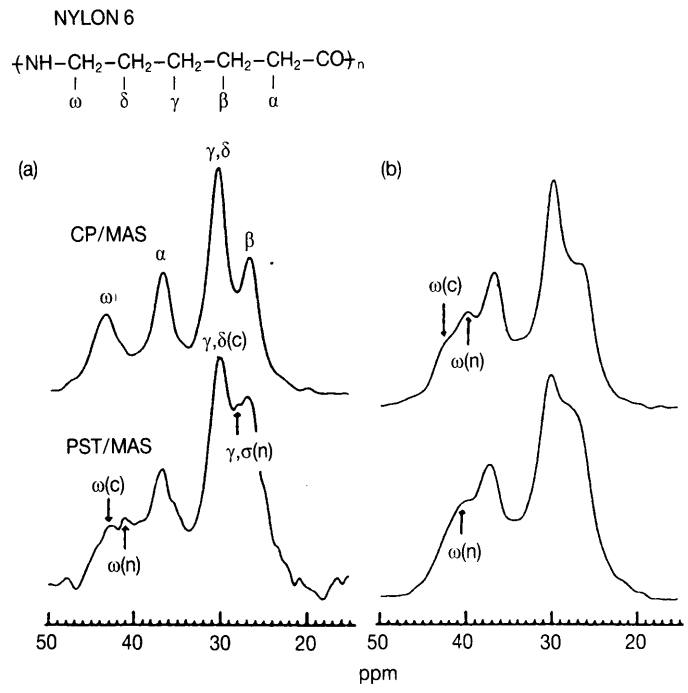

Fig. 17. ^{13}C CP MAS and PST MAS-NMR spectra of nylon 6 (a) single crystal; (b) melt-quenched sample.

samples (Fig. 17). The detailed comparison of these spectra revealed that the amorphous peaks of the ω-CH_2 and $(\delta + \gamma)$-CH_2 carbons of the melt-quenched sample are increased compared with those of the single crystal sample. These spectra show that the amorphous peaks appear at lower frequency than the crystalline peaks. The chemical shift behaviour of these peaks can be understood on the basis of the *γ-gauche* effect. The crystalline state has a *trans* zig-zag structure and the amorphous carbons are undergoing rapid transitions between the *trans* and *gauche* conformations.

Not only the ^{13}C NMR spectra but also the ^{15}N NMR spectra have been observed in the solid state.[27-29] The ^{15}N NMR spectrum of ^{15}N-enriched nylon 6 and computer-fitting with theoretical line shape are shown in Fig. 18. This spectrum shows that there are the crystalline and non-crystalline regions and supports the results of the ^{13}C NMR spectra. The spin-lattice relaxation time analysis of ^{15}N nuclei shows that the rigid crystalline region has a much longer T_{1N} relaxation time than the more mobile amorphous region. The T_{1N} data of the crystalline region are 111–416 s and two non-crystalline regions are observed in the relaxation of the amorphous peak. The faster component has T_{1N} values of 1–3 s and the slower

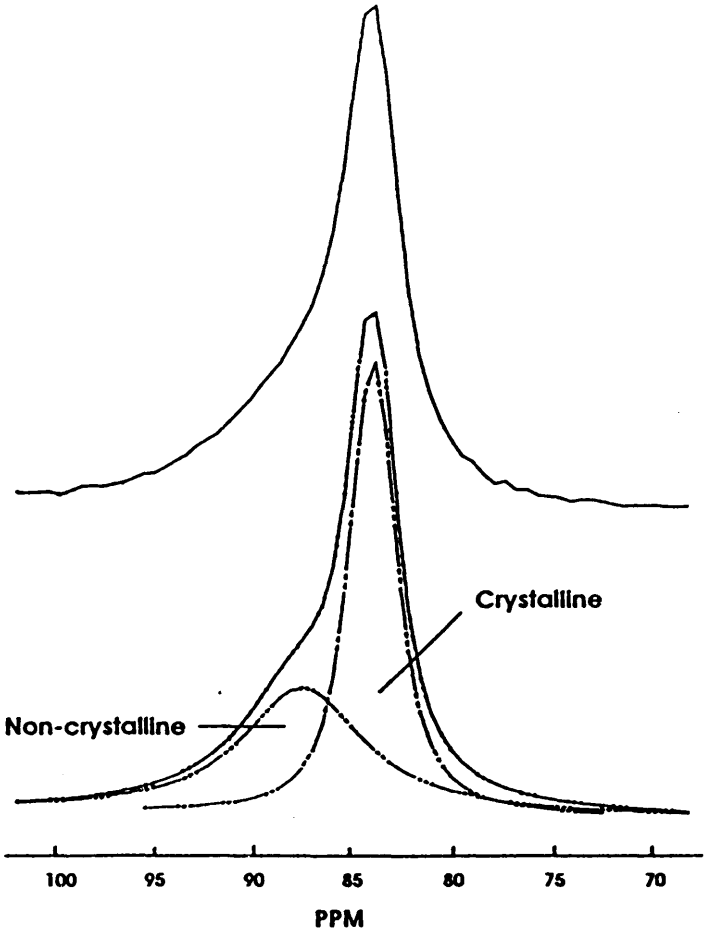

Fig. 18. ^{15}N CP MAS line shape analysis of nylon 6.

component has values for T_{1N} of 19–29 s. Two non-crystalline regions are assigned to the amorphous and non-crystalline interface regions. The ^{15}N chemical shielding anisotropy (CSA) pattern of nylon 6 is observed as a function of temperature (Fig. 19). The CSA powder patterns show the growth of an amorphous signal at elevated temperatures with a chemical shift near the isotropic value obtained with MAS. The σ_{33} component, which lies along the N–H bond of the amide group, becomes less prominent with increasing temperature and finally disappears above 115°C.

Other nylon samples such as nylon 11[30] or nylon 66[31] are also investigated by high-resolution solid-state ^{13}C NMR.

Polyoxymethylene (POM) is the first member of the polyether series

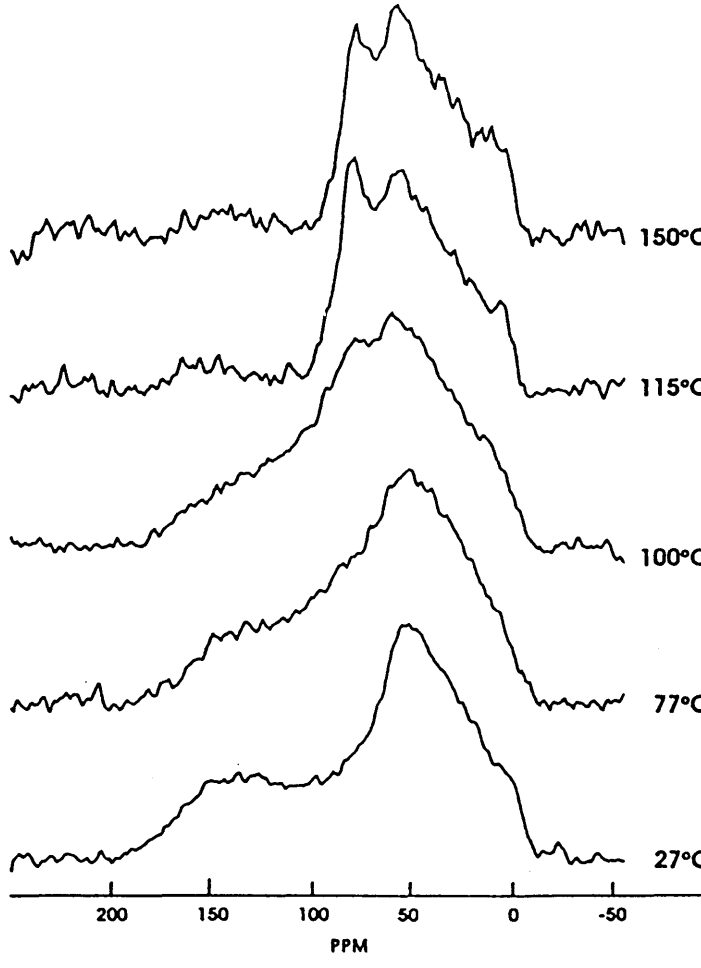

Fig. 19. Static ^{15}N NMR spectrum of annealed nylon 6 sample obtained with CP and high power decoupling at different temperatures.

expressed by the general formula $[(CH_2)_m\text{–O–}]_n$. This polymer has the property of abrasion resistance. From an X-ray diffraction study, POM usually takes the trigonal form with a 9/5 helical (all *gauche*) conformation.[32] Veeman *et al.* have measured the ^{13}C CP and the 90° pulses (without MAS) powder pattern, as shown in Fig. 20.[33] Fig. 20B was observed by the 90° pulses with proton-decoupling and the pulse repetition time is 1 s. This spectrum shows only a mobile region since T_{1C} of the immobile region is longer than the mobile region in the solid state. Therefore, Fig. 20B shows the mobile (non-crystalline) region and Fig. 20A shows both the non-crystalline and crystalline regions with different T_{1C}s. The spin-lattice

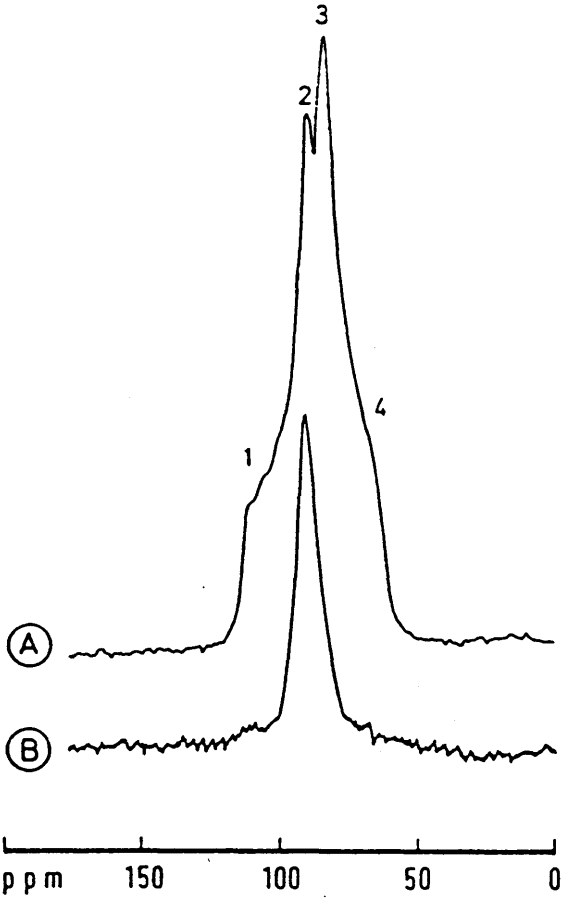

Fig. 20. Proton-decoupled ^{13}C spectra of a non-spinning poly(oxymethylene) (Delrin) sample. Spectrum A results from 10 ms CP, while for spectrum B the carbon magnetization is prepared via a 90° pulse.

relaxation time in the rotating frame ($T_{1\rho}$) measurement of POM also shows that POM has two different kinds of regions with different mobilities.

Kurosu *et al.* have measured the ^{13}C CP MAS and powder pattern of melt-quenched POM in the solid state.[34] It was found that the ^{13}C NMR chemical shifts of the crystal and non-crystalline structures have different chemical shifts. The ^{13}C NMR isotropic chemical shift for the crystalline region appears further towards high frequency by about 2 ppm than that for the non-crystalline region. Further, the principal values of the chemical shielding tensor of POM were determined for the crystalline and non-crystalline regions. These results show that the chemical shielding anisotropy

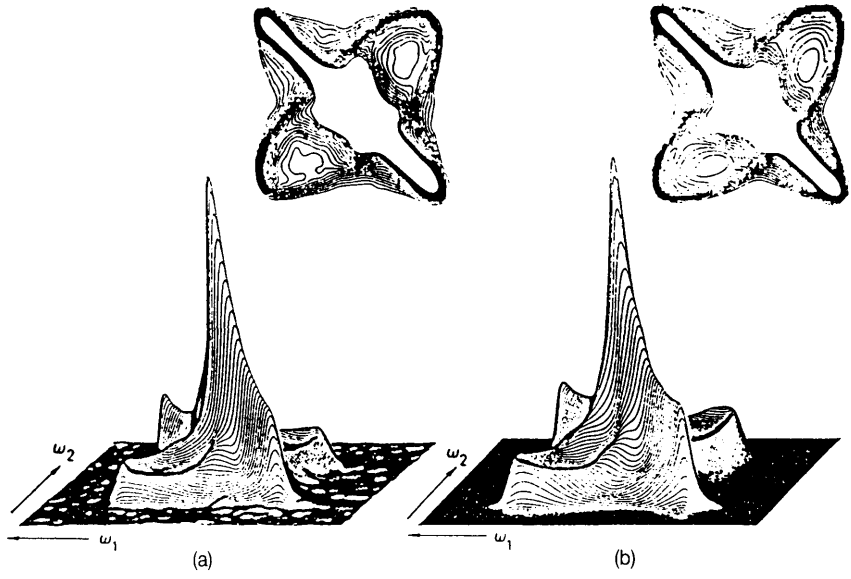

Fig. 21. Pure absorption-mode 2D exchange spectra of isotropic POM: (a) temperature $T = 360$ K and mixing time $t_m = 2$ s; (b) theoretical spectrum of (a) with $x = 2\omega$, $t_m = 2.5$.

$\Delta\sigma$ ($= \sigma_{33} - \sigma_{11}$) of the non-crystalline region is smaller than that of the crystalline region. They also calculated ^{13}C shieldings of POM using crystalline and non-crystalline models. This calculation shows that the $\Delta\sigma$ value of the non-crystalline region is smaller than that of the crystalline region and the isotropic chemical shift of the non-crystalline region is displaced to high frequency as compared with that of the crystalline region.

Recently, two-dimensional solid-state NMR has been developed. The molecular motions of POM have been investigated by this method. The observed ($T = 360$ K, mixing time $t_m = 2$ s) and the calculated two-dimensional exchange spectra of POM are shown in Fig. 21.[35] The spectrum observed at 252 K shows only diagonal signals and this means that there is no molecular motion during the mixing time. On the other hand, if molecular motion occurred during the mixing time, the spectrum would show steric effects as shown in Fig. 22. The calculations are based on the model of helical jump motions assuming a one-dimensional random walk in continuous time with an elementary process of 200° jumps. Thus at $T = 360$ K, the subspectra for the discrete steps of a given CH_2 group of POM experiences, as the helix rotates, can be identified.

Kobayashi *et al.* have investigated the ^{13}C NMR spectra of a needle-like single crystal of trigonal POM (t-POM).[36] The ^{13}C signal in the single crystal

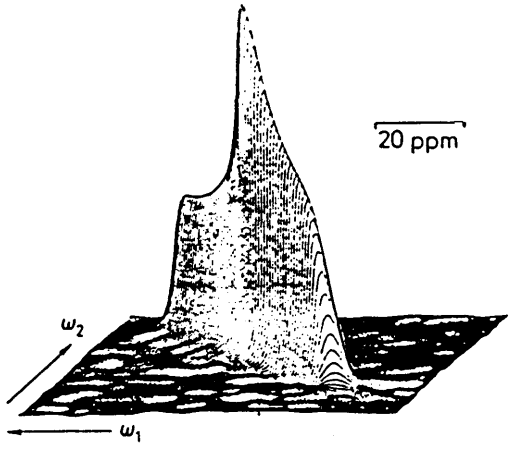

Fig. 22. Pure absorption-mode 2D exchange spectrum at 75.47 MHz of isotropic POM with temperature T = 252 K and mixing time t_m = 1 s.

splits into a doublet at 88.5 and 87.7 ppm in contrast to the singlet at 88.4 ppm in the semicrystalline sample. The resolved pattern is ascribed to the non-equivalent monomeric units in the crystal field of the t-POM lattice. The corresponding ^{13}C signal of a plate-shaped single crystal of orthorhombic POM (o-POM) appears at 82.0 ppm as a singlet as anticipated from the space group of o-POM. The large chemical shift difference (6 ppm) between t-POM and o-POM is interpreted in terms of the intramolecular *γ-gauche* shielding and the intermolecular packing effect.

Since the discovery of polyacetylene film, which becomes electrically conductive by doping, a number of organic conjugated polymers have been synthesized and their electric properties have been studied. The NMR studies on polyacetylene and other conducting polymers have already been reviewed.[2c] In this section, the most recent studies on polypyrrole will be introduced.

Polypyrrole is one of a series of heterocyclic polymers which has attracted much attention due to its characteristic electric and electronic properties. However, there are some problems relating to the physical and material properties which are associated with its structure. The fundamental structural formulae shown in Fig. 23 have been generally proposed for the structures of dedoped and doped polypyrroles, where the aromatic form corresponds to the dedoped state and the quinoid form corresponds to the doped state.[37–39] However, the actual structure appears to be more complicated. At present the exact structure is not known because the polymer is amorphous and insoluble. Consequently, various structures have been proposed for polypyrrole.[38]

High-resolution solid-state NMR spectroscopy provides useful information about the structures of synthetic polymers in the solid state, which sometimes cannot be determined by X-ray diffraction. NMR chemical shifts vary depending on the structure in the solid state and the separable resonance lines lead to an exact structural analysis.

The structure of polypyrrole in the solid state has been studied by means of high-resolution solid-state ^{13}C NMR spectroscopy.[40] However, the structure is insufficiently analysed because of the complexity of the unresolvable broad aromatic ^{13}C signal. This is due to the fact that there are several magnetically non-equivalent aromatic carbons as shown in Fig. 23.

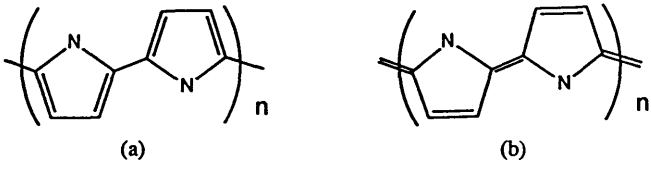

Fig. 23. Aromatic (a) and quinoid (b) structures for polypyrrole.

The structure of polypyrrole, prepared electrochemically, has been analysed by using high-resolution solid-state ^{15}N NMR spectroscopy. The sample used is ^{15}N-labelled in order to obtain ^{15}N spectra with a high signal-to-noise ratio, as attempted by Wehrle *et al.*[41] However, they could not carry out a successful analysis of the ^{15}N CP MAS spectra of the polymers in the solid-state because of insufficient resolution. As expected from Fig. 23, ^{15}N NMR spectroscopy will provide a simpler spectral pattern, when compared with ^{13}C NMR spectroscopy, because a ^{15}N resonance line may correspond to a given structure. Therefore, the structure of doped and dedoped ^{15}N-labelled polypyrrole films can be successfully studied by high-resolution solid state NMR.[42] Doped and dedoped samples were prepared by electrochemical polymerization[43] using 20–30% ^{15}N-labelled pyrrole. In order to obtain a dedoped sample the electrodes were inverted after the doping experiment and the same voltage was applied to them.

The observed ^{15}N CP MAS-NMR spectrum of polypyrrole (sample c; electrical conductivity = 4×10^{-6} S/cm) is shown in Fig. 24(a). It can be seen that the ^{15}N signals of the polypyrroles considered here consist of two major peaks and two minor peaks, which are designated by α, β, γ and δ with decreasing shielding. The four peaks were decomposed by computer fitting, and their ^{15}N chemical shift values are approximately 90, 113, 129 and 145 ppm. This chemical shift range is very large and the results indicate that the polymer has at least four kinds of structure corresponding to the four peaks. The determined ^{15}N chemical shifts, half widths and relative peak intensities of samples a (electrical conductivity = 7×10^{-4} S/cm), b (electrical conductivity = 2×10^{-3} S/cm) and c are summarized in Table 5.

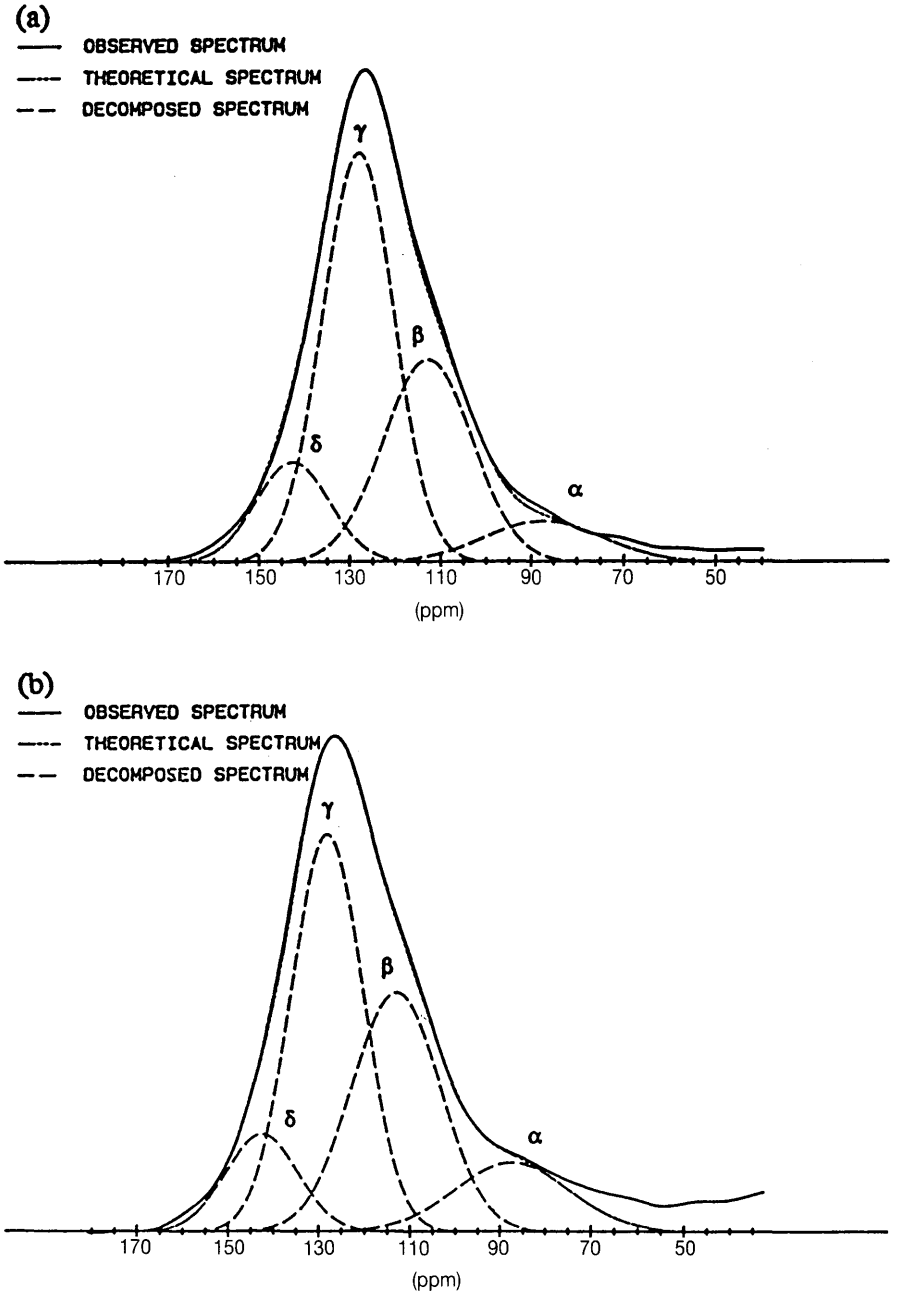

Fig. 24. A 50.55 MHz ^{15}N CP MAS-NMR spectrum and a simulated spectrum of polypyrrole (sample c) in the solid state. The four peaks were decomposed by computer fitting: (a) contact time (CT) = 800 μs and (b) CT = 100 μs.

Table 5. Observed ^{15}N chemical shifts, half widths and relative peak intensities of doped and dedoped polypyrrole samples.[a]

Sample	Peak	^{15}N chemical shift (ppm)	Half width (ppm)	Relative peak intensity (%)
a	α	91.0	30.0	5.1
	β	113.6	23.0	28.8
	γ	129.1	20.6	53.9
	δ	145.5	19.0	12.2
b	α	91.0	30.0	5.5
	β	113.6	23.0	28.7
	γ	129.1	20.6	53.7
	δ	145.5	19.0	12.2
c	α	87.5	30.0	8.0
	β	112.8	23.0	30.2
	γ	128.2	18.6	49.4
	δ	142.5	19.0	12.4

[a]Determined by computer fitting.

As shown in this table, the relative intensities of peaks α and β increase from 5.5 to 8.0% and from 28.7 to 30.2%, respectively, on going from sample b (doped) to sample c (dedoped). However, the relative intensity of peak γ decreases from 53.7 to 49.4% by dedoping. Hence, the relative intensities of peaks α and β increase with a reduction in conductivity, but that of peak γ decreases. In addition, the relative intensity of peak δ does not change with the increase in conductivity. When the ^{15}N CP MAS experiment is performed using a contact time of 100 μs, the intensities of the peaks α and β are relatively enhanced as shown in Fig. 24(b), and the chemical shifts and half widths of the observed shoulder peaks are determined exactly. Furthermore, the difference of the intensity enhancement between peak α, β and peaks γ, δ shows the difference of the magnetic environments, i.e. a difference in T_{NH} values between ^{15}N and ^{1}H and in $T_{1\rho}$, between the peaks α, β and the peaks γ, δ.

In order to get more detailed information about the ^{15}N NMR chemical shift behaviour and physical properties of polypyrrole in the solid state, quantum chemical calculations have been performed. As suggested above, it is thought that polypyrrole predominantly takes the aromatic form and the quinoid form (Fig. 25). The isotropic ^{15}N NMR chemical shifts calculated by the finite perturbation theory (FPT)-INDO method for the aromatic forms are listed in Table 6, and those for the quinoid forms are listed in Table 7. The calculated values are shielding constants, and so the negative sign means deshielding. Since the observed values are the relative chemical shifts and the positive sign corresponds to deshielding, only the relative difference in the calculated ^{15}N NMR shielding constants (σ) should be compared with

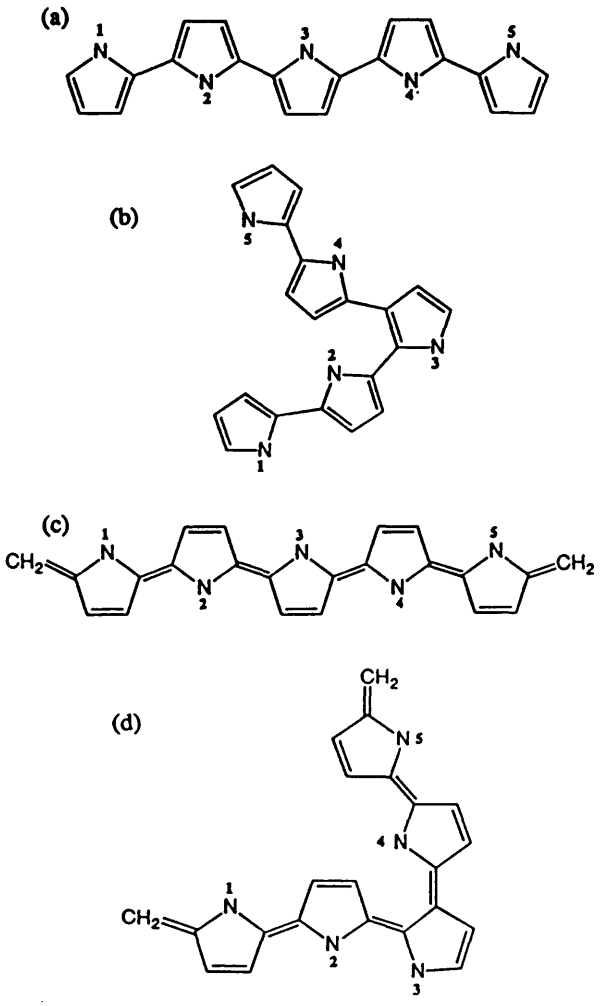

Fig. 25. The structure of models used in the FPT-INDO calculation.

the observed data (δ). As seen from these Tables, the calculated ^{15}N NMR chemical shift for the quinoid form appears towards a high frequency with respect to that for the aromatic one.

Polypyrrole in the solid state is in an amorphous state.[38] Therefore, some local structures are assumed. The calculations for these structures show that the ^{15}N NMR chemical shift moves considerably to high frequency when a hydrogen atom bonded to a nitrogen atom (N2 in Fig. 25(b) and N4 in Fig. 25(d)) is very close to a hydrogen atom bonded to a carbon atom of the other ring. From these calculated results and the experimental findings that

Table 6. Calculated ^{15}N shielding constants for the aromatic models[a] by the FPT-INDO method.

Model	Nitrogen species	Calculated ^{15}N shielding constant σ_{iso} (ppm)
a	N1	−318.81
	N2	−317.33
	N3	−317.34
	N4	−317.23
	N5	−319.49
b	N1	−319.18
	N2	−379.48
	N3	−319.54
	N4	−312.89
	N5	−320.56

[a]See Figs 25(a) and (b).

Table 7. Calculated ^{15}N shielding constants for the quinoid models[a] by the FPT-INDO method.

Model	Nitrogen species	Calculated ^{15}N shielding constant σ_{iso} (ppm)
c	N1	−322.67
	N2	−325.73
	N3	−325.51
	N4	−325.72
	N5	−322.67
d	N1	−324.41
	N2	−329.29
	N3	−315.82
	N4	−367.05
	N5	−324.00

[a]See Figs 25(c) and (d).

the observed ^{15}N NMR chemical shift for the peak γ appears towards a high frequency with respect to that for the peak β, and the fact that the intensity of the peak γ for doped polypyrrole is larger than that for dedoped polypyrrole, it can be concluded that the major peak γ, at about 129 ppm, is assigned to the nitrogen atoms in the quinoid form. The other major peak β, at about 113 ppm, is assigned to the aromatic form, and the minor peak δ at about 145 ppm probably comes from the nitrogen atoms which are bonded to hydrogen atoms approaching other hydrogen atoms bonded to different atoms. From the calculations performed, the other minor peak α, at about 90 ppm, cannot be assigned.

In order to get information about the ^{15}N chemical shifts and electronic energy band structures of an infinite polypyrrole chain with aromatic or quinoid forms, calculations were carried out by the tight binding (TB) INDO/S method. As listed in Table 8, the calculated ^{15}N NMR chemical shift for the quinoid form appears at high frequency compared with that for the aromatic form. This agrees with the results calculated by the FPT-INDO method. The calculated band structures for both the aromatic and quinoid forms are shown in Fig. 26. The band gap is an important factor in determining electrical properties such as electric conductivity, where the band gap is the energy difference between the highest occupied band and

Table 8. Calculated ^{15}N shielding constants and band gaps for the aromatic and quinoid polypyrrole models by the tight-binding INDO/S-SOS method.

Structure	Calculated shielding constant σ_{iso} (ppm)	Band gap (eV)
Aromatic form	−223.50	5.12
Quinoid form	−232.51	2.86

the lowest unoccupied band. Therefore, if this value becomes smaller, the electric conductivity increases. The band gaps for the aromatic and quinoid forms are 5.1 and 2.9 eV, respectively. This result shows that the electric conductivity for the quinoid form is larger than that for the aromatic form. Therefore, it can be expected that if the amount of the quinoid form is increased, polypyrrole with a higher electric conductivity can be obtained.

Fully aromatic polymers that have no aliphatic groups in the main chain make up the upper class of engineering plastics. The representative ones are poly(phenylene oxide), poly(phenylene sulphide), polysulphone, poly(ether sulphone), poly(ether ketone), poly(ether ether ketone), polyamides (aramide), and polyimides. Their high thermal stability, high strength properties, chemical resistance, and electrical properties have attracted attention to their structures.

Poly(phenylene oxide) (PPO), poly(phenylene sulphide) (PPS), and poly(2,6-dimethyl-1,4-phenylene oxide) (PDMPO) adopt the same crystalline conformation illustrated in Fig. 27. The dihedral angles, ϕ, between protonated carbons (C_P) and quarternary carbons (C_Q) are 45° and 45°.

The ^{13}C CP MAS spectrum of solid PDMPO has been reported, where two resonances are observed for the C_P.[44] They attributed this splitting to the non-equivalent environment of the C_P produced by the non-linear C–O–C bonds because the C_P become equivalent only when the phenyl rings rotated 90° out of plane of the oxygen atoms or when the phenyl rings are able to rotate rapidly. One can also expect to see a doubling of the C_P

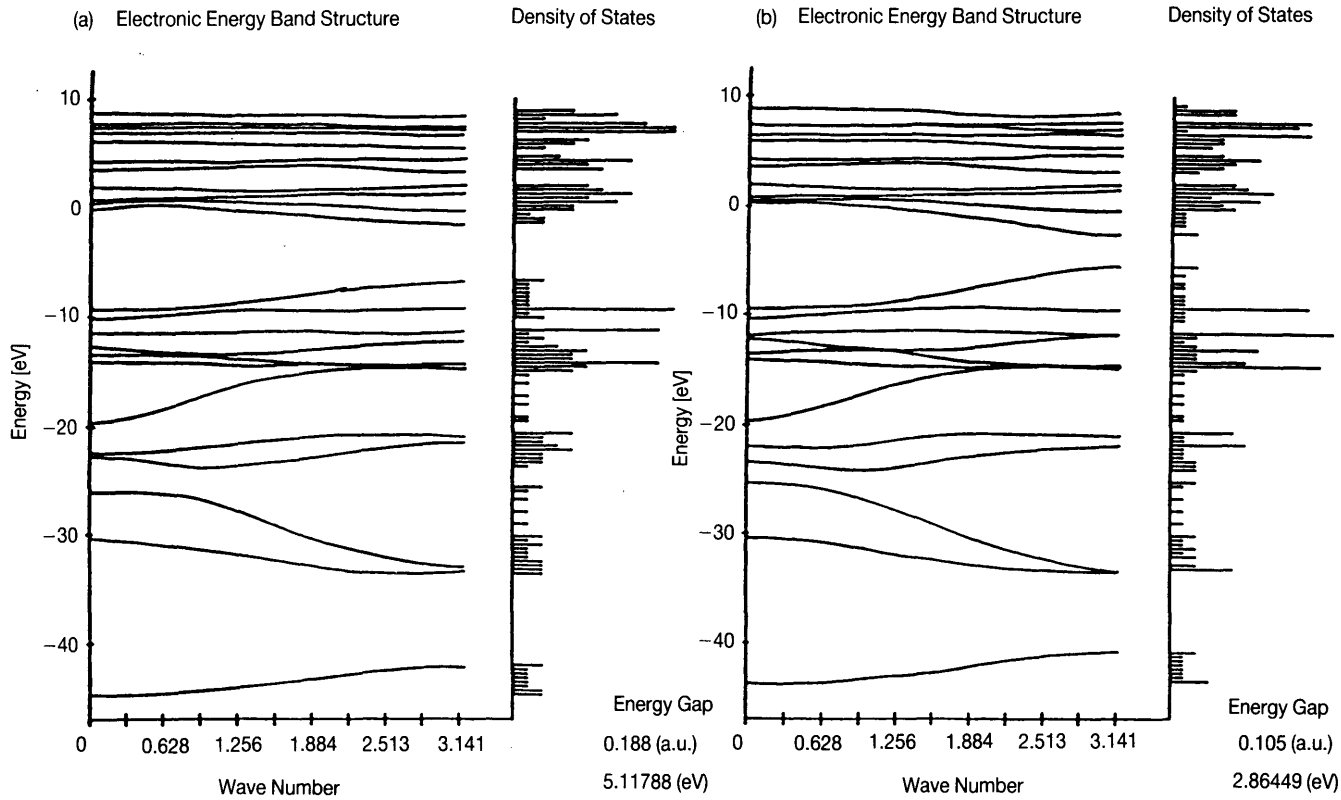

Fig. 26. Electronic energy band structure and density of states of an infinite polypyrrole chain calculated by the TB-INDO/S method: (a) aromatic form and (b) quinoid form.

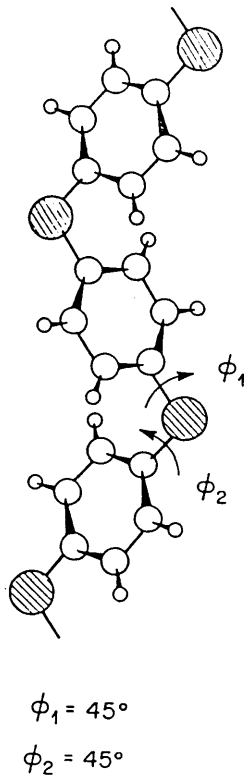

Fig. 27. Schematic drawing of the crystalline conformation of poly(phenylene sulphide) (PPS).

signals in the ^{13}C CP MAS-NMR spectrum. However, the ^{13}C CP MAS spectra of PPS exhibit single resonances for the C_Ps in PPS. Gomez and Tonelli[45] tried to resolve this question by measuring the solid-state NMR spectra of diphenyl sulphide (DPS). Figure 28(c) shows a difference spectrum which shows only the resonances of the protonated carbons C_P. The *m* and *p* resonances are singlets, but the *o*-C_P carbon manifests a resonance doublet centred at 135.5 ppm with a 2:1 ratio of intensities and a singlet resonance ca. 6 ppm upfield at 129.9 ppm corresponding in intensity to a single *o*-C_P carbon. It is shown that the triplet of *o*-C_P carbons is consistent with the conformation, in which the dihedral angles of four CPs are 0°, 180°, 30–40°, and 140–150°, respectively. The least shielded resonances would correspond to the 2 *o*-C_Ps with 140–150° and 180°; the resonance shielded by ca. 1 ppm would correspond to the single *o*-C_P with 30°. The reason why no split was observed in the C_P resonance of PPS was the 1 ppm difference of chemical shift between the resonances with 30–40°

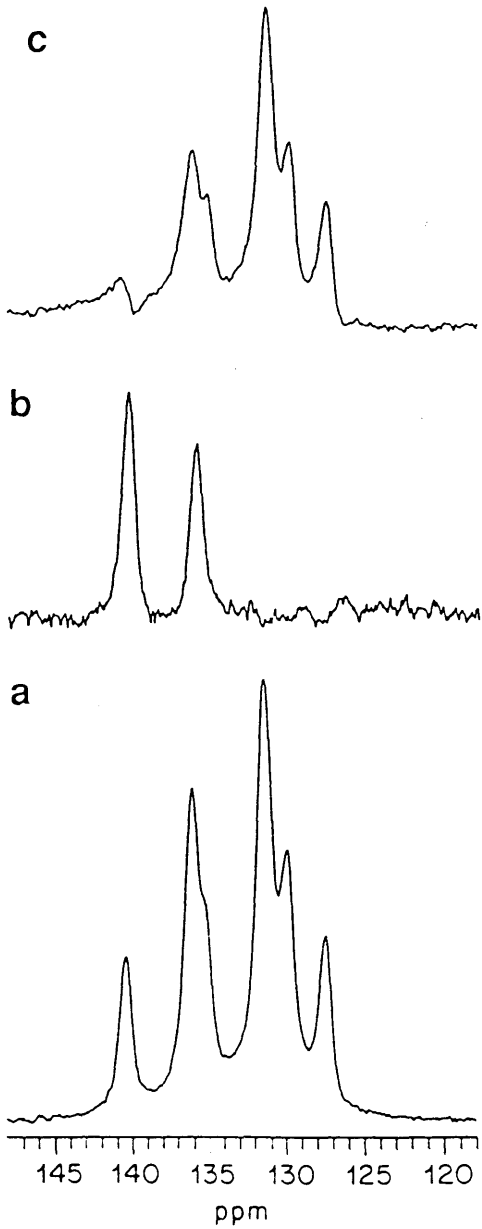

Fig. 28. (a) MAS-DD ^{13}C NMR spectrum of diphenylsulphide (DPS) recorded at $-60°C$ with a 420 s delay between decoupling pulses. (b) CP MAS-DD ^{13}C NMR spectrum of DPS recorded at $-60°C$ with a 100 μs delay (without spin-locking) in the ^{1}H channel after the Hartmann–Hahn match. (c) The difference spectrum [(a) – (b)] showing only protonated carbon resonances.

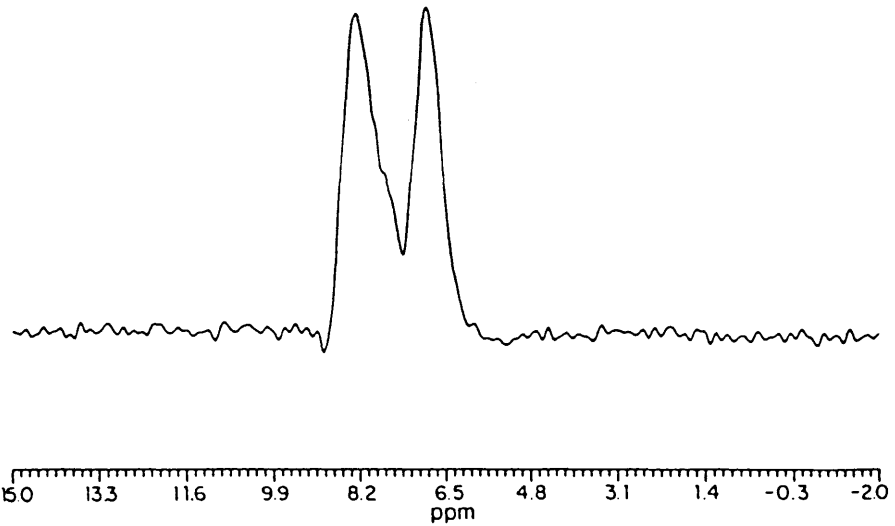

Fig. 29. 300 MHz ^{1}H CRAMPS spectrum of poly(phenylene sulphide) (PPS) obtained using the BR-24 pulse sequence; 64 transients; relaxation delay 8 s.

and 140–150° which are smaller than the ca. 2 ppm line width of the C_P resonance. This implies that the short C–O bonds (ca. 1.4 Å) lead to a greater conformational sensitivity of ^{13}C chemical shifts than the longer C–S bonds (ca. 1.8 Å) in PPS. The spin-lattice relaxation time, T_1, measured for PPS and DPS, of the order of several minutes, indicates the absence of rapid 180° ring flips.

Most recently Zumbulyadis *et al.*[46] have observed the ^{1}H CRAMPS (combined rotation and multiple-pulse spectroscopy) spectrum of semicrystalline PPS (Fig. 29). Two well-resolved resonances, separated by 1.4 ppm, are observed together with a broad shoulder on the high frequency resonance. They interpret this split as reflecting the chemical shift non-equivalence of the two protons expected in the crystalline phase.

Polyimides are usually generated by thermal imidization of poly(amic acid). Water and evaporated solvent bring about voids in the polyimide resins during the reaction. The problem has been solved mainly with the use of acetylene-terminated polyimide prepolymeric resins (Fig. 30) in which homopolymerization at elevated temperatures and pressures occurs without the formation of volatile products. The mechanism of cure is considered to be aromatization of the acetylenic end groups, but this has been impossible to verify because of the intractability of the cross-linked resin. The ^{13}C CP MAS-NMR spectra of the resin and the cured polyimide polymer-measured[47–49] changes in the line shape of the aromatic carbon region are found as well as a diminution of intensity in the acetylene carbon region

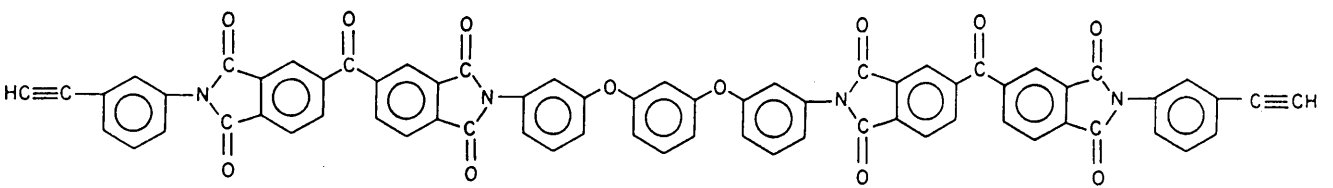

Fig. 30. Structure of acetylene-terminated polyimide.

(Fig. 31). Reactions involving the terminal acetylenic groups of the polyimide resin are involved in the polymerization process, but less than 30% of these acertylenes can undergo cyclotrimerization or other condensation reactions. The remainder appears to be consumed by addition reactions. To make the reaction clear, Swanson *et al.*[50] have studied the solid-state chemical reactions in a ^{13}C-labelled polyimide which had been prepared using starting materials labelled at sites that are thought to be involved in the cure reaction. The acetylene-terminated isoimide structure and ^{13}C-labelled monomers are shown in Figs 32 and 33. Figure 34 shows the ^{13}C CP MAS-NMR difference spectra of acetylene-terminated oligomer labelled at the carboxyl (isoimide/imide) positions. The smaller peak at 148.0 ppm in the uncured oligomer, which is due to the C=N isoimide carbon, disappears, and a single resonance is observed in the spectrum of the cured polymer. This is consistent with the thermal isomerization of the isoimide to the imide. These carbons are not involved in any reactions with the ethynyl (acetylenic) carbons. Similarly, the diaryl carbonyl is not involved in the "cure" chemistry. On the other hand, the difference spectra for the samples which had been selectively ^{13}C-labelled at the C-1 (non-protonated carbon) and C-2 (protonated carbon) ethynyl carbons are shown in Figs 35 and 36. In the delayed decoupling spectra, only the non-protonated carbons are observed. The spectrum of the C-1 labelled cured sample exhibits an intense resonance at 139.6 ppm (non-protonated), a smaller resonance at 129.6 ppm (protonated) in the aromatic region, and a fairly broad resonance at 52 ppm (protonated) in the aliphatic region. The spectrum of the cured C-2 labelled sample shows a distinct peak at 128.7 ppm (protonated), a broad resonance between 58 and 70 ppm (non-protonated), and a shoulder on the high frequency peak at about 138 ppm (non-protonated). The major products of the ethynyl carbons are aromatic groups as evidenced by the largest C-1 and C-2 peaks in the aromatic region. Another reaction product class is the condensed polycyclic aromatic structures as indicated by deprotonation of the C-2 and protonation of the C-1 carbons in the spectra. However, none of the cure products accounts for the resonances in the 50–70 ppm range. The possibility of the further reaction of the Friedel–Crafts backbone addition, which forms a bridged structure, is proposed.

Bismaleimides are also used as void-free high-temperature matrix resins for fibre-reinforced composite materials. The high strength and high modulus properties of these resins persists after hot-wet or hot-dry exposures to 250°C. Bismaleimides by themselves tend to form highly cross-linked networks which produce brittle resins. To alleviate this problem, chain extenders are introduced into the resins to lower the cross-link density and thereby increase the fracture toughness of the cured composite. Fry and Lind[51] have measured the ^{13}C CP MAS-NMR spectra of 1,1′-(methylenedi-4,1-phenylene)-bismaleimide (BMI) as received, after

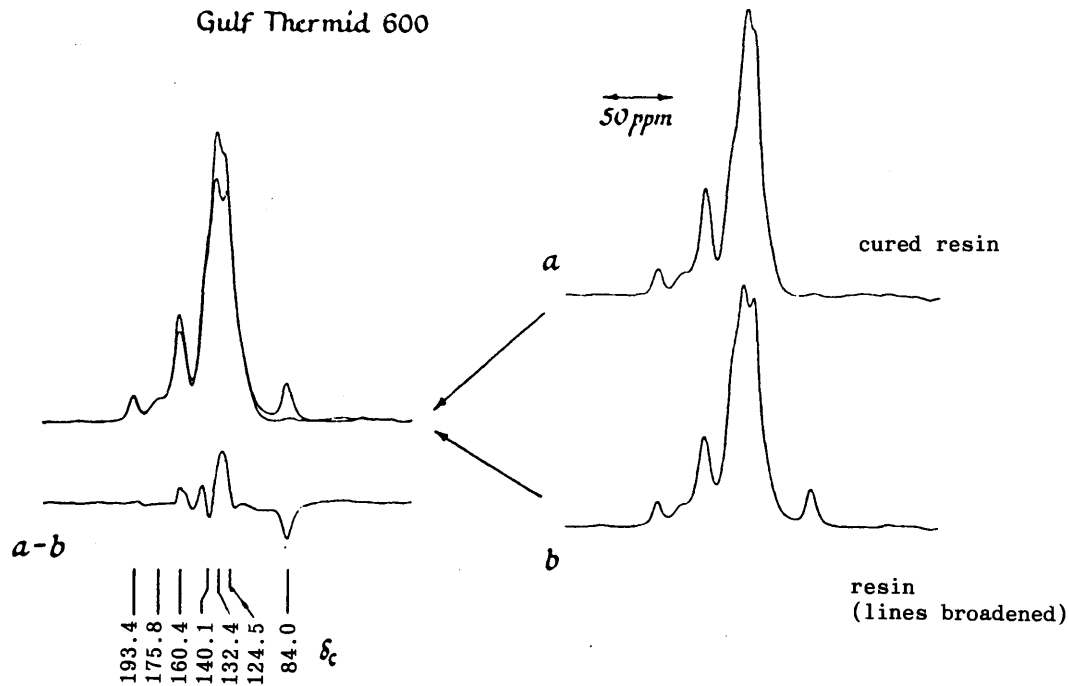

Fig. 31. Difference spectrum (a – b) obtained by subtraction of the polyimide resin spectrum (with lines artificially broadened, b) from that of the cured polyimide polymer (a). Small deviations in the difference spectrum should be ignored since line broadening across the cured polymer spectrum may not be uniform.

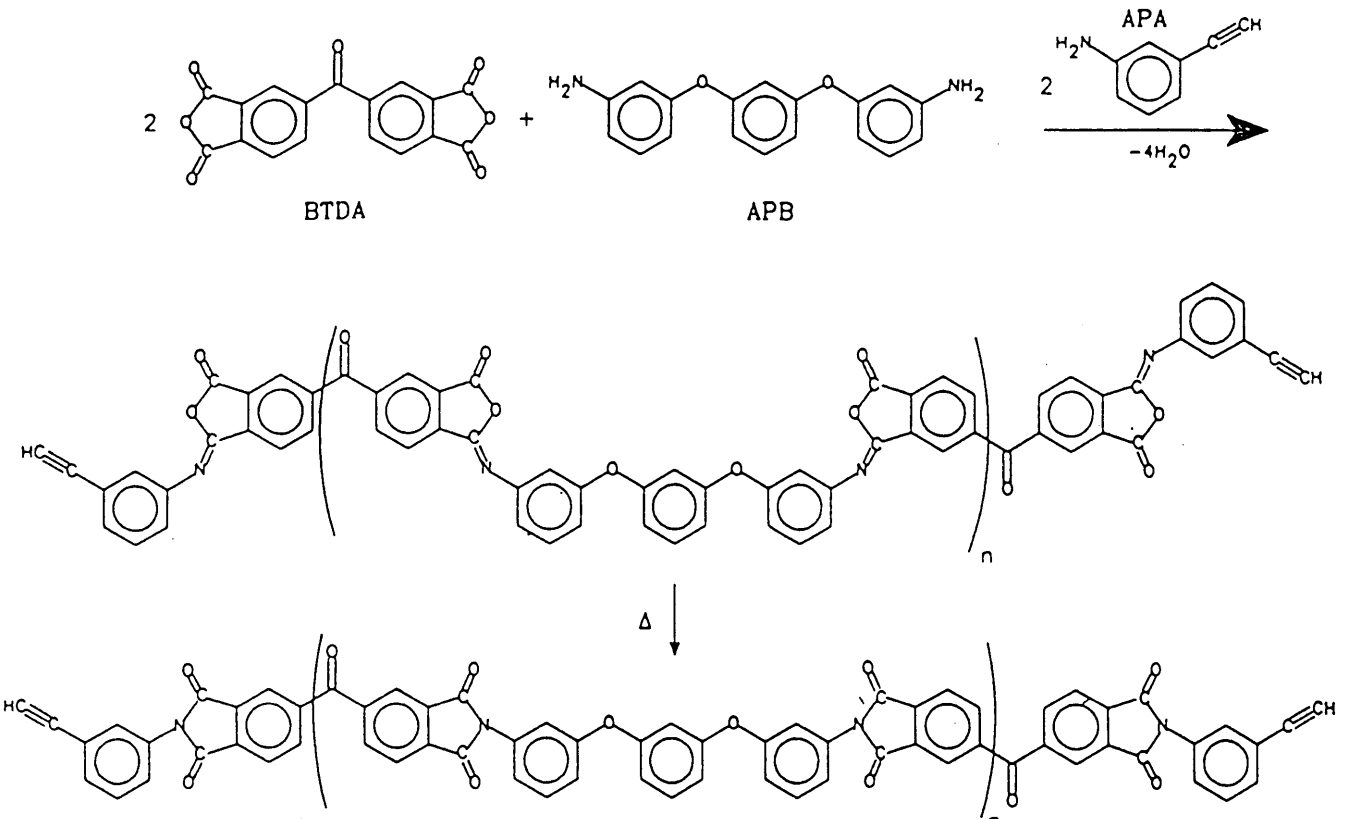

Fig. 32. Synthesis of acetylene-terminated isoimide oligomer and cure to imide oligomer.

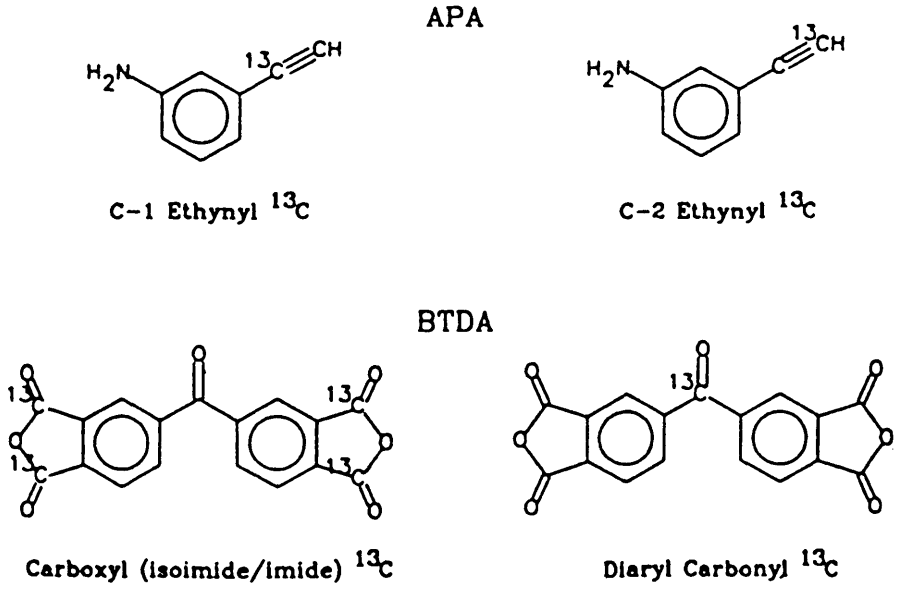

Fig. 33. ^{13}C-labelled monomers.

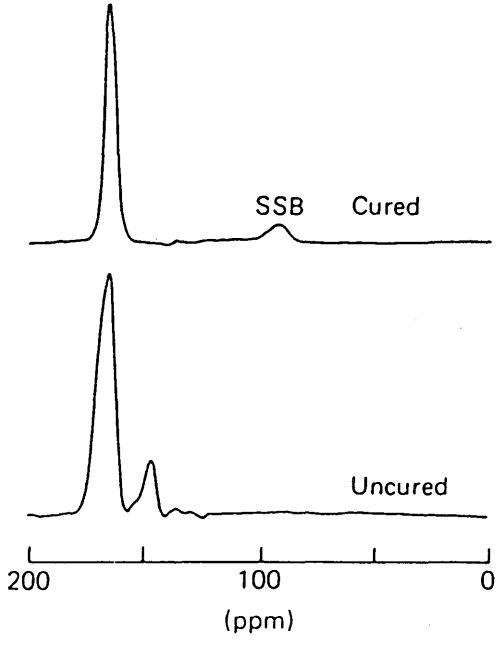

Fig. 34. ^{13}C NMR difference of acetylene-terminated oligomer labelled at the carboxyl(isoimide/imide) positions.

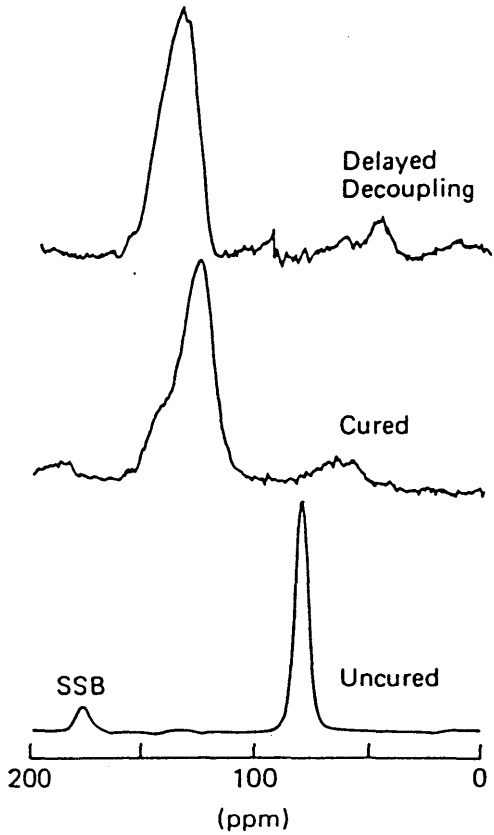

Fig. 35. ^{13}C NMR difference spectra of acetylene-terminated oligomer labelled at the C-1 ethynyl position.

quenching, and after curing for 4 h at 493 K (Fig. 37). The cured BMI spectrum clearly shows a new carbonyl resonance at 175 ppm. A decrease is observed in the intensity of the resonance at 132 ppm, and a new resonance occurs at about 45 ppm. Two primary reactions, shown in Fig. 38, appear to take place during curing: (R1), the cross-linking reaction, and (R2), the chain extension reaction. In the (R2) reaction, the chain extender is methylene dianiline (MDA). Figure 39 shows the assignments for the reactants and products. As the maleimide rings react to form substituted succinimides (the products of R1 and R2), the carbonyl concentration at 169 ppm shifts to 175 ppm. The ratio of $a_{175}/(a_{175}+a_{169})$ provides a good measure of the extent of cure as shown in Fig. 40 (a_x is the area of the resonance at x ppm estimated from curve fitting). On the other hand, since the 45 ppm and the 52 ppm resonances occur only as the products in (R1) and in (R2), respectively, the ratios involving a_{45} and a_{52} suggest the preference of these

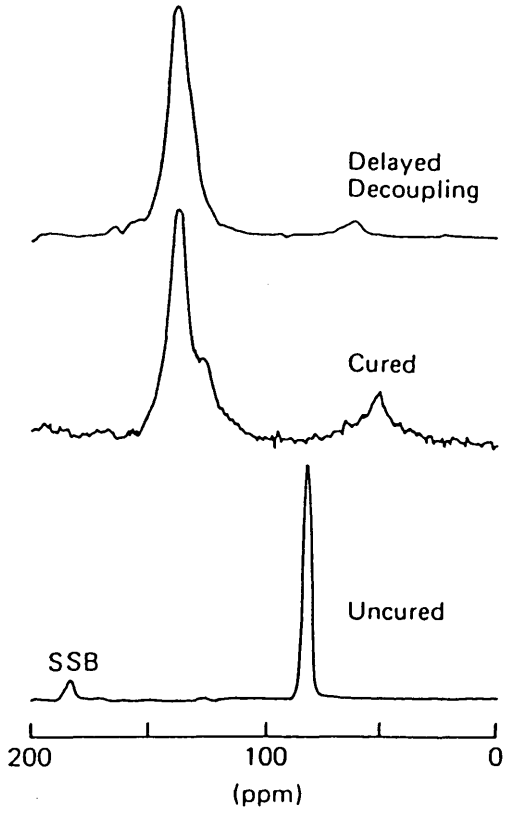

Fig. 36. ^{13}C NMR difference spectra of acetylene-terminated oligomer labelled at the C-2 ethynyl position.

reactions under a certain cure condition. Figure 41 thus clearly shows that the chain extension reaction (R2) is favoured at 418 K, whereas the cross-linking reaction (R1) occurs to a greater extent at 493 K (the 39 ppm resonance should be constant).

Other examples of the application of ^{13}C CP MAS-NMR to engineering plastics can be found in the literature,[52–54] including studies on polycarbonate,[55] poly(ethylene terephthalate),[56] sulphones[53] and polyimides.[57] In addition, recent studies are found for polycarbonate,[58] poly(ethylene terephthalate),[59] poly(butylene terephthalate),[60] poly(ether ether ketone)[61] and polyamide.[62]

Above any specified temperature, bulk polymers sometimes form a liquid crystalline phase before going from solid to liquid. For example, in a series of poly (L-glutamate)s with long *n*-alkyl side chains[63–65] or *n*-alkenyl side chains,[66] the side chains form a crystalline phase at low temperature, but at

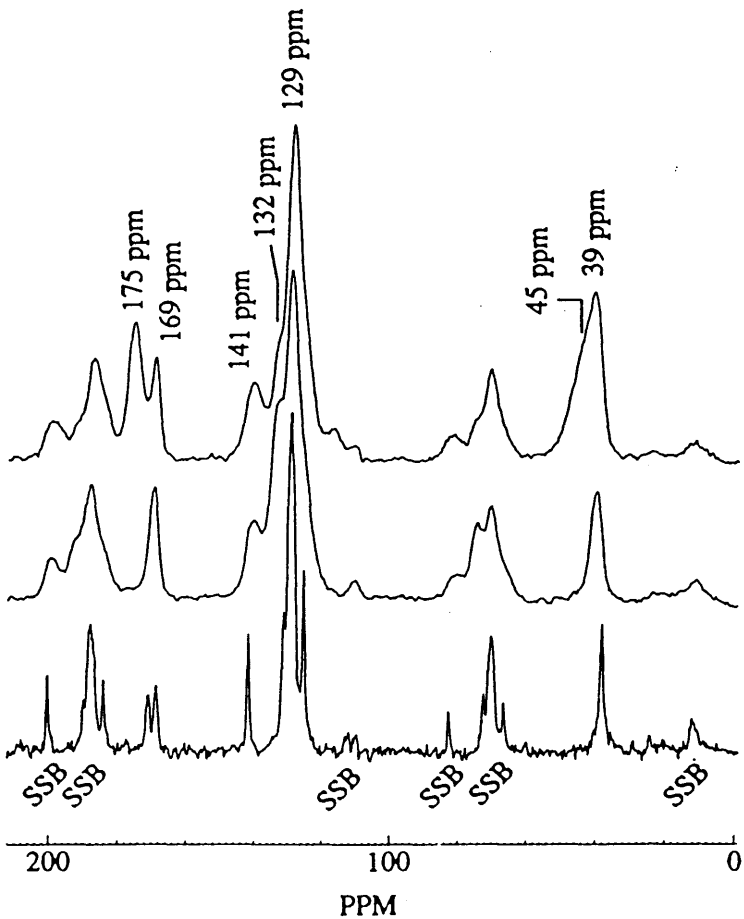

Fig. 37. ^{13}C CP MAS spectra of BMI as received (bottom), after quenching (middle), and after curing for 4 h at 493 K (top). Spinning sidebands are labelled SSB.

higher temperatures the side chains melt like liquid *n*-alkanes or liquid alkenes and the polymers have a liquid crystalline character. The thermotropic behaviour of poly(L-glutamate)s with long *n*-alkyl side chains or with oleyl side chains with double bonds have been investigated by VT CP MAS-NMR and pulse NMR.

Figure 42 shows the ^{13}C CP MAS-NMR spectrum of poly(γ-*n*-octadecyl-L-glutamate) at room temperature together with the assignment of peaks. It has been demonstrated that ^{13}C chemical shift values of CO (amide) and C_α carbons and interior CH_2 carbons depend on the conformation and crystal structure. At room temperature, ^{13}C chemical shift values of the CO (amide) and the C_α carbons are 176.0 and 57.6 ppm, respectively. These

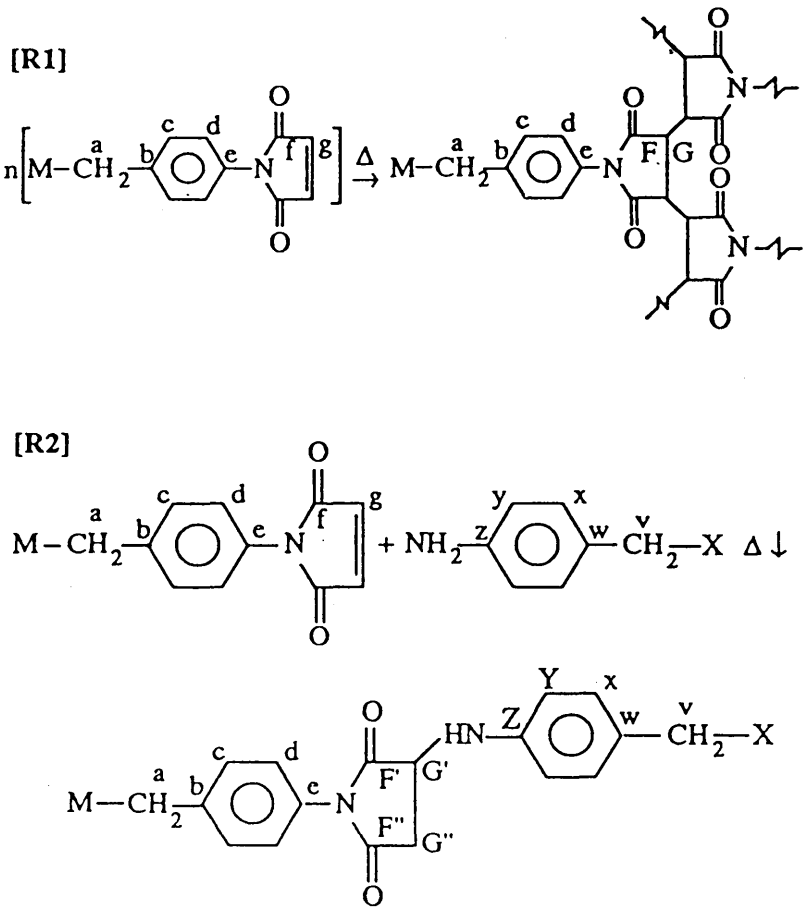

Fig. 38. Reactions [R1] and [R2].

values show that the main chain takes an α-helix conformation. On the other hand, the interior CH_2 signal splits into two peaks at 33.4 and 30.6 ppm indicated by I and A, respectively. From the reference data of *n*-alkanes and polyethylene, it is seen that peak I arises from the CH_2 carbons in the all-*trans* zig-zag conformation in the crystalline state and that peak A arises from the CH_2 carbons in the non-crystalline phase or the liquid phase.

Figure 43 shows the VT ^{13}C CP MAS-NMR spectra of the polymer at temperatures ranging from room temperature to 100°C.[64] (It is demonstrated that the polymer forms a liquid crystalline phase above 40°C.) The *n*-alkyl peaks change observably as the temperature is increased. Peak I

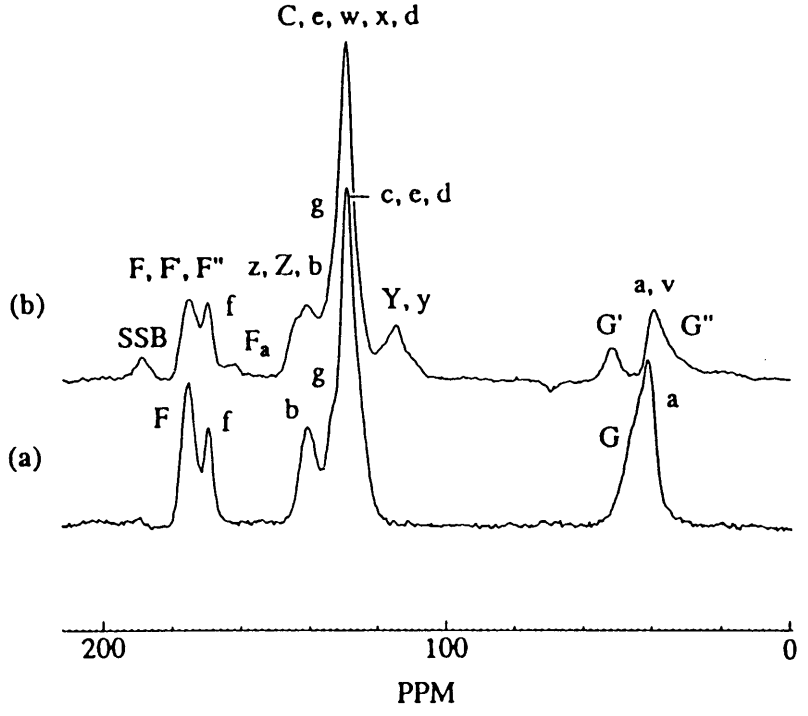

Fig. 39. ^{13}C TOSS spectrum of (a) pure BMI cured 4 h at 498 K and (b) 1.5:1 BMI:MDA cured 1 h at 418 K. Assignments are listed in Table 2.

disappears above 35°C and the intensity of peak A increases noticeably. This is due to the melting of side chain crystallites. On the other hand, as for the CO (amide) and C_α carbons, a progressive broadening of these carbons is observed. At about 40°C, the peaks are broadened to the point of disappearing from the spectrum. At higher temperature the peaks appear at the same chemical shift values again. This means that the main chain takes an α-helix conformation. The broadening can be explained on the basis that the reorientation rate of the main chain becomes insufficient to average dipolar interactions with protons. This reduces the efficiency of the radiofrequency decoupling and leads to a maximum line width of the carbons when the molecular motion occurs at the frequency corresponding to the amplitude of the proton decoupling field (about 60 kHz for the experiment). Therefore, it can be said that the main chain with the α-helix form is undergoing reorientation at a frequency of about 60 kHz in the liquid crystalline phase.

The VT ^{13}C CP MAS experiments on poly(γ-oleyl-L-glutamate)[66] with unsaturated long side chains show that the main chain takes the α-helix form

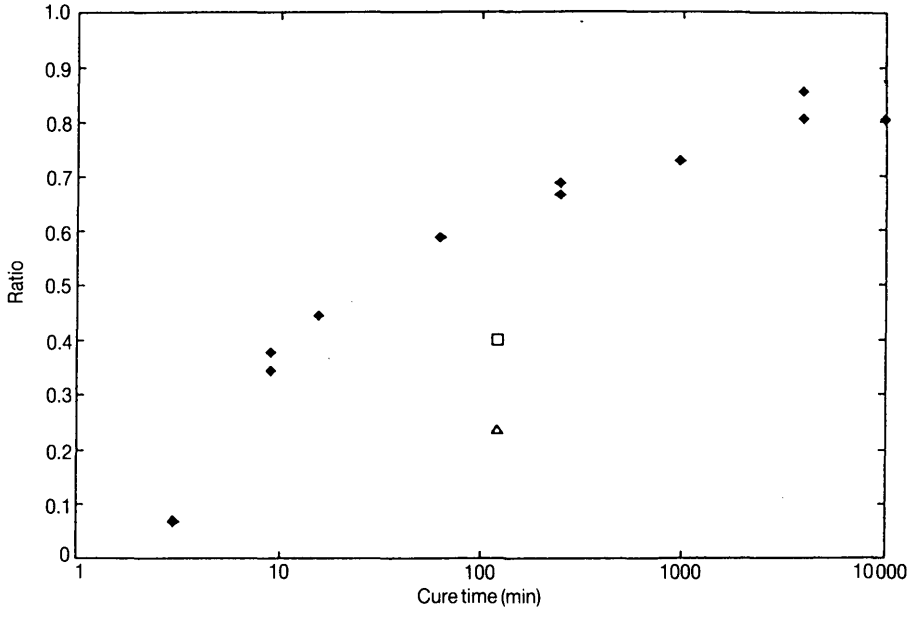

Fig. 40. The ^{13}C NMR carbonyl concentration ratios $a_{175}/(a_{175}+a_{169})$ for the 1:0 BMI:MDA resin cured at 493 K for up to 10 000 min are shown by solid points. The square point represents a 1:0 sample that was first dissolved in chloroform and then held at 418 K for 2 h. The triangle point represents a 1:0 sample that was quickly melted and then quenched before curing at 418 K for 2 h.

within the temperature range from −40 to 80°C, while the long side chains are in a mobile state above −40°C. Such a situation is very similar to the case of poly(γ-*n*-octadecyl-L-glutamate). A detailed discussion of the dynamics of these two polymers is based on proton relaxation times and proton line widths measured over a wide range of temperatures from −150 to 120°C.[67]

Long *n*-alkanes, on going from the crystalline state to the liquid state, take the hexagonal form in the narrow temperature range prior to the melting point, in which the *n*-alkane chains are rotating about their long axes. The hexagonal form is the so-called "rotator phase" like the liquid crystalline phase. Ishikawa *et al.*[68] have investigated this problem by VT ^{13}C CP MAS-NMR experiments over a wide range of temperatures. It is revealed that the ^{13}C chemical shift value of the interior CH_2 carbons in *n*-$C_{24}H_{50}$ moves from 34.2 to 33.3 ppm on going from the triclinic form to the rotator phase, and the ^{13}C chemical shift of the interior CH_2 carbons of *n*-$C_{19}H_{40}$ and *n*-$C_{32}H_{66}$ move from 32.8 to 33.3 ppm on going from the orthorhombic form to the rotator phase. From these results, it can be said that ^{13}C chemical shift values of *n*-alkanes in the rotator phase are the same

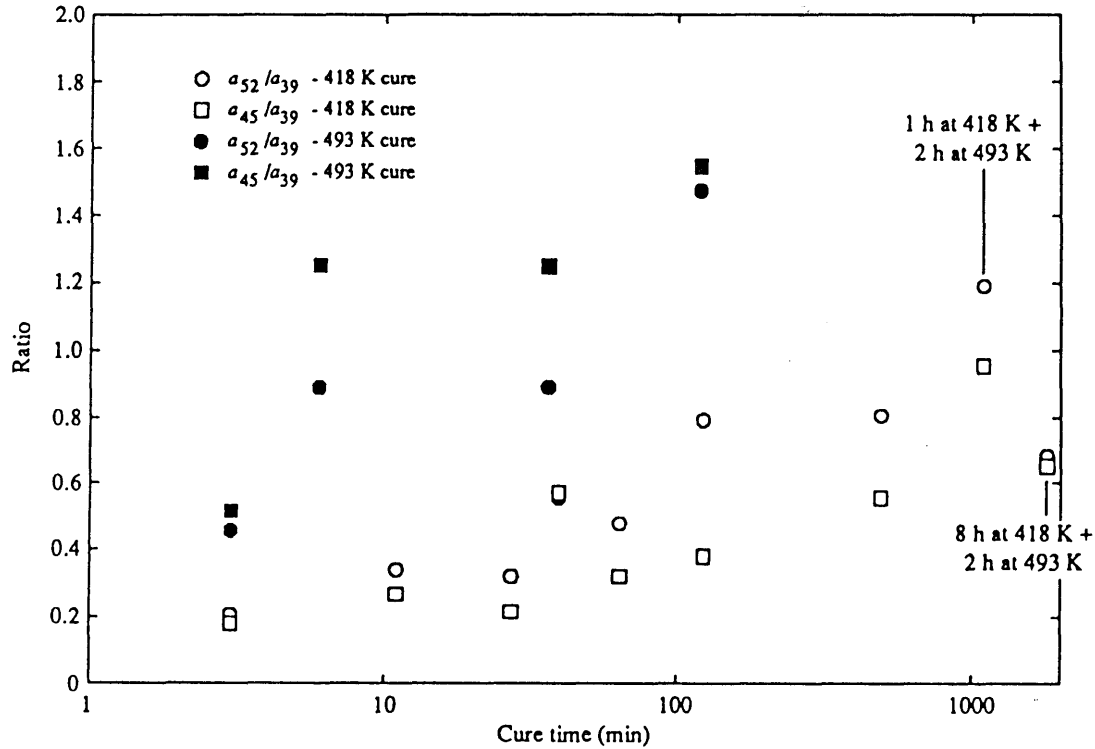

Fig. 41. Ratios of ^{13}C CP MAS resonance areas for the chain-extension methylene at 53 ppm (circles) and the cross-linking methylene at 45 ppm (squares) to the diphenyl methylene at 39 ppm are shown for cures performed at 418 K (open points) and at 493 K (solid points) for the 2.5:1 BMI:MDA system.

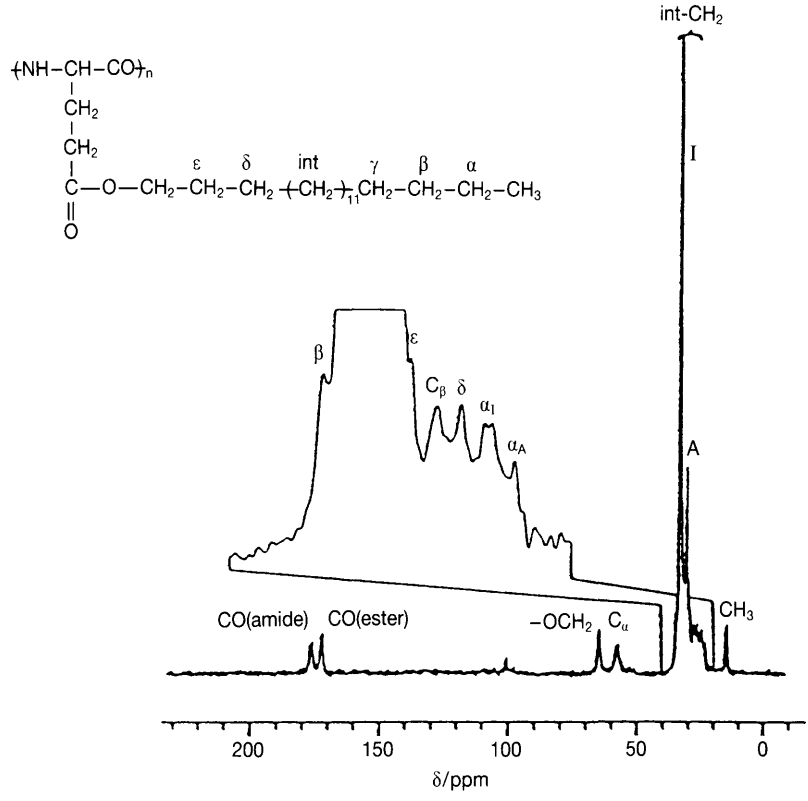

Fig. 42. ^{13}C CP MAS-NMR spectrum of poly(γ-*n*-octadecyl-L-glutamate) at room temperature. Peaks in the vicinity of 30 ppm are expanded. Assignment of each peak is done by reference to the data for poly(γ-benzyl-L-glutamate) and *n*-alkanes in the solid state.

irrespective of chain length and therefore every *n*-alkane in the rotator phase has the same structural aspects.

Further, in order to study the dynamic features of *n*-alkanes in the rotator phase, the ^{13}C T_1 values of *n*-$C_{32}H_{66}$ in the crystalline phase, rotator phase and liquid phase were measured by Torchia's pulse sequence method and the inversion-recovery pulse sequence method as shown in Fig. 44.[69] The order of the magnitudes of the T_1 values for the CH_2 carbons is α-$CH_2 < \beta$-$CH_2 <$ interior CH_2 in the crystalline phase, in contrast to that in the melting phase. According to BBP theory,[70] as the correlation time for molecular motion increases, T_1 first decreases and then increases again, passing through a minimum. Therefore, it can be said that the molecular motion of the CH_2 carbons of *n*-$C_{32}H_{66}$ in the crystalline state at 60°C is in the slow motion region and that the molecular motion of the CH_2 carbons in

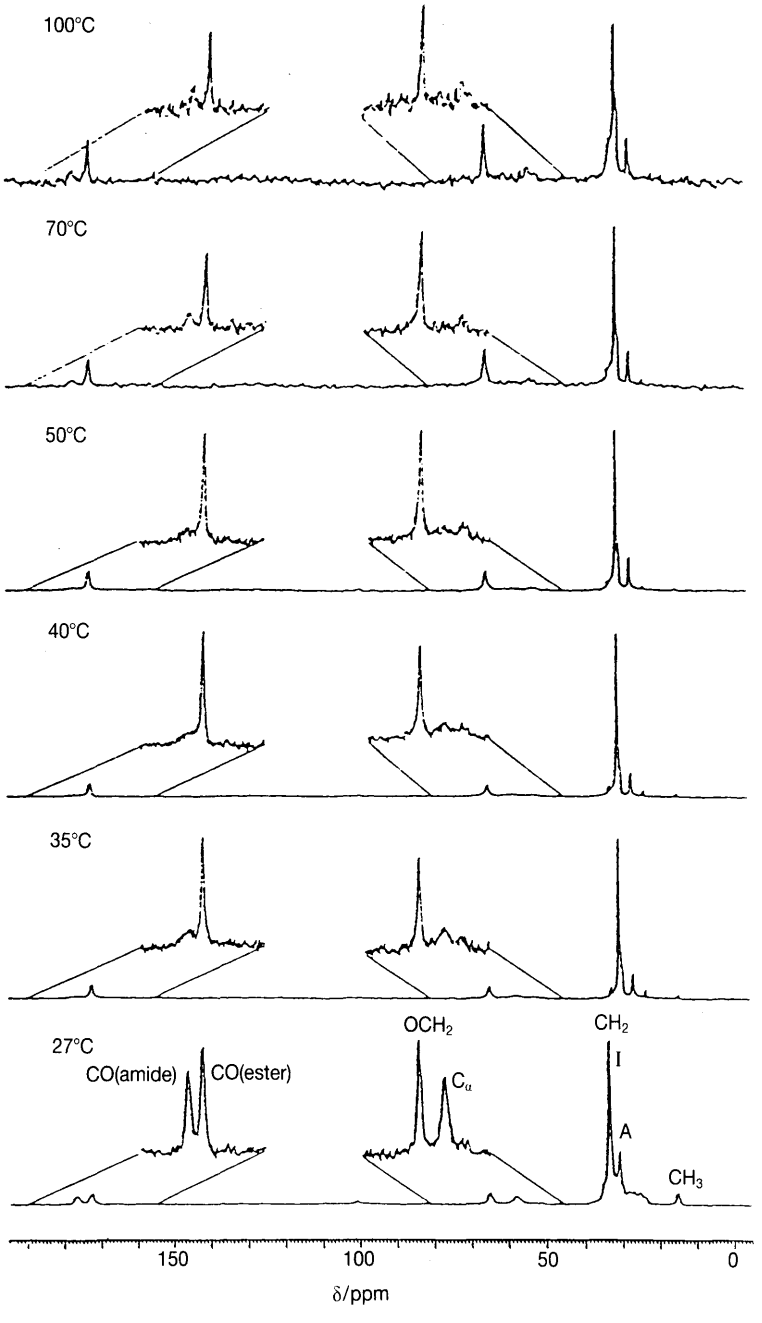

Fig. 43. ^{13}C CP MAS-NMR spectra of poly(γ-*n*-octadecyl-L-glutamate) as a function of temperature. The main chain carbon peaks are expanded.

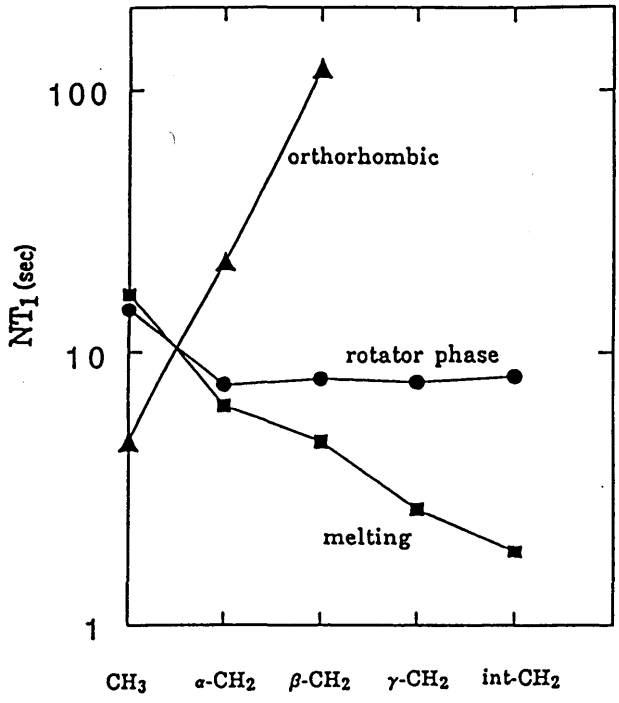

Fig. 44. ^{13}C spin-lattice relaxation times NT_1 for n-$C_{32}H_{66}$ chain at various temperatures. N indicates the number of protons bonded to each carbon considered.

the liquid phase at 80°C is in the extreme narrowing region. However, for T_1 values in the rotator phase at 70°C, α-$CH_2 \approx \beta$-$CH_2 \approx \gamma$-$CH_2 \approx$ interior CH_2. This means that every CH_2 carbon in the rotator phase is undergoing molecular motion with the same mode. Therefore, it can be said that all-*trans* zig-zag chains in the rotator phase rotate about their long axes.

Mathias[71] has examined the structural behaviour of long *n*-alkyl side chains of some comb polymers with the following structures which form a liquid crystalline phase above about 40°C, through the observation of the VT ^{13}C CP MAS-NMR spectra. A ^{13}C chemical shift of about 3 ppm to low frequency is observed for the methylene carbons as the side chain crystallite is melted. The CP efficiency for the main chain carbons is decreased. These behaviours are similar to that of poly(γ-*n*-alkyl-L-glutamate) mentioned above. Cooling the liquid crystals below the melting transition associated with the liquid crystalline transition results in broadened lines.

The relaxation times of the liquid crystalline polymer, shown below, which has a liquid crystalline transition at 44°C, show that below the melting transition the mesogenic unit and the spacer carbons alpha to the mesogen

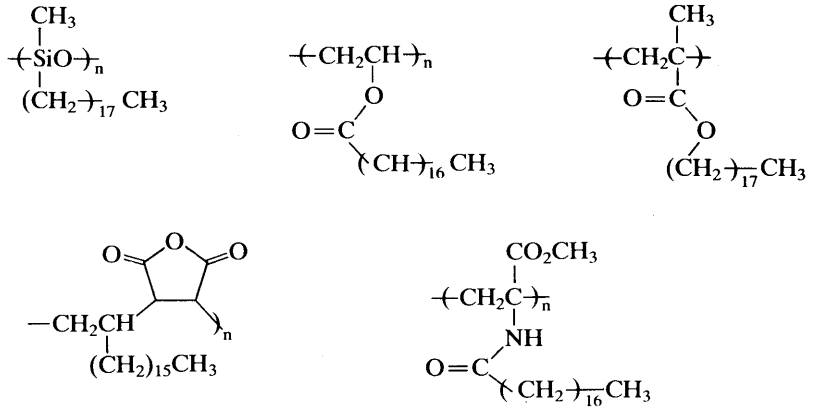

are quite rigid.[72] The spacer has a substantial degree of mobility and the backbone has a much higher relative mobility compared to the flexible free substituent methyl carbons. ^{13}C CP MAS spectra for the liquid crystal as a function of thermal history are shown in Fig. 45. Heating to 100°C and cooling cause excessive broadening of all the lines indicative of an amorphous polymer. Heating to 70°C, the top of the liquid crystalline transition, narrows the lines and this is maintained when cooled below the glass transition.

Spiess *et al.*[73–77] have indicated that the orientational order is maintained when cooled below the glass transition for side chain liquid crystals. Positional order is also required to crystallize.

Further, the other liquid crystalline polymers such as polyester, side chain polysiloxane liquid crystals, polyamide, etc., have been investigated by solid-state NMR.[78–83]

The structural change of lipids, dimyristoylphosphatidylcholine and distearoylphosphatidylcholine, in going from the crystalline phase to the liquid crystalline phase was investigated by VT ^{13}C CP MAS-NMR at temperatures from −90 to 140°C.[84] The experimental results show that the conformational change of the *n*-alkyl chains of DMPC and DSPC in the liquid crystalline state is very similar to that of *n*-alkanes in the liquid state near the melting point, and below the crystalline–liquid crystalline transition temperature the *n*-alkyl chains are still reorientating with some degree of disorder.

3. POLYMER ALLOYS

The physical blending of two or more polymers provides new polymer materials with suitable physical properties.[85] Such polymer blends are often referred to as "polymer alloys" to use a term from metallurgy. The

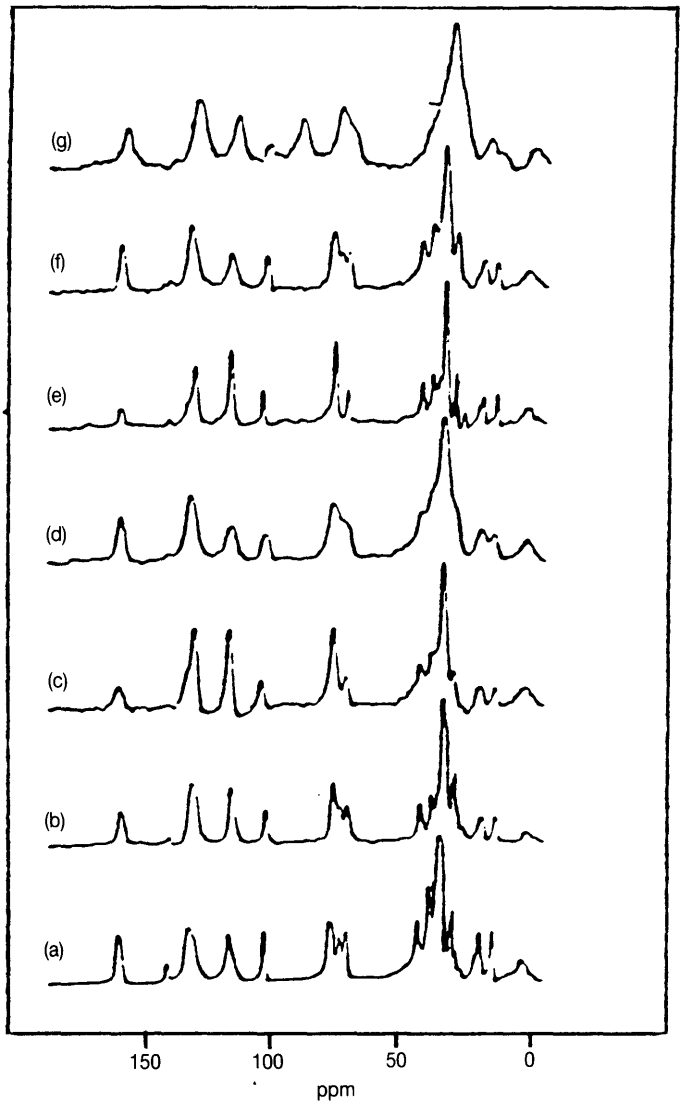

Fig. 45. The effect of thermal history on the ^{13}C CP MAS-NMR spectra of the liquid crystalline polymer in scheme (below). (a) 20°C, (b) 40°C, (c) 70°C, (d) 20°C after cooling from 100°C, (e) 70°C after heating d, (f) 20°C after cooling from 70°C, and (g) 20°C after cooling from 100°C.

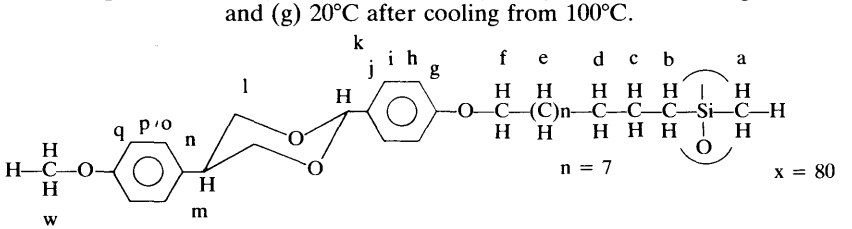

thermodynamics of polymer–polymer mixtures plays an important role in the molecular state of dispersion, leading to an understanding of the morphology of two phase mixtures and the interface between phases.

In the polymer blends, it is very important to understand the size of the phases or domains on a molecular or segmental scale. In this section, most recent NMR studies will be introduced on these subjects. In polymer blends, spin diffusion between individual polymers can occur when they are intimately mixed. From such a point of view, miscibility in polymer–polymer mixtures has been the subject of considerable discussion through the 2D NMR and CP MAS-NMR results.

The first 2D ^{1}H NMR experiments on a mixture of polystyrene and poly(vinyl methyl ether) (PVME), one of the typical polymer alloys, was carried out by Ernst *et al.*[86] The cross-peaks between signals coming from polymers, when cast from toluene solution, were successfully observed but not when cast from chloroform solution. In the former blend well-mixed domains exist, but in the latter blend they do not. Ernst *et al.* have suggested that through the observation of the quantitative determination of cross-peak intensities and spin diffusion rates, the fraction of mixed domains and domain size can be estimated.

^{13}C CP MAS spectra of the mechanically mixed deuterated polystyrene (d-PS)/poly(vinyl methyl ether) sample were measured[87] as a function of contact time at $-33°C$, since poly(vinyl methyl ether) has a proton $T_{1\rho}$ minimum at room temperature which makes cross-polarization ineffective. The spectrum is dominated by the signals of PVME. However, at longer contact times, a signal coming from the aromatic carbons of d-PS is observed. This comes from domains where interfacial mixing has occurred between the PVME, which is above its glass temperature when mixed, and the d-PS. ^{13}C CP MAS-NMR spectra of the same sample, heated to 130°C for 30 min and quenched, were measured under identical conditions as before, as shown in Fig. 46. In addition to the PVME signals, a very intense signal due to the phenyl carbons of the d-PS and resonances due to the d-PS methylene and methine backbone carbons appear. The signal intensities decrease at long contact times due to PVME proton $T_{1\rho}$ relaxation. Further, the ^{13}C CP MAS-NMR experiments on two blends of d-PS and poly(methyl methacrylate) (PMMA) were performed but no signal due to d-PS was observed. The above technique demonstrates that d-PS and PVME are compatible, but d-PS and PMMA are not compatible. As seen from these experiments, the polarization transfer has an r^{-6} spatial dependence[88] which generally limits effective transfer to distances of less than about 20 Å.

Parmer *et al.*[89] determined polymer–polymer miscibility by ^{13}C CP MAS-NMR in blends of deuterated and protonated polymers, d-PS/PVME, deuterated PMMA (d-PMMA)/PS and deuterated PMMA/poly(vinyl chloride) (PVC). ^{13}C CP MAS experiments on d-PS/PVME and d-PMMA/PS were done and similar results found. In Fig. 47 the ^{13}C CP MAS-NMR

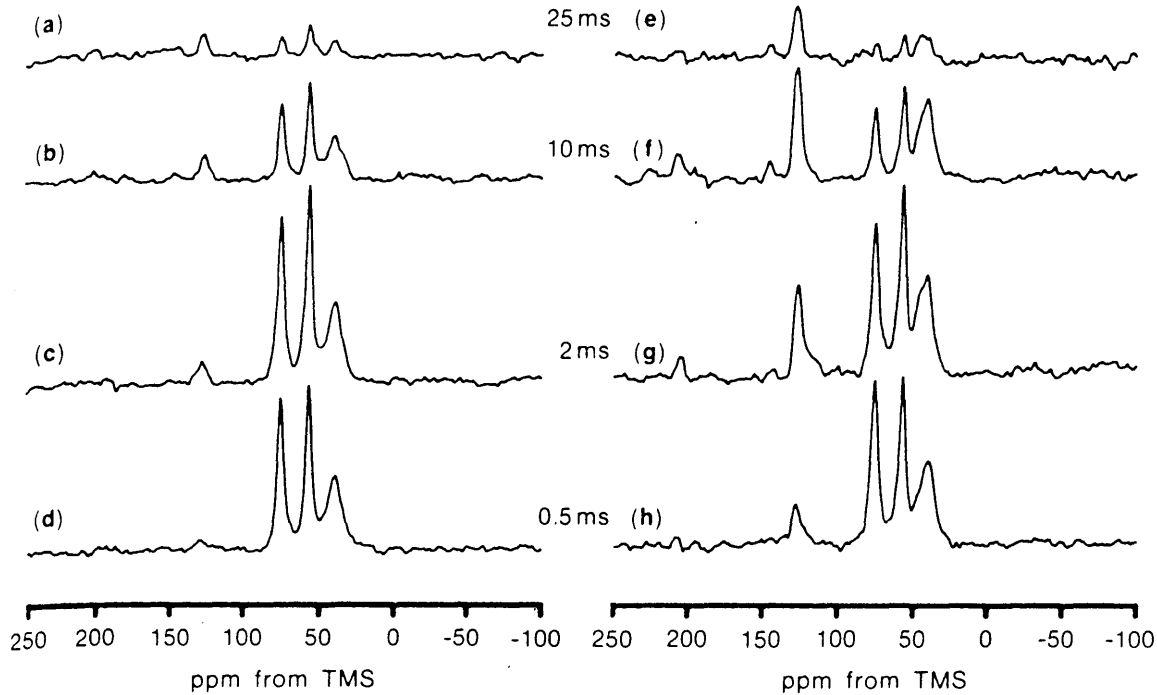

Fig. 46. 50.17 MHz ^{13}C CP MAS-NMR spectra of a 50:50 mechanical mixture by weight of deuterated polystyrene/poly(vinyl methyl ether) (d-PS/PVME) blends as a function of contact time at −33°C. Cross-polarization and decoupling fields are ca. 55 kHz. The number of accumulations is 128. (a)–(d) are of the mechanical mixture before heating. (e)–(h) are of the same sample after heating to 130°C for 2 × 30 min and quenching after each heating cycle.

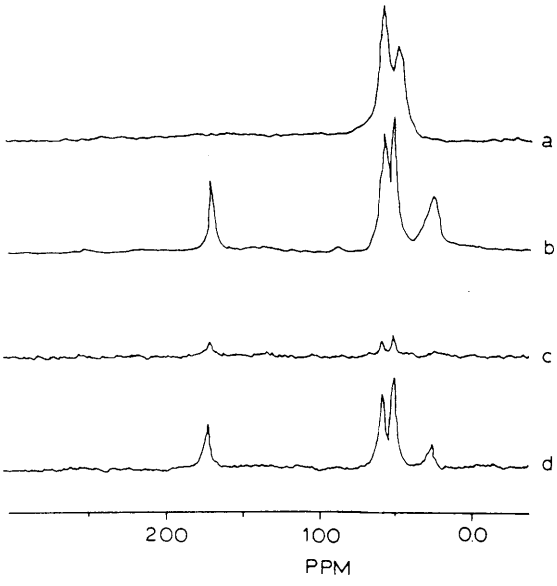

Fig. 47. 50 MHz ^{13}C CP MAS-NMR spectra of: (a) poly(vinyl chloride) (PVC); (b) poly(methyl methacrylate) (PMMA); (c) 95% deuterated PMMA/5% PVC and (d) a spectrum of (c) obtained with a dipolar decoupling delay of 40 μs.

spectra of PVC (a), PMMA (b) and a blend of 95% of d-PMMA and 5% of PVC (c and d) are shown. In the ^{13}C CP MAS spectrum of the blend the PVC resonances are suppressed by a delayed dipolar decoupling sequence. Even though Fig. 47d shows the spectrum from less than half of the transients used to obtain Fig. 47c, the signals are three to four times more intense. This shows not only miscibility at the molecular level but also the applicability of the technique to blends containing only a few per cent of protonated polymer components.

The miscibility enhancement of PS/PMMA blends[90] through ionic interactions was studied by the intermolecular cross-polarization method as mentioned above. When PS is slightly sulphonated (3.3 mol% of $-SO_3H$) and PMMA is copolymerized with 2.3 mol% 4-vinylpyridine (4VP), the miscibility of the blend is enhanced, due to proton transfer from the $-SO_3H$ to the 4VP moiety with the formation of ionically interacting sites on the d-PS and the PMMA. By the introduction of about 9.5 mol% of interacting groups ($-SO_3H$ and 4VP), the blend shows a much greater enhancement in miscibility. When the $-SO_3H$ on the d-PS is neutralized with $N(CH_3)_4OH$ and the 4VP is quaternized with CH_3I, the blends exhibit similar or even better miscibility compared with the proton-transfer blends. This is attributed to direct ion–ion interactions in the blends.

Chu *et al.*[91] have studied thermally induced phase separation in PS/PVME blends through the observation of the proton spin-lattice relaxation, in both the laboratory and the rotating frame, for the entire range of blend composition. Under conditions in which the blends are compatible, ^{1}H $T_{1\rho}$ results obtained at −5°C showed microheterogeneity at a 10 Å scale using the relation[92] given by $\langle L^2 \rangle \approx (T_1/T_2)\langle r^2 \rangle$ where $\langle L^2 \rangle$ is the molecular contacts over a coherence scale L, (T_1/T_2) is a ratio of spin-lattice relaxation time to spin–spin relaxation time and r is the average distance between protons. ^{1}H $T_{1\rho}$ values at room temperature are closer to the longer relaxation time of PS than that expected from a simple weighted average of the relaxation times of the constituent homopolymers. This shows incomplete averaging by spin diffusion and a restraining effect of PS on the segmental motions of PVME. These blends are heated to cause phase separation. From the biphase decay of ^{13}C magnetization, the compositions of the separated phases give a lower critical solution temperature phase diagram. NMR relaxation in PVME blends with PS molecular weights of 9, 100, and 900 K are compared.

By the observation of the temperature dependence of the ^{13}C line width, for the CH carbon of PVME in a PS/PVME blend, the effects of blending on molecular motion of the individual polymer components have been investigated.[93] This shows that the molecular motion averages the distribution of isotropic chemical shifts in the glassy state and the interference between local anisotropic motion and high power proton decoupling is also noted.

Solid-state phase behaviour and molecular level mixing phenomena in a strongly interacting poly(ethylene oxide) (PEO) and resorcinol mixture have been investigated through ^{13}C CP MAS-NMR and ^{1}H CRAMPS[94] experiments.[95] One-dimensional (1D) ^{1}H CRAMPS spectra of the polymer blend are shown in Fig. 48. The aromatic proton signal of resorcinol in the beta phase is 1 ppm to high frequency of its counterpart in the undiluted crystalline state of the small molecule. The hydroxyl proton signal of resorcinol in the weaker hydrogen-bonded phase beta is shifted slightly to low frequency relative to that characteristic of phase gamma. The above results are consistent with the FT IR results. These experiments provide substantial evidence that PEO and resorcinol in the molecular complex (phase beta) are intimately mixed on a molecular level. Order-of-magnitude estimates of interproton separations based on a spin-diffusion coefficient of 5×10^{-12} cm^2/s suggest that dipolar distances of 1, 10 and 100 Å should produce proton spin diffusion on a time scale of 20 μs, 2 ms and 200 ms, respectively. In this respect, ^{1}H CRAMPS spectra are capable of distinguishing between proton spin diffusion in intimately mixed and phase-separated blends. The duration of the mixing period necessary to detect spin diffusion depends on the solid-state morphology.

Figures 49 and 50 show the 2D proton spin-diffusion spectrum of the

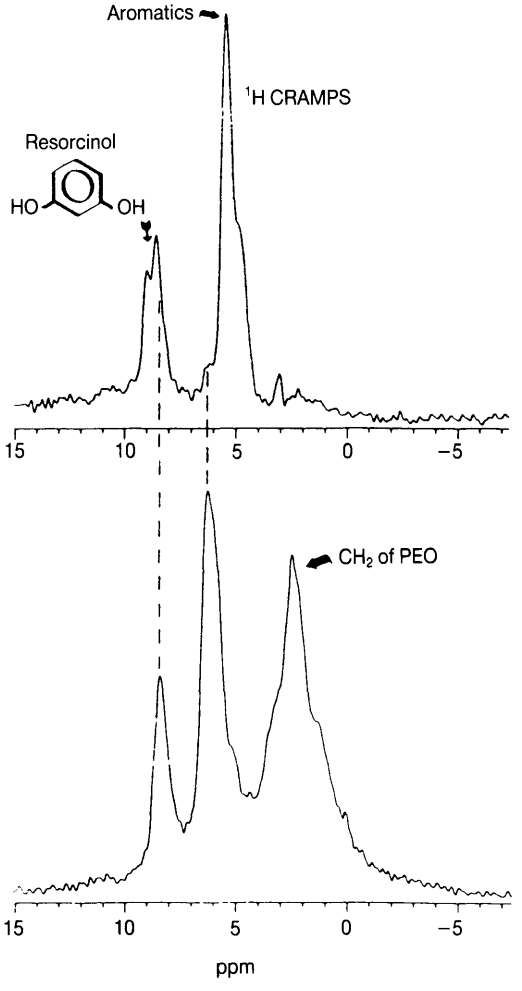

Fig. 48. ^{1}H CRAMPS spectra of undiluted crystalline resorcinol (upper spectrum) and the molecular complex of poly(ethylene oxide) and resorcinol (lower spectrum). The concentration of resorcinol in the molecular complex (phase beta) is 33 mol%.

PEO/resorcinol blend. This allows us to distinguish the signal contours of the methylene protons of PEO from the aromatic and hydroxyl proton signal contours of resorcinol. In these figures, the signal contours on the main diagonal from lower left to upper right are assigned, respectively, to the hydroxyl protons of resorcinol, the aromatic protons of resorcinol, and methylene protons of PEO. After 100 μs of proton dipolar interaction, spin diffusion between PEO and resorcinol can be observed in Fig. 49, through off-diagonal contours indicated by the arrows. This shows that proton

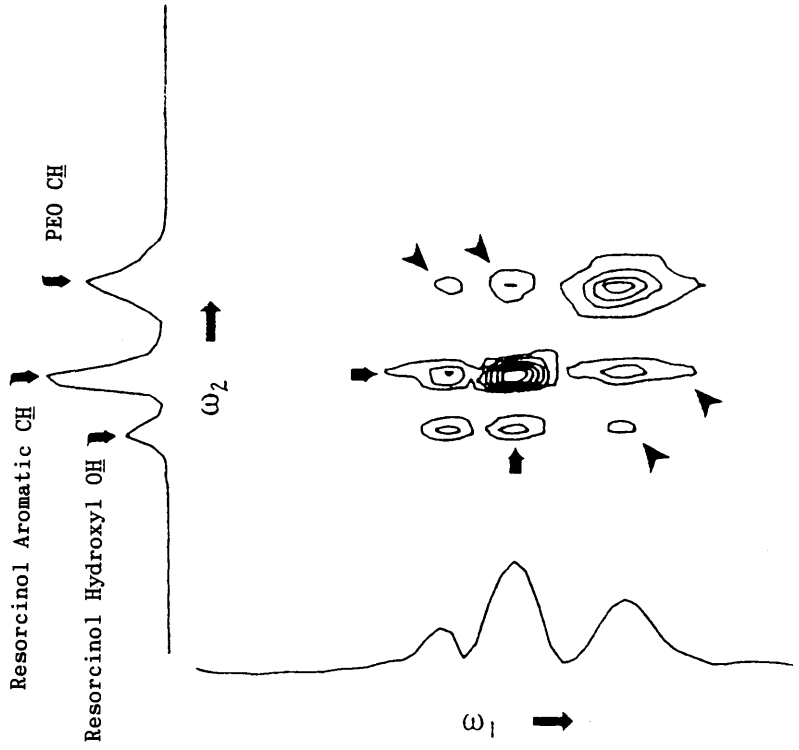

Fig. 49. 2D ^{1}H spin diffusion spectrum of the molecular complex of poly(ethylene oxide) and resorcinol. The mixing period persists for 200 μs in the presence of proton dipolar interactions. The horizontal and vertical arrows identify off-diagonal contours generated via proton dipolar communication (aromatic-hydroxyl) within the resorcinol molecule. The slanted arrows identify off-diagonal contours generated *via* intermolecular dipolar couplings between poly(ethylene oxide) and resorcinol.

magnetization transport between PEO and resorcinol in phase beta is operative on the 100 μs time scale, suggesting that intermolecular proton distances are in the range of 2–5 Å. Figure 49 shows that spin diffusion between PEO and resorcinol is absent when homonuclear ^{1}H dipole–dipole interactions are applied for 40 μs. Four of the six off-diagonal contours (Fig. 49) are absent in Fig. 50. Dipole–dipole couplings between the methylene protons of PEO and the hydroxyl protons of resorcinol, and the methylene protons of PEO and the aromatic CH protons of resorcinol do not produce off-diagonal contours in the 2D ^{1}H NMR experiment on a time scale of 40 μs. This is a consequence of dipolar couplings between protons that are separated by more than 2 Å.

Miscible blends of polybenzimidazole (PBI) with an aromatic polyimide

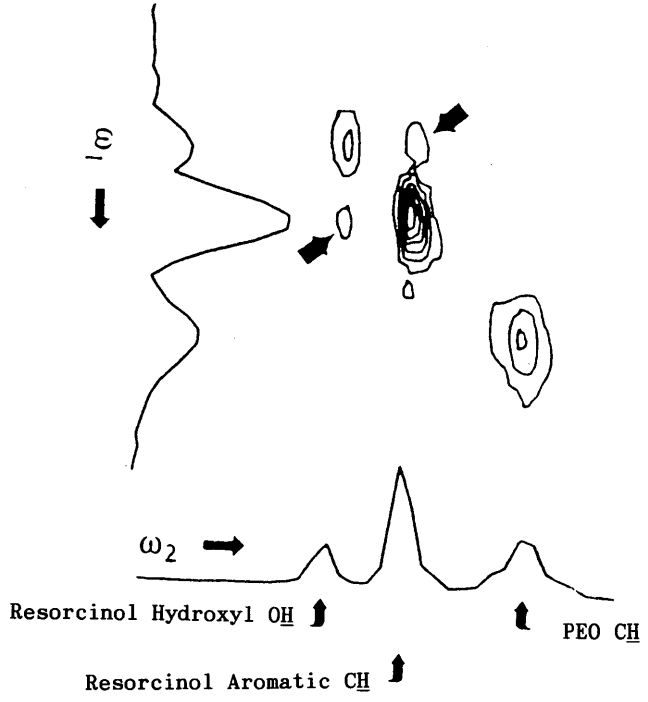

Fig. 50. 2D ^{1}H spin-diffusion spectrum of the molecular complex of poly(ethylene oxide) and resorcinol (phase beta). Dipolar couplings are exerted for 40 μs during the mixing period. Only the aromatic-hydroxyl off-diagonal proton contours, generated *via* dipolar communication within resorcinol, can be observed at this shorter spin-diffusion mixing time.

and a polyetherimide were investigated by ^{13}C CP MAS-NMR.[96] The ^{13}C CP MAS experiments show that specific hydrogen bonds exist between the phthalimide carbonyl of polyimide and the imidazolic amine bond of PBI. This evidence comes from a change in the carbonyl signal of polyimide. Addition of PBI broadens this signal, principally in the high frequency direction, and a high frequency carbonyl chemical shift shows the existence of a fraction of the carbonyl to amine hydrogen bonds. Further, miscibility in the blends has also been confirmed by a study of the proton rotating frame spin-lattice relaxation behaviour.

Charge-transfer interactions in polymer blends containing the electron donor (*N*-ethylcarbazol-3-yl)methyl methacrylate (NEC-MM) and the electron acceptor 2-[(3,5-dinitrobenzoyl)oxy]ethyl methacrylate (DNBEM) moieties were investigated by ^{13}C CP MAS-NMR and differential scanning calorimetry (DSC).[97] The number of inter- vs intramolecular charge-transfer interactions was varied by preparing blends of polydonor with acceptor, as

well as blends containing a homopolymer and an acceptor–donor copolymer. The blends were one phase for NECMM contents greater than 35 mol%. At lower donor contents, two phases with different amounts of charge transfer complexation were shown to exist.

NMR, via ^1H $T_{1\rho}$ and DSC, via T_g (glass transition temperature) indicate that charge-transfer interactions result in restricted mobility and reduced free volume and interatomic distances in the bulk polymer blends. Intermolecular charge-transfer complexes are decomplexed on heating above 185°C, and two phases, composed of only one blend component, are formed. A chemical shift observation by charge transfer suggests that the complex has an asymmetrical structure.

Phase behaviour of blend systems containing nitrile copolymers (acrylonitrile/methyl acrylate/butadiene terpolymer) (B210) with poly(ethylene-co-maleic anhydride) (PEMA) and poly(oxycarbonyloxyl-1,4-phenyleneisopropylylidene-1,4-phenylene) (PC) was investigated by ^{13}C CP MAS-NMR and DSC.[98] Spin-lattice relaxation times of the protons in the rotating frame for blends and pure components have been measured by monitoring the CP MAS generated carbon signal intensities as a function of a variable proton spin-lock time. Since single-component NMR relaxation behaviour was observed over the entire range of compositions, phase homogeneity was demonstrated for the B210/PEMA system. These monophase blends exhibit single-component rotating frame spin-lattice relaxation times, intermediate in value as compared to the pure components. The DSC examinations also show that B210/PEMA blends have a single composition-dependent glass transition temperature. In contrast, the CP MAS-NMR experiment of B21/PC blends shows that they display multicomponent relaxation behaviour indicating the presence of a mixed phase along with pure phases of each individual polymer.

The modulus and transition temperature of polymer materials can be controlled through the addition of low molecular weight diluents. From this point of view, diluent motion in a glassy blend such as a 50/50 blend of poly(phenylene oxide) (PXE) and PS plus a phosphate ester diluent, tetraxylyl hydroquinone diphosphate (HQDP), was investigated through 2D ^{31}P NMR.[99] 2D ^{31}P NMR spectra of the polymer blends are shown as a function of mixing time at 71 and 83°C (Fig. 51). The first static 2D spectrum (a) is measured at 71°C and a mixing time of 1 s, at which a mechanical loss peak is observed. The spectrum shows only intensity along the diagonal corresponding to the axially asymmetric chemical shift anisotropy line shape. The absence of off-diagonal peaks eliminates the presence of ^{31}P spin diffusion on this time scale. The 2D spectrum (e) at 83°C and a mixing time of 1 s, at which the dynamic mechanical spectrum shows an increased loss, shows significant diagonal peaks. This can arise from molecular reorientation with a time constant less than, or equal to, the mixing time of the pulse sequence. The rate and amplitude of the motion can be further character-

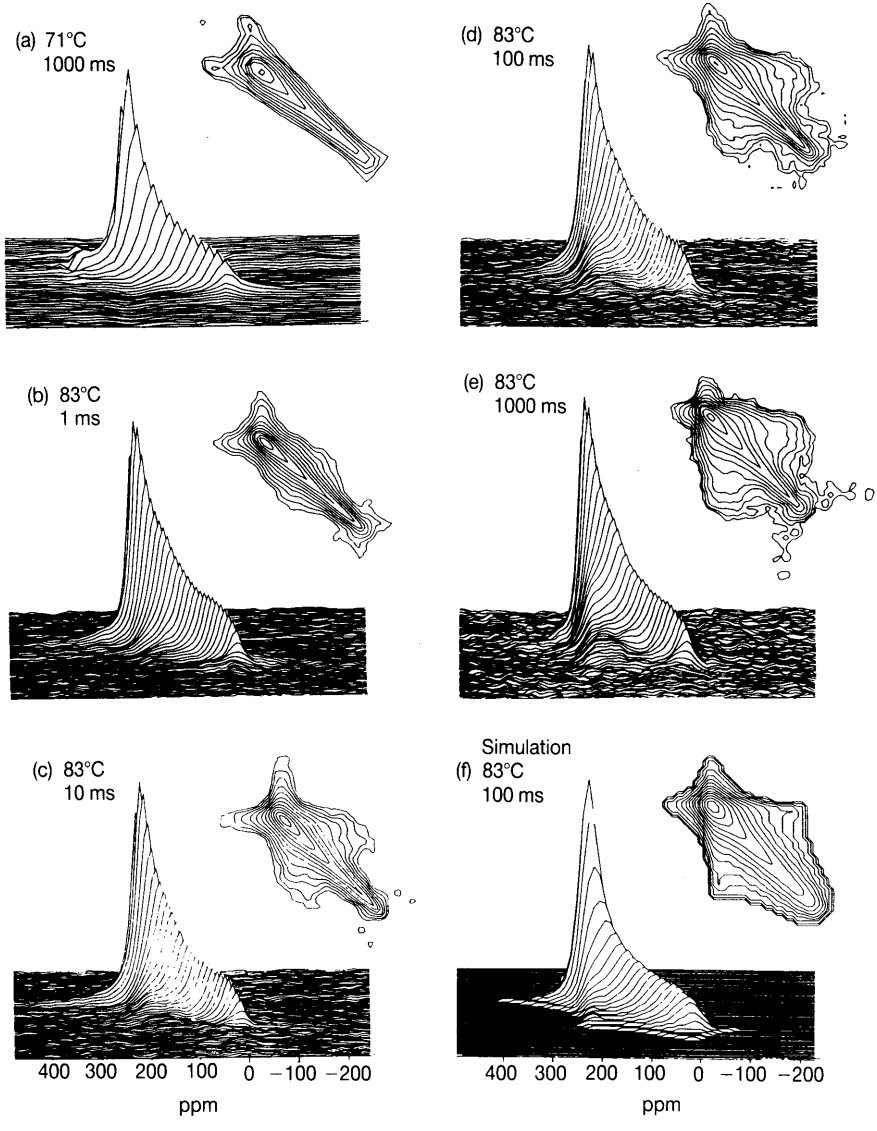

Fig. 51. (a) ^{31}P 2D line-shape pattern at 71°C and a mixing time 1 s. (b–e) 2D line-shape pattern at 83°C and mixing times of 1, 10, 100, 1000 ms. (f) Calculated 2D line-shape pattern for comparison with the pattern obtained at 83°C and a 100 ms mixing time.

ized by acquiring 2D patterns at several times, 1, 10, 100 and 1000 ms. From these spectral patterns a variety of specific descriptions of molecular motion may be presented.

Using the similar 2D ^{13}C NMR method, a blend of PS and ^{13}C-labelled poly(2,6-dimethylphenylene oxide) was investigated as a function of temperature, and mixing time, in the vicinity of the thermal glass transition.[100] Chain motion of the ^{13}C-labelled polymer on a ms time scale commenced at temperatures of approximately 10°C below the thermal glass transition, in contrast to a single-component polymeric glass which only shows such motion at temperatures above the glass transition.

The miscibility and separation of solution-cast blends of poly(vinylidene fluoride) (PVF2) and PMMA, with ageing, for a range of composition was examined by ^{13}C CP MAS-NMR.[101] One amorphous phase and intimate mixing of the polymer chains in this phase existed for all compositions of the blends, even after 2 months of ageing at room temperature as determined by the ^1H $T_{1\rho}$ and the T_{CH}. The ^1H $T_{1\rho}$ shows the presence of phases or domains in the amorphous component of the blend larger than approximately 19 Å. The T_{CH} values increase with ageing for all the carbons of PMMA. This shows that a subtle separation between polymer chains is occurring on the scale of 4–5 Å and that transfer of polarization is not as efficient with ageing.

A partially miscible blend of d-PMMA/solution chlorinated PE (d-PMMA/SCPE) has been examined through the CP time T_{CH} obtained by ^{13}C CP MAS-NMR.[102] The mean internuclear distance between SCPE protons and d-PMMA carbons was estimated by use of the T_{CH} data of the well-defined SCPE methylene carbon. Proton to carbon intramolecular T_{CP} values are proportional to r^6, where r is the internuclear distance, and also proportional to n^{-1}, where n is the number of protons attached to the carbon. Thus, the two protons on the SCPE methylene at a distance of 1.09 Å give rise to a T_{CH} of 25 μs. It is not possible to know how many SCPE protons are involved in interchain CP to the d-PMMA carbons, but an approximation can be made that on average four SCPE protons are near any one d-PMMA carbon. Therefore, the value obtained for T_{CP} of 11 ms for the d-PMMA methyl carbon is calculated to result from interactions with four protons ($n = 4$) at a mean distance of 3.4 Å.

The scale of miscibility of blend films of cellulose (CELL) with poly(vinyl alcohol) (PVA), polyacrylonitrile (PAN), poly(ε-caprolactane) (PCL) and nylon 6 was estimated by solid-state NMR relaxation measurements.[103] The miscibility of the synthetic polymers with CELL, as obtained from NMR relaxation measurements, follows the order PAN $\approx$ PVA > PCL > nylon 6. This order agrees well with one deduced from the comparison of the dynamic mechanical analysis of the different blends. By combining NMR and dynamic mechanical analysis results it is possible to estimate more precisely the domain size produced upon blending two polymers; hence,

blends can be looked at on a scale of 1 nm (CP MAS), 4 nm ($T_{1\rho}$), 15 nm (dynamic mechanical analysis), and 25–40 nm (T_1).

The elastomeric components of several tyre sections were examined by multiple-slice, three-dimensional ^{1}H NMR imaging at medium resolution (100–200 μm) and short echo times (0.5–2 ms).[104] The various rubber layers and cords were readily distinguished for a non-steel-belted tyre section at 200 μm resolution, presumably based on T_2 differences among the different components. ^{13}C MAS-NMR spectra of samples from each layer provided elastomer composition, which supported the origin of the intensity differences seen by NMR imaging. Experimental tyre tread sections with good and poor carbon black dispersions produced substantially different images at 150 μm in-plane resolution.

Hikichi *et al.*[105] have investigated the miscibility and domain structure of PVA/poly(vinylpyrrolidone) (PVP) blends through the ^{13}C CP MAS spectra and intermolecular cross-polarization. It was demonstrated that a hydrogen-bonding interaction between the two polymers occurs. The ^{1}H T_1 and $T_{1\rho}$ results show that the blends are miscible for all components on a scale of 200–300 Å. On a scale of 20–30 Å, however, the miscibility of the blends depends significantly on the composition. When the PVA composition is more than 46%, the blends are composed of two phases, an amorphous miscible phase of PVA and PVP and a pure PVA phase. The crystallinity of the PVA phase decreases rapidly with decreasing PVA composition. When the PVA composition is less than 46%, the blend is completely miscible. The composition of the PVA phase in the blends was inferred from the results of ^{1}H $T_{1\rho}$. Further, they have investigated the miscibility of PVA/poly(methacrylic acid),[106] PVA/poly(acrylic acid),[107] polycarbonate/PMMA[108] and poly(vinyl phenol)/poly(methyl acrylate)[109] blends using similar methods.

Spevacek *et al.*[110] have investigated the mechanism of stereocomplex formation for a mixture of isotactic and syndiotactic PMMAs by ^{13}C CP MAS-NMR.

4. NATURAL POLYMERS

To clarify the structures and functions of proteins is very important for understanding life processes and provides an index with respect to the design of artificial biomaterials. Therefore, new methods, which can exactly determine the protein structure, have been urgently required. Solid-state NMR is a powerful tool for the determination of protein structure and satisfies this requirement. The advantages of this method have been described in many monographs and reviews.[111–119] In this section, through recent studies on fibrous, membrane, globular, and conjugated proteins, we

show that the solid-state NMR methods are useful for the structural analysis of proteins.

4.1. Fibrous proteins

Since fibrous proteins generally have periodical amino acid sequence and higher-order structure, the clarification of their fine structure in the solid state becomes very important not only when discussing the physical and chemical properties, but when obtaining information about the molecular design of synthetic polypeptides. Actually, the comparison of some fibrous proteins and their model synthetic polypeptides has been carried out. The conformation-dependent ^{13}C CP MAS-NMR chemical shifts[120–141] are particularly useful for the determination of the conformational features of fibrous proteins.

Because silk fibroin is one of the fibrous proteins having a simple amino acid composition and the isotopic enrichment can be easily performed, the peak assignments of its NMR spectra are almost accomplished[142–146] and more detailed analyses for static or dynamic structures have been made by solid-state NMR.[113,147–156] Amino acid composition of silk fibroin varies with the species of silkworms. In fact, fibroin from *Phylosamia cynthia ricini* contains alanine (Ala) (48.4%), glycine (Gly) (32.2%), serine (Ser) (5.5%), and tyrosine (Tyr) (4.5%), while fibroin from *Bombyx mori* contains Gly (42.9%), Ala (30.0%), Ser (12.2%), and Tyr (4.8%).[157] In reflecting the higher Ala content of *P.c. ricini* fibroin it is shown that the ^{13}C NMR chemical shifts of the Ala residues of a dried sample, taken from the silk gland of *P.c. ricini*, are identical to those of the α-helical $(Ala)_n$. By contrast, the cocoon of *P.c. ricini* is found to have the anti-parallel β-sheet form, as determined from the ^{13}C NMR chemical shift of the Ala and Ser residues. On the other hand, the ^{13}C peaks of the Ala and Gly residues of the silk II form of *Bombyx mori* silk fibroin are in good agreement with those of $(Ala\text{-}Gly)_n$ II as well as $(Gly)_n$ II and $(Ala)_n$ of the β-sheet form. The ^{13}C NMR chemical shifts of samples taking the silk I form are significantly displaced from those of the silk II form. Models for the silk I structure of *B. mori* silk fibroin have been proposed on the basis of ^{13}C NMR data, X-ray diffraction data, and conformational energy calculations.[158] Recently, on the basis of this information the solvent- and mechanical-treatment-induced conformational transitions of silk fibroins were studied by means of ^{13}C CP MAS-NMR.[152] In addition, the dynamic features of side chains of silk fibroins in the solid state were also studied by ^{2}H NMR and ^{13}C CP MAS methods.[150,151] For the Ser residue of *B. mori* silk fibroin, especially, it was suggested that the hydroxyl groups might be hydrogen-bonded to the C=O or NH groups in intra- or interchain bonding. Most recently, ^{15}N solid-state NMR techniques were applied to elucidate the

atomic resolution details of the silk II conformation of silk fibroins.[154,155] The ^{15}N NMR chemical shift tensors of the sites, [^{15}N]Gly, [^{15}N]Ala, and [^{15}N]Tyr were determined for the ^{15}N-labelled powder samples. ^{15}N CP NMR spectra of the oriented silk fibroin block were observed by setting it parallel and perpendicular with respect to the applied magnetic field. The static spectra were simulated with ^{15}N chemical shift tensors as functions of several Euler angles and distribution of fibre axis (Fig. 52). Then, the torsion angles (ϕ, ψ) of the site-specific amino acid residues of silk fibroins were determined (Table 9), using the results of a ^{13}C–^{15}N double-labelled model compound.

Collagen has a rod-like shape, a dimension of about 3000×15 Å and is composed of a triple-stranded helix which is assembled into cylindrical fibrils having a diameter of 50–2000 Å.[159] The individual triple chains are composed of a repeating pattern $(Gly\text{-}X\text{-}Y)_n$, where X and Y are frequently occupied by proline (Pro) and hydroxyproline (Hyp) residues, respectively. Torchia *et al.* have reported substantial works on the molecular dynamics of collagens by means of multinuclear solid-state NMR spectroscopy, using isotopically labelled samples which were obtained by cultivation techniques.[111,160–175] Fujiwara and Kuboi have reported the ^{13}C and ^{31}P CP MAS-NMR spectra of dentin collagen.[176] Saito *et al.* have found that most of the ^{13}C signals of collagen fibrils from bovine tendon and skin are in good agreement with those of $(Pro\text{-}Gly\text{-}Pro)_n$, although some peaks of collagen are slightly displaced from those of the model polypeptides.[177] Most recently, they attempted to assign all of the ^{13}C CP MAS-NMR peaks of collagen fibrils on the basis of computer simulation by utilizing amino acid composition and chemical shift data from both the solid state and solution, and confirmed that some unassigned peaks were not ascribable to a denatured portion but to the minor amino acid residues.[178] Furthermore, they found that the ^{13}C spin-lattice relaxation times (T_1) of both the C_β and C_γ carbons of Pro and Hyp in fibrils are substantially reduced as compared with those of some crystalline oligopeptides. It was shown that the presence of rapid ring puckering motion in these residues results in a reduction of the NT_1 values, where N stands for the number of protons attached to the carbon under consideration. The ^{13}C CP MAS-NMR signals of the soluble collagens in the anhydrous state are generally broader than those of the insoluble collagen and they are substantially narrowed upon hydration (Fig. 53). In particular, it is noteworthy that the carbonyl signal is split into an asymmetrical doublet or three signals upon hydration, which can be considered as characteristic of the presence of the native collagen structure. Collagens with various degrees of cross-linking were also studied by high-resolution liquid and solid-state ^{13}C NMR methods, especially by means of relaxation time measurements.[179]

^{13}C CP MAS-NMR spectra of tropomyosin, one of muscle proteins, were measured in the solid state, in order to elucidate the higher-order structure

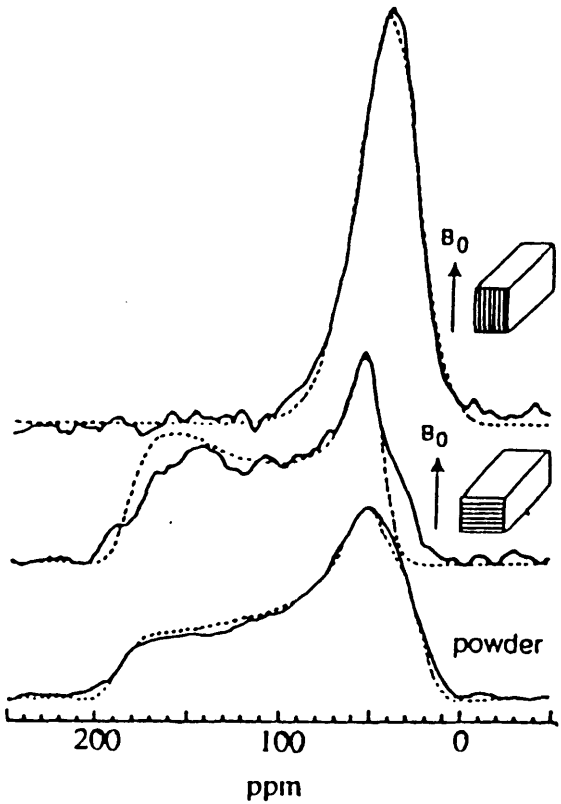

Fig. 52. ^{15}N solid-state NMR spectra of [^{15}N]Gly-labelled silk fibroin. Solid line: observed; broken line: calculated.

Table 9. ^{15}N chemical shift tensors, Euler angles and torsion angles of *B. mori* silk fibroin.

	Gly	Ala	Tyr
Chemical shift tensors (ppm)			
σ_{11}	22	33	32
σ_{22}	54	56	54
σ_{33}	186	200	194
Euler angles (deg)			
α_F	24 ± 10	2 ± 10	22 ± 10
β_F	72 ± 2	70 ± 2	72 ± 2
Torsion angles (deg)			
ϕ	-141 ± 5	-139 ± 5	-139 ± 5
ψ	147 ± 5	146 ± 5	147 ± 5

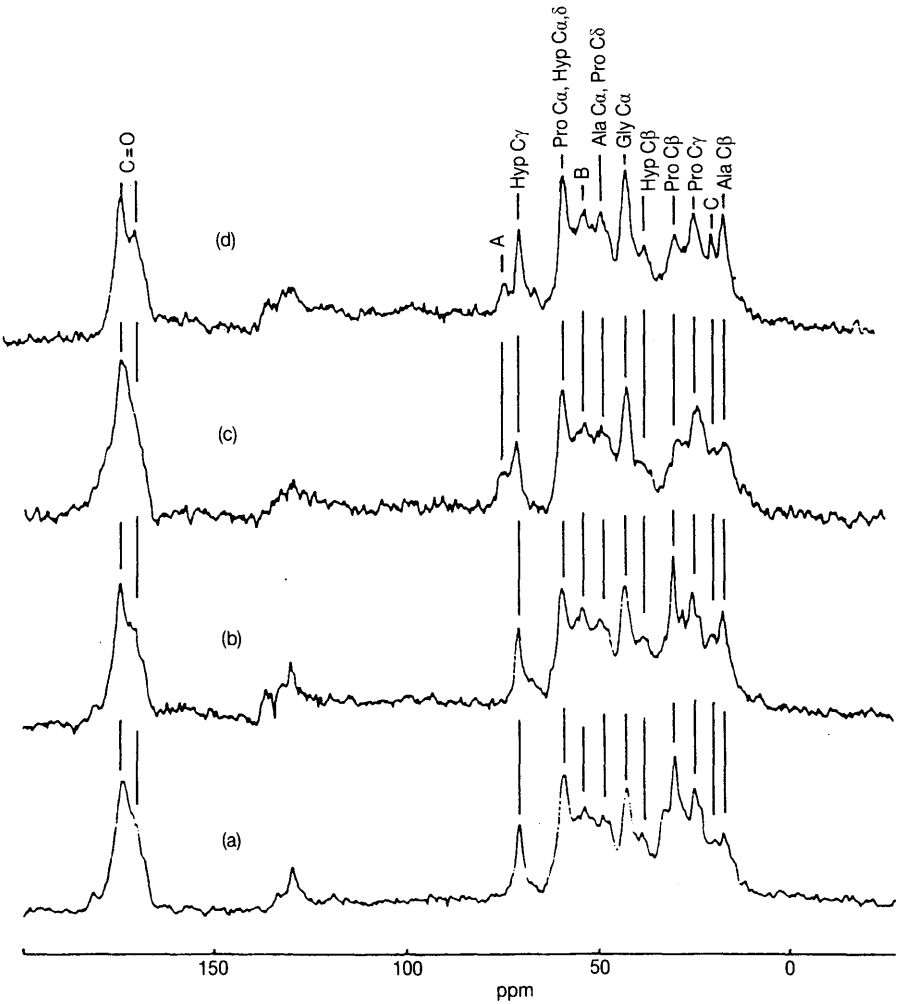

Fig. 53. 75.46 MHz ^{13}C CP MAS-TOSS-NMR spectra of insoluble bovine tendon (sigma) collagen (A and B) and acid-soluble collagen from calf skin (C and D). A and C, anhydrous sample; B and D, hydrated sample after humidification in a desiccator at 96% RH for 12 h.

of the protein through the observation of the ^{13}C NMR chemical shifts of the amino acid residues and their mobility.[180–182] The higher-order structure of tropomyosin is a right-handed α-helix coiled-coil structure, which contains two different sites, which are characterized as the internal hydrophobic site and the external hydrophilic site (Fig. 54A).[183] A typical ^{13}C CP MAS-NMR spectrum for tropomyosin in the solid state is shown in Fig. 54B. Since the Ala residue is one of the major components, the ^{13}C

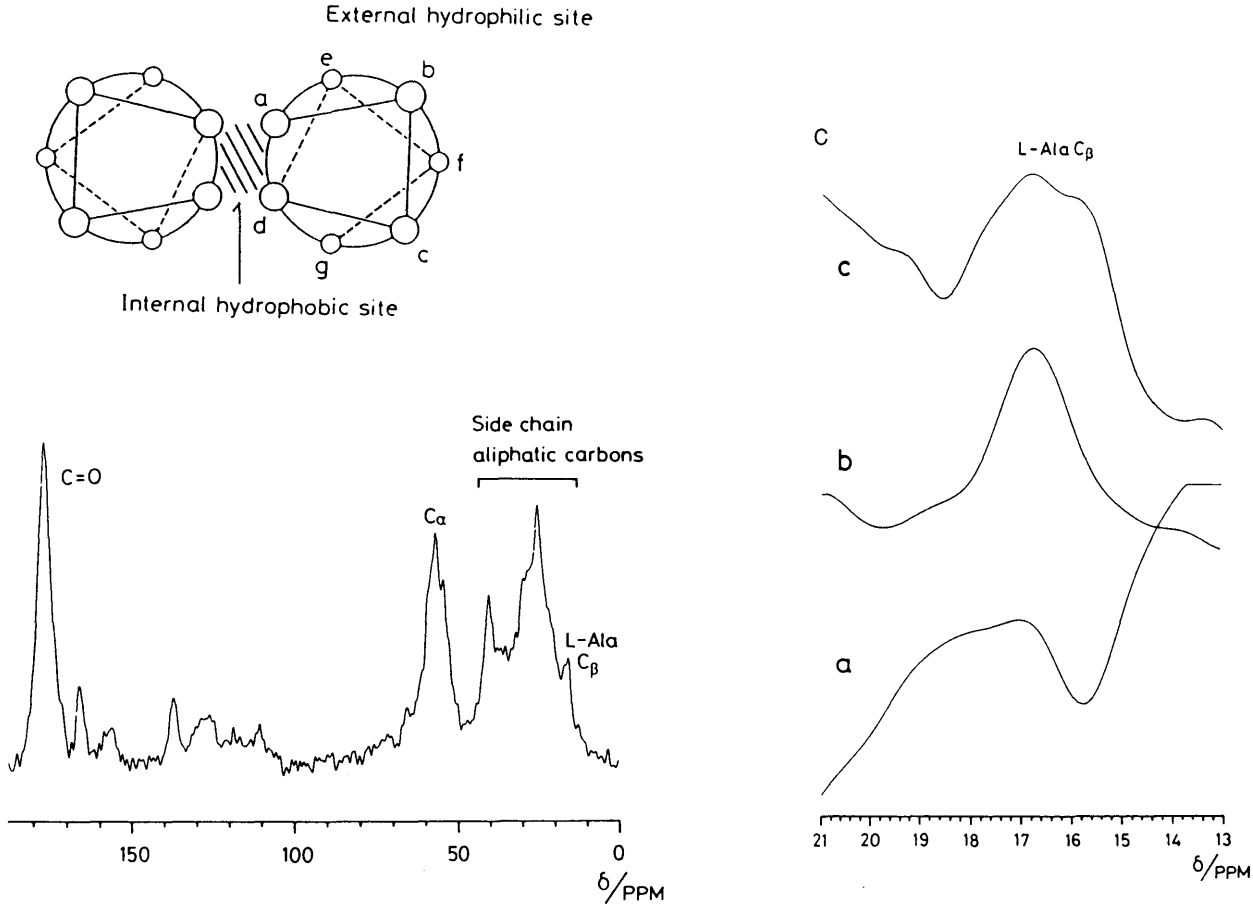

Fig. 54. (A) A schematic picture of the cross-section of the coiled-coil structure in tropomyosin. (B) The typical ^{13}C CP MAS-NMR spectrum of tropomyosin at room temperature. (C) The expanded ^{13}C NMR spectra of the Ala C_β carbon atoms of tropomyosin, measured using the inversion-recovery method at room temperature. Recovery time, t,: (a) 10 ms; (b) 500 ms; (c) 3500 ms.

signal which appears at 15–17 ppm can be easily assigned to the Ala C_β carbons, and it can be seen that this signal consists of two peaks. Figure 54C shows the expanded Ala C_β signal, measured using the inversion–recovery method. From these spectra, there are at least two kinds of Ala C_β carbons. Further, the carbons contributing to the peak at 15.8 ppm have a longer T_1 value than those at 16.7 ppm. This indicates that the former carbons are more mobile than the latter carbons, because the Ala C_β carbons in tropomyosin have correlation times with values appearing in an extremely narrow region at toom temperature. The distance between the two α-helical axes in the coiled-coil structure is shorter than the coiled-coil helicles which are packed in parallel in native muscle from X-ray studies.[184] Therefore, it can be said that the mobility of the Ala C_β carbons in the internal site is expected to be more restricted than that in the external site. From such a situation, the two peaks at 15.8 and 16.7 ppm are assigned to the Ala C_β carbons in the external and internal sites of the coiled-coil structure, respectively.

On the other hand, high-resolution solid-state ^{13}C NMR studies of wool keratin proteins have been systematically carried out.[185–189] The native wool fibre consists of intermediate filaments (termed "microfibrils") composed of low-sulphur proteins which are embedded in a non-filamentous matrix. The non-filamentous matrix usually contains two classes of proteins; one is a high-sulphur protein and the other is a protein containing Gly and Tyr residues.[190] Wool keratin can be divided into three main fractions after reducing disulphide bonds and protection of the resulting thiol groups with iodoacetic acid to form *S*-carboxymethyl kerateine (SCMK).[191,192] The ^{13}C CP MAS-TOSS-NMR spectra of wool and four kinds of SCMKs extracted from wool [low-sulphur fractions (SCMKA), helix-rich fragments (SCMKA-hf), high-sulphur fractions (SCMKB), and high-Gly-Tyr fractions (HGT)] in the solid state are shown in Fig. 55, and the observed ^{13}C chemical shift values in these samples are summarized in Table 10 together with the assignments which are made using their amino acid compositions and the ^{13}C chemical shift data[120–141] with respect to homopolypeptides in the solid state. For characterization of the main chain conformation of polypeptides and proteins in the solid state, it is very useful to use the ^{13}C chemical shift value of the main chain carbonyl carbon, because it is strongly influenced by the conformation of the main chain but not by varieties of amino acids and/or a specific amino acid sequence.[120,121] Therefore, it can be said that the line shape of the ^{13}C signals in the carbonyl region for proteins is varied with the conformations. The carbonyl ^{13}C signal can be decomposed to four peaks by computer-fitting (Fig. 56) and the results for the main chain carbonyl carbons are summarized in Table 11. The relative intensity of the high frequency peak at ca. 176 ppm corresponds to the proportions of the α-helix component because this peak comes from the main chain carbonyl carbons in the α-helix form. The proportion of the α-helix component

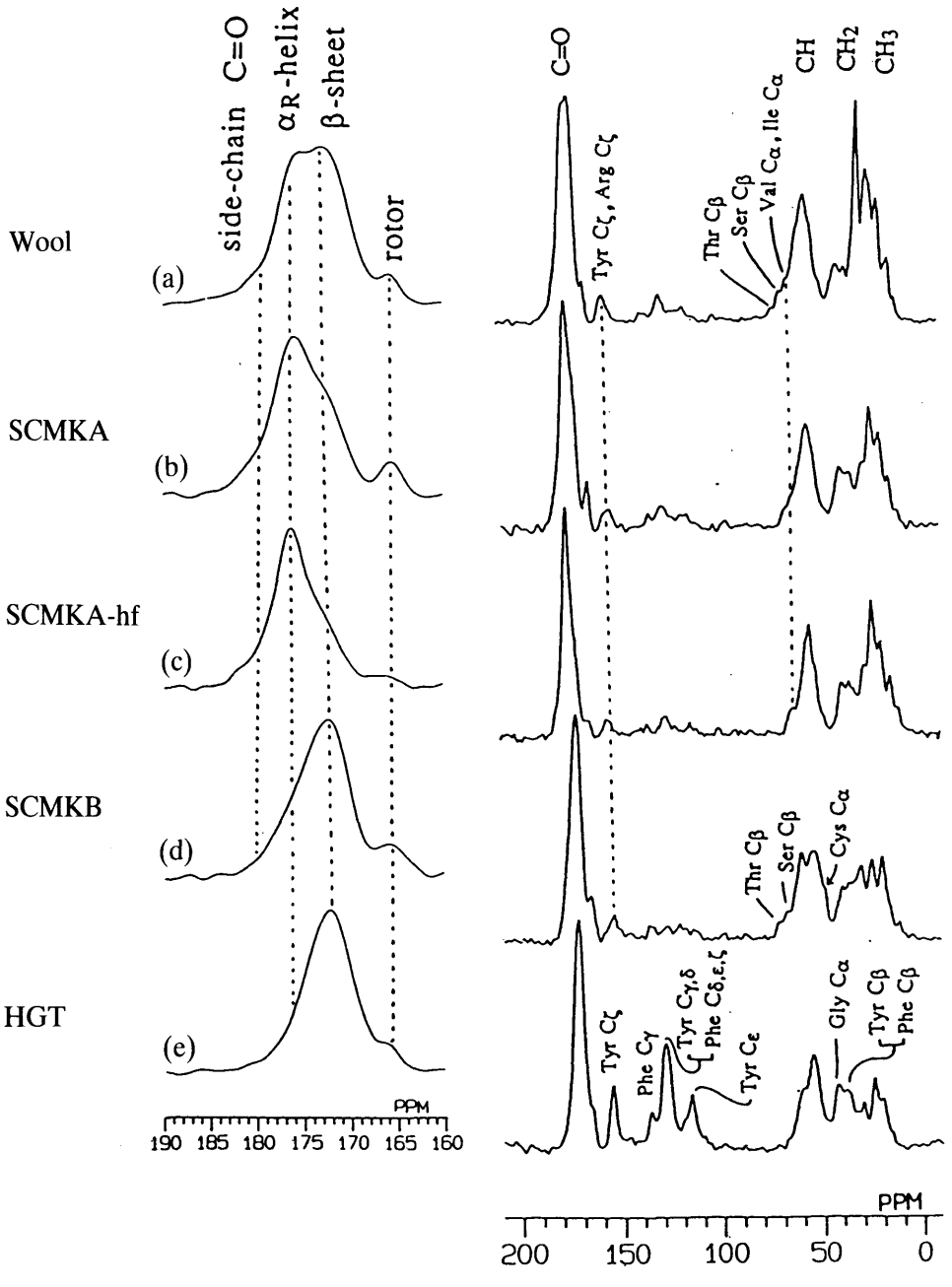

Fig. 55. ^{13}C CP MAS-TOSS-NMR spectra of (a) wool, (b) SCMKA, (c) SCMKA-hf, (d) SCMKB, and (e) HGT and their expanded spectra for the carbonyl carbon region.

Table 10. Observed ^{13}C NMR chemical shifts for wool, SCMKA, SCMKA-hf, SCMKB, and HGT in the solid state.

Chemical shifts[a] (ppm)					
Wool	SCMKA	SCMKA-hf	SCMKB	HGT	Assignment[b]
175.3	176.0	176.3			Carbonyl carbons (αh)
173.2			172.8	172.3	Carbonyl carbons (βs)
156.2	155.1	157.2	154.8	156.0 (156.4)	Tyr C_ζ and Arg C_ζ
				136.9 (137.3)	Phe C_γ
128.5	129.1	128.2		128.9 (128.9)	Phe $C_{\delta,\varepsilon,\zeta}$ and Tyr C_γ
				116.3	Tyr C_ε
72.2			71.8		Thr C_β (βs)
68.6			67.8		Ser C_β (βs)
65.2	[c]	64.4			Val C_α and Ile C_α (αh)
			60.6		Thr C_α (βs) and Pro C_α
				60.2	[d]
56.6	56.9	56.4	54.8	54.6	C_α methine carbons
				42.5	Gly C_α
40.5	40.3	40.3	40.1		[d]
				38.4	Tyr C_β and Phe C_β
36.3	35.6	36.7	36.6		[d]
30.1 (30.0)					Mainly CH_2 in lipid
	28.8	28.9	30.8	30.2	[d]
25.4	25.0	25.2	25.4	24.6	[d]
(23.1)	[c]	(23.7)		(23.1)	Leu C_δ
20.3 (20.3)	20.7 (20.9)	21.0 (21.1)		20.6 (20.8)	Mainly Val C_γ
			20.3 (20.7)		Mainly Thr C_γ (βs)
[c] (16.5)	16.2 (16.5)	16.1 (16.5)	[c]		Mainly Ala C_β (αh)
14.9 (14.8)					Mainly Ile $C_{\gamma'}$
11.9 (11.7)	12.1	12.4 (11.9)	12.1		Ile C_δ

[a]The numbers in the parentheses are chemical shifts of the peaks observed in ^{13}C CP MAS-DDph spectra.

[b]The assignment was made by reference data of homopolypeptides in the solid state (refs 120–136). αh and βs in the parentheses mean the α_R-helix and β-sheet forms, respectively.

[c]Observed as the shoulder peak.

[d]Unassigned at this stage.

increases in the order of wool, SCMKA and SCMKA-hf. On the other hand, the low frequency peak at 172 ppm comes appreciably from the main chain carbonyl carbons in the β-sheet form. From the conformational characterization on the basis of the above assignment, it can be said that the β-sheet form is rich in SCMKB and HGT. These findings are also confirmed from the peaks in other carbon regions. Further, it is suggested that the coiled-coil structure exists in wool, SCMKA, and SCMKA-hf, because the ^{13}C chemical shift values of the Ala C_β carbons in these samples coincide in experimental error with that of the Ala residue located in the internal site of the coiled-coil structure in tropomyosin (Table 11). This conformational

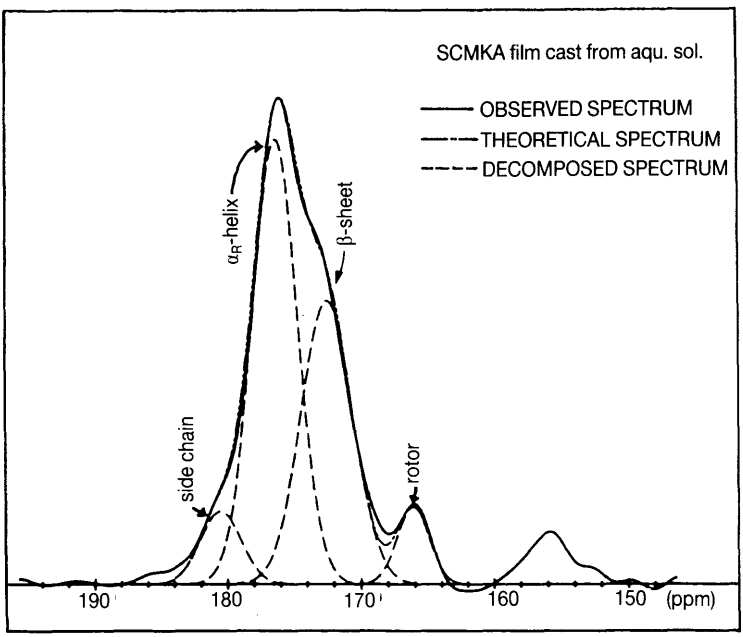

Fig. 56. ^{13}C NMR spectra for the carbonyl carbon region in SCMKA deconvoluted by computer fitting with Gaussian functions. The minor peak appearing at about 166 ppm comes from the NMR rotor.

Table 11. Observed ^{13}C NMR chemical shifts, half widths, and relative peak intensities of the main chain carbonyl carbons in wool, SCMKA, SCMKA-hf, SCMKB, and HGT.[a]

	^{13}C chemical shift (ppm)	Half width (ppm)	Relative peak intensity (%)
Wool	176.3	4.0	42
	172.2	4.8	58
SCMKA	176.2	4.0	56
	172.5	4.8	44
SCMKA-hf	176.4	3.6	65
	173.0	4.5	35
SCMKB	176.0	3.7	25
	172.5	4.6	75
HGT	176.6	4.0	8
	172.2	5.6	92

[a]Determined by computer fitting.

analysis, using the conformation-dependent ^{13}C CP MAS-NMR chemical shifts, has been applied to estimate the conformational transition of SCMKA by stretching, heating, or steam-treating.[186–189] The β-sheet form appears and the proportion of the α-helix form decreases upon stretching and steam-treating. For the SCMKA heated at 200°C for 3 h *in vacuo*, the ^{13}C MAS-NMR spectrum shows that each peak is broader than those of other treated specimens. This indicates the existence of various conformations and/or different microenvironments in the heated SCMKA. Thus, it can be said that the random coil form appears by heating. From the X-ray diffraction, the α-helix form completely vanishes in the SCMKA heated under the same conditions.[193] The result obtained by ^{13}C CP MAS-NMR spectroscopy, however, indicates that the α-helix form remains to an appreciable extent in the heated sample, although the random coil form also appears. The difference between the results from X-ray diffraction and NMR spectroscopy suggests that only the packing of the ordered structure (the α-helix form) in the SCMKA is disrupted by heating, but that the secondary structure is retained. On the other hand, in the case of the structural transition for the same protein, the change of the line shape for the C_α methine carbons can be mainly attributed to the conformational change. Figure 57 shows the observed and simulated ^{13}C CP MAS-NMR spectra for the C_α methine carbon region in SCMKA films. Spectrum simulation was performed by taking into account the experimental fact that the ^{13}C chemical shift value of the C_α methine carbon is influenced by both the main chain conformation and the variety of amino acid residues in contrast to the ^{13}C chemical shift behaviour of the carbonyl carbons.[120,121] As shown in Fig. 57, there is a tendency for the intensity of the peak appearing at about 52–53 ppm to increase as the stretching ratio is increased. This can be interpreted by means of the conformation dependence of the ^{13}C chemical shifts.

^{13}C CP MAS-NMR spectra of horse hoof, horse hair, parrot feather, and human hair were reported by Kricheldorf and Muller.[194] The dynamics and structure of mouse keratin intermediate filaments were investigated by solid-state ^{13}C and ^{2}H NMR spectroscopy, using isotopically labelled samples.[195]

4.2. Membrane proteins

The structural and dynamic analyses of membrane proteins are well carried out by solid-state NMR. The reasons are as follows: first, biological membranes greatly restrict the motion of embedded proteins and consequently are difficult to study by solution NMR methods. Second, only a few membrane proteins have been crystallized and studied by X-ray diffraction methods. Third, if the membrane protein is uniaxially oriented in the lipid,

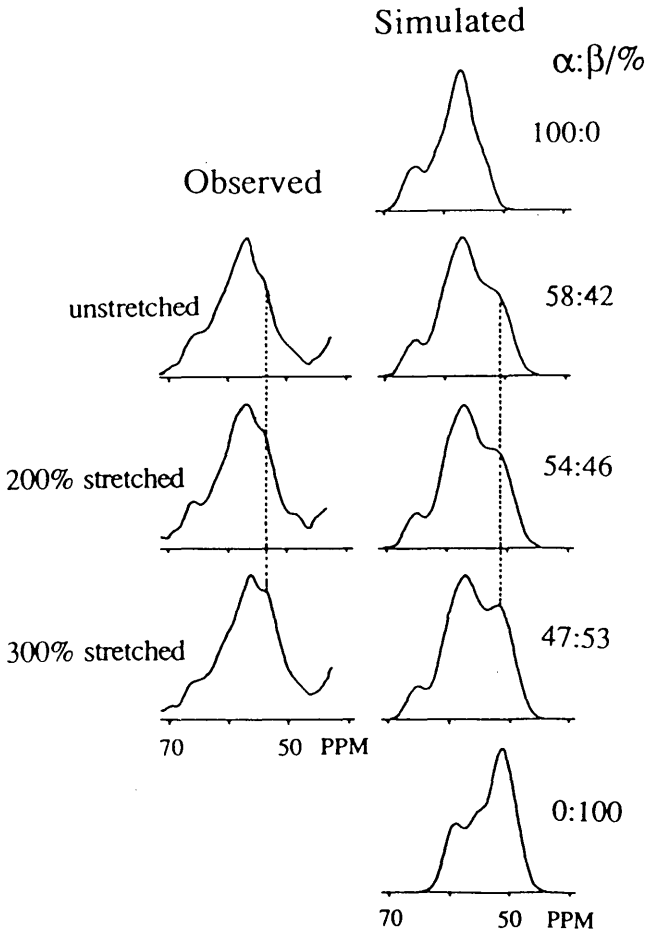

Fig. 57. Observed and simulated ^{13}C CP MAS-NMR spectra for the C_α methine carbon region in SCMKA films prepared from an aqueous solution. The Gaussian function for a peak with half width 3.5 ppm is assumed, and the chemical shift positions of the amino acid residues constituting SCMKA determined from reference data of homopolypeptides are used. Further, the corresponding peak heights are estimated from the amino acid composition of SCMKA. Under these assumptions, the spectrum simulation is carried out as follows: at first, two reference spectra are simulated, one for the case in which all the amino acid residues take the α-helix form, and the other for the case in which all the amino acid residues take the β-sheet form. Next, using the two reference spectra, some spectra with a given specified ratio of the α-helix to β-sheet form content are simulated, where this ratio is determined from the carbonyl carbon signal (see Fig. 55).

there is the advantage of being able to determine the structure at the atomic level by NMR as well as by X-ray crystallography. Fourth, since phospholipids in many cases coexist, the NMR method is still suitable because of its ability to observe selectively by means of isotopic labelling, multinuclear NMR, and by utilizing the differences of relaxation times. Therefore, phospholipids are well studied by solid-state NMR methods including ^{31}P NMR.[196,197]

Gramicidin A (GA) is a pentadecapeptide consisting of 15 alternating L- and D-amino acids and has the following chemical formula:[198]

$$\text{HCO-L-Val}_1\text{-Gly}_2\text{-L-Ala}_3\text{-D-Leu}_4\text{-L-Ala}_5\text{-D-Val}_6\text{-L-Val}_7\text{-D-Val}_8\text{-L-Trp}_9\text{-}$$
$$\text{D-Leu}_{10}\text{-L-Trp}_{11}\text{-D-Leu}_{12}\text{-L-Trp}_{13}\text{-D-Leu}_{14}\text{-L-Trp}_{15}\text{-NHCH}_2\text{CH}_2\text{OH}$$

This sequence allows the peptide to fold into a unique secondary structure, the β-helix. When GA is incorporated into a lipid environment, it forms a helical channel that transports monovalent cations. On the basis of a variety of spectroscopic data and model building, a structure has been proposed for the channel conformation that is an amino terminus to amino terminus dimer (the head-to-head dimer of single helices).[199] This structure has been confirmed by solid-state NMR methods.[200–212] Until recently, it was generally accepted that the sense of the helix was left-handed.[199,213] However, it has now been shown by solid-state NMR studies that in a fully hydrated lipid environment the helix is right-handed.[206,207,212]

^{13}C CP MAS spectra of ^{13}C-labelled GA were measured to determine directly the structure of this peptide in a lipid membrane.[200–202] The seven GA analogs, each labelled in a single carbonyl group of Gly_2, L-Ala_3, D-Leu_4, L-Val_7, D-Leu_{10}, D-Leu_{12}, or D-Leu_{14} were synthesized by the solid-phase method. These ^{13}C-labelled GAs were incorporated into aligned multilayers of dimyristoylphosphatidylcholine (DMPC) or diether lipid bearing 14- or 16-carbon chains, at a 1:15 peptide:lipid molar ratio. ^{13}C CP NMR spectra were obtained at several temperatures and over a range of sample orientations with respect to the spectrometer magnetic field. The results are summarized in Table 12. The observed chemical shielding anisotropies indicate that all of the labelled carbonyl bonds are oriented almost parallel to the molecular long axis and perpendicular to the lipid bilayer plane. These orientations are consistent with GA forming a β 6.3 single-strand helix that is oriented parallel to the methylene chains of the lipid molecules. Comparison of the line widths from labelled residues that are in the innermost turn of the helix (Gly_2, L-Ala_3, and D-Leu_4), in the centre of the molecule (L-Val_7), and in the turn nearest the lipid bilayer surface (D-Leu_{10}, D-Leu_{12}, and D-Leu_{14}) suggests that although the peptide behaves largely as a right-handed barrel, segments of the peptide close to the membrane surface possess greater motional freedom.

Table 12. Reduced chemical shift anisotropies (CSA) and line widths from the labelled carbonyl sites in gramicidin A analogues, and CSAs for lipid carbonyl and methylene resonances.

Label position	Lipid	Gramicidin CSA (ppm)	Gramicidin line width (Hz)	Lipid CSAs	
				Carbonyl	Methylene
Gly^2	DMPC DTPC DMPC	11 ± 2	800 ± 100	27 ± 1	17 ± 1
Ala^3	DTPC DHPC	16 ± 1	800 ± 100	28 ± 1	15 ± 1
D-Leu^4	DMPC	12 ± 2	800 ± 100	25 ± 1	14 ± 1
Val^7	DMPC	16 ± 1	800 ± 100	30 ± 1	15 ± 1
D-Leu^{10}	DMPC DHPC	9 ± 2	400 ± 70	25 ± 1	16 ± 1
D-Leu^{12}	DMPC	11 ± 1	400 ± 70	25 ± 1	16 ± 1
D-Leu^{14}	DMPC DHPC	13 ± 1	400 ± 70	27 ± 1	14 ± 1

Measurements were performed on samples containing a 1:15 peptide/lipid molar ratio at 307 K in DMPC and DTPC, and at 325 K in DHPC.

Recently, an analytical method for the determination of torsion angles of the GA backbone from solid-state ^{15}N NMR spectroscopic data has been demonstrated.[204–210] Advantage is taken of the ^{15}N–^{1}H and ^{15}N–^{13}C dipolar interactions as well as the ^{15}N chemical shift interaction in the oriented samples. The torsion angles for the L-Ala_3 site are determined by obtaining the NMR data for both the Gly_2-L-Ala_3 and L-Ala_3-D-Leu_4 peptide

Fig. 58. Method for simulation of spectra obtained from oriented samples at temperatures below the phase transition. (a) The PAS (σ_{11}, σ_{22}, σ_{33}) representation of the ^{15}N chemical shift tensor is known in the defined initial position ($\phi = 0$) with respect to the laboratory reference frame (X, Y, Z). The axis of local motion, e, is fixed relative to both frames of reference. The line defined by the intersection of planes Σ and Ω is placed coincident with Y, where Σ is the $\boldsymbol{\sigma}_{11}\boldsymbol{\sigma}_{33}$ plane and Ω is the plane perpendicular to e and passing through the origin. Since the chosen position in the XY plane is arbitrary in the NMR experiment, when $\boldsymbol{B}_0$ is the Z_{1ab} direction, subsequent rotation of the PAS through θ about e results in a new orientation that can be fully described by ϕ, the angle between e and the XY plane, and θ. (b) Continuous line: as the PAS is rotated about e, the Z-component of the chemical shift tensor, σ_{obs}, is plotted as a function of θ. Dotted line: a Gaussian probability distribution is assumed, characterized by the mean orientation, θ, and the amplitude, δ (half width at half height). (c) The chemical shift spectrum resulting from applying the assumed probability distribution to the calculated trajectory of the chemical shift is shown.

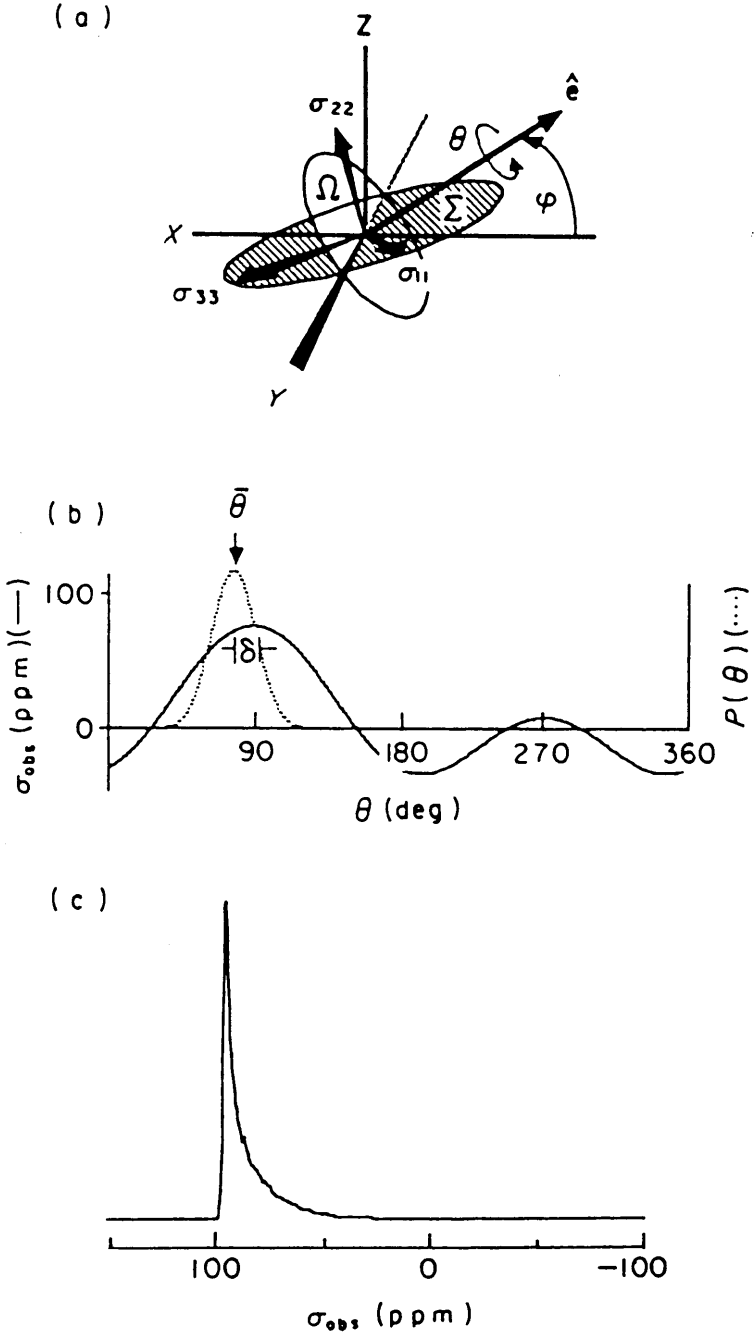
(a)
Z
σ_{22}
$\hat{e}$
θ
Ω
Σ
φ
X
σ_{11}
σ_{33}
Y
(b)
$\bar{\theta}$
100
$\Delta\delta$
0
90
180
270
360
σ_{obs} (ppm)(—)
$P(\theta)$(····)
θ (deg)
(c)
100
0
−100
σ_{obs} (ppm)

linkages.[208] Two possible sets of torsion angles for the L-Ala_3 site are obtained ($\phi, \psi = -129°$, 153° and $-129°$, 122°), both of which are consistent with a right-handed α-helix. In addition, the dynamics of the backbone of GA in DMPC bilayers have been investigated using solid-state ^{15}N NMR.[209] ^{15}N CP NMR spectra of single-site ^{15}N-labelled GA at 8°C are analysed to yield a spatial model for local backbone motion. This model includes the axis of motion, the mean orientation, and the maximum amplitude of displacement for individual peptide planes (Fig. 58). Specific sites in the first turn of the amino terminus were investigated, with emphasis on the L-Ala_3 and D-Leu_4 linkages, for which the orientation of the ^{15}N chemical shift tensor with respect to the molecular frame has been determined. Figure 59 shows the simulation of spectra obtained from oriented bilayer samples containing specific-site ^{15}N-labelled GA at 8°C. Samples were placed in the magnet such that the bilayer normal was parallel to the direction of the field. The effect of bilayer defect structure, and of parabolic focal conics[214] is included in the spectral simulation. From these simulations, it is found that only relatively small amplitude motions are possible at the two sites, with amplitudes of not more than ±8° and ±15° for the L-Ala_3 and D-Leu_4 sites, respectively.

Bacteriorhodopsin and rhodopsin are integral membrane proteins that contain vitamin A aldehyde retinal as a photoreactive chromophore. Many works on the structure and environment of the retinal chromophore in these proteins by means of solid-state NMR have been reported, using mainly specifically ^{13}C-labelled retinals.[115,215–225] So far, it can be said that the structure of retinal in bacteriorhodopsin and rhodopsin has been determined only by solid-state NMR. Therefore, solid-state NMR is the only experimental procedure for the clarification of the sense of sight. Most recently, the ^{13}C CP MAS-NMR spectra of ^{13}C-labelled bacteriorhodopsin in purple membranes were measured.[226] On the basis of the ^{13}C CP MAS-NMR experiments, a discussion has been presented of the change of the manner of mutual orientation between α-helices as induced by hydration/dehydration.

Fig. 59. Simulations of spectra obtained from oriented samples in the gel phase that superimpose the effects of local disorder due to backbone dynamics and global channel axis disorder due to the PFC (parabolic focal conics) defect structure. The chemical shift scales are relative to $\sigma_{iso} = 0$ ppm. (a) Experimental spectrum recorded for the D-Leu_4 site at 8°C. (b) Simulation for the D-Leu_4 site using a local motion defined by $\phi = 5°$, $\theta = 262°$ and $\delta = 15°$, and a slow global lateral diffusion through the PFC defect structure (10 ppm line broadening applied). (c) Same as in (b), with 2 ppm line broadening applied. (d) Experimental spectrum recorded for the L-Ala_3 site at 8°C. (e) Simulation for the L-Ala_3 site using a local motion defined by $\phi = 19.5°$, $\theta = 82°$, and $\delta = 8°$, and a slow global lateral diffusion through the PFC defect structure (10 ppm line broadening applied). (f) Same as in (e), with 2 ppm line broadening applied.

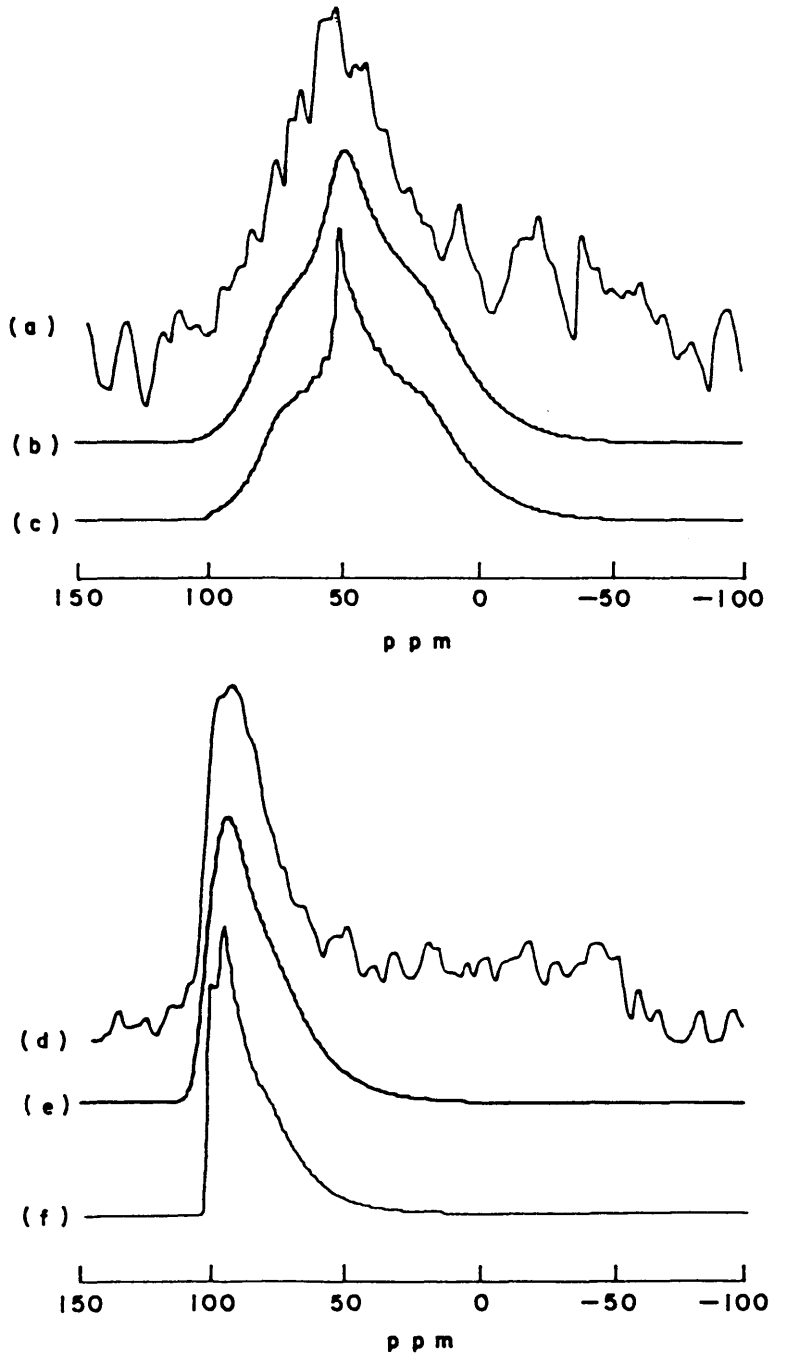
(a)
(b)
(c)
150
100
50
0
−50
−100
p p m
(d)
(e)
(f)
150
100
50
0
−50
−100
p p m

4.3. Miscellaneous biopolymers

The solid-state NMR method complements and extends other structural methods such as X-ray diffraction and solution NMR. Soluble proteins such as enzymes and conjugated proteins such as glycoproteins have been investigated by solid-state NMR.[227–242]

Ellis and coworkers have characterized the ^{113}Cd chemical shielding tensor in Cd complexes, particularly those containing oxygen ligands, and then studied the metal binding site in lyophilized metalloprotein samples by solution and solid-state ^{113}Cd NMR spectroscopy.[229–233] Principal elements of the ^{113}Cd chemical shielding tensor have been determined by spinning sideband analysis of CP MAS spectra for the calcium-binding sites in parvalbumin and for the manganese (S1) and calcium (S2) sites in concanavalin A. Similarities in isotropic chemical shifts and in its tensor parameters for the parvalbumin calcium sites and for the S2 site in concanavalin A reflect similar metal-coordination environments in the two proteins. Santos *et al.* have also reported the solid-state ^{113}Cd and ^{119}Hg spectra of some model complexes for biologically occurring [M(S-Cys)$_2$(His)$_2$] centres of metalloproteins.[234,235]

^{13}C CP MAS-NMR spectroscopy has been used to characterize covalent conjugates of alachlor, an α-chloroacetamide hapten, with glutathione (GSH) and bovine serum albumin (BSA).[236] The solid-state NMR method demonstrates definitively the covalent nature of these conjugates and can also be used to characterize the sites of ^{13}C-labelled hapten attachment to proteins. Three different sites of alachlor binding are observed in the BSA system. Accurate quantitation of the amount of hapten covalently bound to GSH and BSA is possible. The solid-state ^{13}C NMR technique can easily be generalized to study other small molecule/protein conjugates and can be used to assist the development and refinement of synthetic methods needed for the successful formation of such protein alkylation products. Similar methods have been applied to characterize enzyme–substrate interactions[237,238] and aromatic cross-links in insect cuticle,[239] respectively.

On the other hand, for proteins which are in more complex systems, molecular motion is mainly characterized by solid-state NMR. The motional dynamics of lens cytoplasmic proteins present in calf lens homogenates have been investigated by solid-state NMR techniques in order to define further the organizational differences between the cortex and nucleus.[240] Mainly from the results of the spin-locking experiments at several temperatures, it has been established that both mobile and solid-like protein phases are present in calf lens nuclear homogenate. However, for the native cortical homogenate, within the detection limits of NMR, the protein phase is mobile, except at low temperature where a small fraction of solid-like protein phases is present. The dynamics of intact lime cuticle and its two components, cutin and wax, have been similarly investigated.[241] For wheat

gluten, four different subsets are identified by solid state and solution ^{13}C NMR methods.[242]

5. CONCLUSION

The present chapter shows that solid-state high-resolution NMR spectroscopy provides great perspectives for elucidating the high-order structure of polymers such an engineering plastics, high-performance polymers, polymer alloys and natural polymers in bulk. It is clear that solid-state high-resolution NMR is an indispensable technique for the routine analysis as well as for the study of the structures and dynamics of polymers in bulk. Another important future role for solid-state high-resolution NMR might be an extension to NMR imaging as a tool for materials research, although this is outside the scope of this chapter.

REFERENCES

1. H. S. Gutowsky, A. Saika, M. Takeda and D. E. Woessner, *J. Chem. Phys.*, 1957, **27**, 537.
2. For example, (a) J. Schaefer and E. O. Stejskal, *Topics in Carbon-13 NMR Spectroscopy* (ed. G. C. Levy), Vol. 3, p. 283. Wiley, New York, 1979; (b) R. A. Komoroski (ed.), *High Resolution NMR of Synthetic Polymers in Bulk*. VCH Publishers, Florida, 1986; (c) I. Ando, T. Yamanobe and T. Asakura, *Progress in NMR Spectroscopy* (eds J. W. Emsley, J. Feeney and L. H. Sutcliffe), Vol. 22, p. 349. Pergamon Press, Oxford, 1990.
3. I. Ando, T. Sorita, T. Yamanobe, T. Komoto, H. Sato, K. Deguchi and M. Imanari, *Polymer*, 1985, **26**, 1864.
4. D. L. VanderHart and F. Khoury, *Polymer*, 1984, **25**, 1589.
5. W. L. Earl and W. L. VanderHart, *Macromolecules*, 1979, **12**, 762.
6. T. Yamanobe, T. Sorita, T. Komoto and I. Ando, *J. Mol. Struct.*, 1985, **31**, 267.
7. H. Kurosu, T. Yamanobe and I. Ando, *J. Mol. Struct. (Theochem.)*, 1989, **201**, 239.
8. T. Kitamaru, F. Horii and K. Murayama, *Macromolecules*, 1986, **19**, 636.
9. H. Tadokoro, *Kobunshi*, 1983, **32**, 202.
10. I. Ando and T. Yamanobe, *Seni to kogyo*, 1985, **41**, 255.
11. T. Nakai, J. Asada and T. Terao, *J. Chem. Phys.*, 1988, **88**, 6049.
12. I. Ando, T. Yamanobe, S. Akiyama, T. Komoto, H. Sato, T. Fujito, K. Deguchi and M. Imanari, *Solid State Commun.*, 1987, **62**, 785.
13. T. Yamanobe, M. Tsukahara, T. Komoto, J. Watanabe, I. Ando, I. Uematsu, K. Deguchi, T. Fujito and I. Imanari, *Macromolecules*, 1988, **21**, 48.
14. S. Akiyama, T. Komoto, I. Ando and H. Sato, *J. Polym. Sci.: Part B: Polym. Phys.*, 1990, **28**, 587.
15. I. Ando, T. Yamanobe, S. Akiyama, T. Komoto, H. Sato, T. Fujito, K. Deguchi and M. Imanari, *Solid State Commun.*, 1987, **62**, 785.
16. I. Ando and G. A. Webb, *Theory of NMR Parameters*. Academic Press, London, 1983.
17. N. Kasai and M. Kakubo, *IUPAC International Symposium on Macromolecular Chemistry*, Prague, 1965, p. 491.

18. Q. Chen, T. Yamada, H. Kurosu, I. Ando, T. Shiono and Y. Doi, *J. Polym. Sci.: Part B: Polym. Phys.*, 1992, **30**, 591.
19. J. J. Dechter, R. A. Komoroski, D. E. Axelson and L. Mandelkern, *J. Polym. Sci. Polym. Phys.*, 1981, **19**, 631.
20. B. Schroter and A. Posern, *Makromol. Chem.*, 1981, **182**, 675.
21. R. Kitamaru, F. Horii and K. Murayama, *Polym. Bull.*, 1982, **7**, 583.
22. D. E. Axelson, *High Resolution NMR Spectroscopy of Synthetic Polymers in Bulk* (ed. R. A. Komoroski), Ch. 5, p. 197. VCH Publishers, Florida, 1986.
23. Q. Chen, T. Yamada, H. Kurosu, I. Ando, T. Shiono and Y. Doi, *J. Mol. Struct.*, 1991, **263**, 319.
24. T. Terao, S. Maeda and A. Saika, *Macromolecules*, 1983, **16**, 1535.
25. F. Horii, S. Hu, T. Ito, H. Odani, R. Kitamaru, S. Matsuzawa and K. Yamaura, *Polymer*, 1992, **33**, 2299.
26. (a) K. Kubo, T. Yamanobe, T. Komoto, I. Ando and T. Shiibashi, *J. Polym. Sci. Part B: Polym. Phys.*, 1989, **27**, 929; (b) K. Kubo, I. Ando, T. Shiibashi, T. Yamanobe and T. Komoto, *J. Polym. Sci.: Part B: Polym. Phys.*, 1991, **29**, 57.
27. D. G. Powell and L. J. Mathias, *J. Am. Chem. Soc.*, 1990, **112**, 669.
28. G. R. Hatfield, J. H. Glans and W. B. Hammond, *Macromolecules*, 1990, **23**, 1654.
29. L. J. Matias, D. G. Powell, J. Autran and R. S. Porter, *Mater. Sci. Eng.*, 1990, **A126**, 253.
30. P. Holstein, J. Spevacek, D. Geschke and V. Thiele, *Progr. Colloid Polym. Sci.*, 1991, **85**, 60.
31. S. Yamazaki, T. Kimura, K. Neki and N. Tamura, *Anal. Sci.*, 1991, **7**, 1613.
32. G. Carazzolo and M. Mammi, *J. Polym. Sci., Part A*, 1964, **1**, 965.
33. W. S. Veeman, E. M. Menger, W. Ritchey and E. de Boer, 1979, **12**, 924.
34. H. Kurosu, T. Komoto and I. Ando, *J. Mol. Structures*, 1988, **176**, 279.
35. A. Hagemeyer, K. Schmidt-Rohr, H. W. Spiess, *Adv. Magn. Reson.*, 1989, **13**, 85.
36. M. Kobayashi, M. Murano and A. Kaji, *Macromolecules*, 1990, **23**, 3051.
37. J. L. Bredas and G. B. Street, *Acc. Chem. Res.*, 1985, **18**, 309.
38. M. G. Kanatzldis, *Chem. Eng. News*, 1990, **3**, 36.
39. J. L. Bredas, B. Themans, J. G. Fripiat and J. M. Andre, *Phys. Rev. B*, 1984, **29**, 6761.
40. F. Devreux, G. Bidan, A. A. Syed and C. Tsintavis, *J. Phys..*, 1985, **46**, 1595.
41. B. Wehrle, H. H. Limbach, J. Mortensen and J. Heinze, *Synth. Meth.*, 1990, **38**, 293.
42. M. Kikuchi, H. Kurosu and I. Ando, *J. Mol. Struct.*, 1992, **269**, 183.
43. N. Ogata, *Doudenseikoubunshi (Conducting Polymers)*. Koudansha, Tokyo, 1990.
44. J. Schaefer and E. O. Stejskal, *Topics in Carbon-13 NMR Spectroscopy* (ed. G. C. Levy), Vol. 4, p. 283. Wiley-Interscience, New York, 1979.
45. M. A. Gomez and A. E. Tonelli, *Polymer*, 1991, **32**, 796.
46. N. Zumbulyadis, J. M. O'Reilly and D. M. Teegarden, *Macromolecules*, 1992, **25**, 3317.
47. J. Schaefer and E. O. Stejskal, *J. Am. Chem. Soc.*, 1976, **98**, 1031.
48. J. Schaefer and E. O. Stejskal, *Macromolecules*, 1977, **10**, 384.
49. M. D. Sefcik, E. O. Stejskal, R. A. McKay and J. Schaefer, *Macromolecules*, 1979, **12**, 423.
50. S. A. Swanson, W. W. Fleming and D. C. Hofer, *Macromolecules*, 1992, **25**, 582.
51. C. F. Fry and A. C. Lind, *New Polym. Mater.*, 1990, **2**, 235.
52. J. Schaefer and E. O. Stejskal, *Macromolecules*, 1977, **10**, 384.
53. J. R. Havens and J. L. Koenig, *Appl. Spectrosc.*, 1983, **37**, 226.
54. J. R. Lyerla, in *High Resolution NMR Spectroscopy of Synthetic Polymers in Bulk* (ed. R. A. Komoroski), Ch. 3. VCH Publishers, Florida, 1986.
55. J. Schaefer, E. O. Stejskal, R. A. McKay and W. T. Dixon, *Macromolecules*, 1984, **17**, 1479.
56. M. D. Sefcik, J. Schaefer, E. O. Stejskal and R. A. McKay, *Macromolecules*, 1980, **13**, 1132.

57. J. R. Havens, H. Ishida and J. L. Koenig, *Macromolecules*, 1981, **14**, 1327.
58. J. Schaefer, B. Hansen, B. Bluemich and H. W. Spiess, *J. Non-Cryst. Solids*, 1991, **131–133**, 777.
59. D. L. Tzou, P. Desai, A. S. Abhiraman and T. H. Huang, *Polym. Prep. (Am. Chem. Soc.)*, 1990, **31**, 157.
60. M. A. Gomez, M. H. Cozine and A. T. Tonelli, *Macromolecules*, 1988, **21**, 388.
61. M. D. Poliks and J. Schaefer, *Polym. Prep. (Am. Chem. Soc.)*, 1990, **31**, 109.
62. S. A. Curran, C. P. LaClair and S. M. Aharoni, *Macromolecules*, 1991, **24**, 5903.
63. M. Tsukahara, T. Yamanobe, T. Komoto, J. Watanabe and I. Ando, *J. Mol. Struct.*, 1987, **159**, 345.
64. T. Yamanobe, M. Tsukahara, T. Komoto, J. Watanabe, I. Ando, I. Uematsu, K. Deguchi, T. Fujito and M. Imanari, *Macromolecules*, 1988, **21**, 48.
65. T. Yamanobe, H. Tsukamoto, Y. Uematsu, I. Ando and I. Uematsu, *J. Mol. Struct.*, 1993, **295**, 25.
66. B. Mohanty, T. Komoto, J. Watanabe, I. Ando and T. Shiibashi, *Macromolecules*, 1989, **22**, 4451.
67. B. Mohanty, J. Watanabe, I. Ando and K. Sato, *Macromolecules*, 1990, **23**, 4908.
68. S. Ishikawa, H. Kurosu and I. Ando, *J. Mol. Struct.*, 1991, **248**, 361.
69. S. Ishikawa and I. Ando, *J. Mol. Struct.*, 1992, **273**, 227.
70. N. Bloembergen, E. M. Purcell and R. V. Pound, *Phys. Rev.*, 1948, **73**, 679.
71. L. J. Mathias, *Polym. Commun.*, 1988, **29**, 352.
72. B. C. Perry and J. L. Koenig, *J. Appl. Polym. Sci., Appl. Polym. Symp.*, 1989, **43**, 165.
73. H. W. Spiess, *Pure Appl. Chem.*, 1987, **57**, 1717.
74. H. W. Spiess, R. Ebelhauser and T. Fahmy, *Makromol. Chem., Rapid Commun.*, 1984, **5**, 333.
75. H. W. Spiess and R. Ebelhauser, *Makromol. Chem., Rapid Commun.*, 1984, **5**, 4038.
76. H. W. Spiess, H. Sillescu and E. Rossler, *Polymer*, 1985, **26**, 203.
77. U. Pschorn, H. W. Spiess, B. Hisgen and H. Ringsdorf, *Makromol. Chem.*, 1986, **187**, 2711.
78. F. Laupretre, C. Noel, W. N. Jenkins and W. N. Williams, *Faraday Discuss. Chem. Soc.*, 1985, **79**, 191.
79. T. Kato, G. M. A. Kabir and T. Uryu, *J. Polym. Sci., A, Polym. Chem.*, 1989, **27**, 1447.
80. J. Hong and G. S. Harbison, *Colloids Surf.*, 1990, **45**, 313.
81. U. Wiesner, K. Schmidt-Rohr, C. Boeffel, U. Pawelzik and H. W. Spiess, *Adv. Mater.*, 1990, **2**, 484.
82. S. A. Curran, C. P. LaClair and S. M. Aharoni, *Macromolecules*, 1991, **24**, 5903.
83. D. Geschke and G. Fleischer, *Prog. Colloid Polym. Sci.*, 1991, **85**, 127.
84. S. Ishikawa and I. Ando, *J. Mol. Structure*, 1992, **271**, 57.
85. D. R. Paul and S. Newman (eds), *Polymer Blends*, Academic Press, New York, 1978.
86. P. Caravatti, P. Neuenschwander and R. P. Ernst, *Macromolecules*, 1985, **18**, 119.
87. G. C. Gobbi, R. Silvestri, T. P. Russell, J. R. Lyerla, W. W. Fleming and T. Nishi, *J. Polym. Sci., Polym. Lett.*, 1987, **25**, 61.
88. S. R. Hartmann and E. L. Hahn, *Phys. Rev.*, 1962, **128**, 2040.
89. J. F. Parmer, L. C. Dickinson, J. C. W. Chien and R. S. Porter, *Macromolecules*, 1987, **20**, 2308.
90. X. Zhang, A. Natansohn and A. Eisenberg, *Macromolecules*, 1990, **23**, 412.
91. C. W. Chu, L. C. Dickinson and J. C. W. Chien, *J. Appl. Polym. Sci.*, 1990, **41**, 2311.
92. V. J. McBrierty and D. C. Douglas, *J. Polym. Sci., Macromol. Rev.*, 1981, **16**, 295.
93. K. Takegoshi and K. Hikichi, *J. Chem. Phys.*, 1991, **94**, 3200.
94. R. K. Harris, P. Jackson, L. H. Merwin, B. J. Say and G. Haegele, *J. Chem. Soc., Faraday Trans. 1*, 1988, **84**, 3649.
95. L. A. Belfiore, T. J. Litz, C. Cheng and C. E. Bronnimann, *J. Polym. Sci., B, Polym. Phys.*, 1990, **28**, 1261.

96. J. Grobelny, D. M. Rice, F. E. Karasz and W. J. MacKnight, *Macromolecules*, 1990, **23**, 2139.
97. A. Simmons and A. Natansohn, *Macromolecules*, 1991, **24**, 3651.
98. S. Percec and T. Hammond, *Polymer*, 1991, **32**, 1252.
99. C. Zhang, P. Wang, A. A. Jones, P. T. Inglefield and R. P. Kambour, *Macromolecules*, 1991, **24**, 338.
100. Y. H. Chin, C. Zhang, P. Wang, P. T. Inglefield, A. A. Jones, R. P. Kambour, J. T. Bendler and D. M. White, *Macromolecules*, 1992, **25**, 3031.
101. R. A. Grinsted and J. Koenig, *J. Polym. Sci., B, Polym. Phys.*, 1990, **28**, 177.
102. R. Ibbett, D. Bucknall and H. S. Higgins, *Polymer*, 1992, **33**, 423.
103. J. F. Masson and R. St. J. Manley, *Macromolecules*, 1992, **25**, 589.
104. S. N. Sarkar and R. A. Komoroski, *Macromolecules*, 1992, **25**, 1420.
105. X. Zhang, K. Takegoshi and K. Hikichi, *Polymer*, 1992, **33**, 712.
106. X. Zhang, K. Takegoshi and K. Hikichi, *Polym. J.*, 1991, **23**, 79.
107. X. Zhang, K. Takegoshi and K. Hikichi, *Polym. J.*, 1991, **23**, 83.
108. A. Asano, K. Takehoshi and K. Hikichi, *Polym. J.*, 1992, **24**, 473.
109. X. Zhang, K. Takegoshi and K. Hikichi, *Polym. J.*, 1992, **24**, 1403.
110. B. Schneider, J. Spevacek, J. Straka and J. Stokr, *Makromol. Chem., Macromol. Symp.*, 1990, **34**, 213.
111. D. A. Torchia and D. L. VanderHart, in *Topics in Carbon-13 NMR Spectroscopy* (ed. G. C. Levey), Vol. 3, Ch. 5. Wiley, New York, 1979.
112. C. A. Fyfe, *Solid State NMR for Chemists*. C.F.C. Press, Guelph, Canada, 1983.
113. H. Saito, T. Tabeta, A. Shoji, T. Ozaki, I. Ando and T. Asakura, in *Magnetic Resonance in Biology and Medicine* (eds G. Govil, C. L. Kheterapal and A. Saran), p. 195. Tata McGraw-Hill, New Delhi, 1985.
114. G. A. Hatfield and G. E. Maciel, *Methods Protein Anal.*, **1988**, 214.
115. S. O. Smith and R. G. Griffin, *Ann. Rev. Phys. Chem.*, 1988, **39**, 511.
116. (a) S. J. Opella and P. L. Stewart, *Methods Enzymol.*, 1989, **176**, 242; (b) K. V. Ramanathan and S. J. Opella, *Trans. Am. Crystallogr. Assoc.*, 1989, **24**, 145; (c) S. J. Opella, *Biol. Magn. Reson.*, 1990, **9**, 177; (d) L. E. Chirlian and S. J. Opella, *New Polym. Mater.*, 1990, **2**, 278.
117. M. A. Keniry, *Methods Enzymol.*, 1989, **176**, 376.
118. M. A. Hemminga and T. W. Poile, *Spec. Publ. R. Soc. Chem.*, 1989, **74**, 74.
119. A. E. Derome and S. Bowden, *Chem. Rev.*, 1991, **91**, 1307.
120. H. Saito and I. Ando, *Ann. Rep. NMR Spectrosc.*, 1989, **21**, 210.
121. A. Shoji, S. Ando, S. Kuroki, I. Ando and G. A. Webb, *Ann. Rep. NMR Spectrosc.*, 1993, **26**, 55.
122. T. Taki, S. Yamashita, M. Satoh, A. Shibata, T. Yamashita, R. Tabeta and H. Saito, *Chem. Lett.*, **1981**, 1803.
123. H. Saito, R. Tabeta, A. Shoji, T. Ozaki and I. Ando, *Macromolecules*, 1983, **16**, 1050.
124. H. Saito, R. Tabeta, I. Ando, T. Ozaki and A. Shoji, *Chem. Lett.*, **1983**, 1437.
125. I. Ando, H. Saito, R. Tabeta, A. Shoji and T. Ozaki, *Macromolecules*, 1984, **17**, 457.
126. A. Shoji, T. Ozaki, H. Saito, R. Tabeta and I. Ando, *Macromolecules*, 1984, **17**, 1472.
127. A. Shoji, T. Ozaki, H. Saito, R. Tabeta and I. Ando, *Makromol. Chem., Rapid Commun.*, 1984, **5**, 799.
128. T. Yamanobe, I. Ando, H. Saito, R. Tabeta, A. Shoji and T. Ozaki, *Bull. Chem. Soc. Jpn*, 1985, **58**, 23.
129. T. Yamanobe, I. Ando, H. Saito, R. Tabeta, A. Shoji and T. Ozaki, *Chem. Phys.*, 1985, **99**, 259.
130. S. Ando, T. Yamanobe, I. Ando, A. Shoji, T. Ozaki, R. Tabeta and H. Saito, *J. Am. Chem. Soc.*, 1985, **107**, 7648.
131. S. Tuzi, T. Komoto, I. Ando, H. Saito, A. Shoji and T. Ozaki, *Biopolymers*, 1987, **26**, 1983.

132. H. Miyamoto, R. Takezaki, T. Komoto and I. Ando, *J. Mol. Struct.*, 1988, **172**, 395.
133. H. Saito, R. Tabeta, F. Formaggio, M. Crisma and C. Toniolo, *Biopolymers*, 1988, **27**, 1607.
134. S. Ando, I. Ando, A. Shoji and T. Ozaki, *J. Mol. Struct.*, 1989, **192**, 153.
135. S. Ando, K. Matsumoto, I. Ando, A. Shoji and T. Ozaki, *J. Mol. Struct.*, 1989, **212**, 123.
136. H. Miyamoto, T. Komoto, H. Kurosu, I. Ando, T. Ozaki and T. Shoji, *J. Mol. Struct.*, 1990, **220**, 251.
137. H. R. Kricheldorf, M. Mutter, F. Mazer, D. Muller and D. Forster, *Biopolymers*, 1983, **22**, 1357.
138. H. R. Kricheldorf and D. Muller, *Macromolecules*, 1983, **16**, 615.
139. H. R. Kricheldorf, D. Muller and K. Ziegler, *Polym. Bull.*, 1983, **9**, 284.
140. H. R. Kricheldorf and D. Muller, *Int. J. Biol. Macromolecules*, 1984, **16**, 145.
141. D. Muller and R. H. Kricheldorf, *Polym. Bull.*, 1981, **6**, 101.
142. T. Asakura, Suzuki and Y. Watanabe, *Macromolecules*, 1983, **16**, 1024.
143. T. Asakura, Y. Watanabe, A. Uchida and H. Minagawa, *Macromolecules*, 1984, **17**, 1075.
144. T. Asakura, Y. Watanabe and T. Itoh, *Macromolecules*, 1984, **17**, 2421.
145. T. Asakura and T. Murakami, *Macromolecules*, 1985, **18**, 2614.
146. T. Asakura, H. Kashiba and H. Yoshimizu, *Macromolecules*, 1988, **21**, 644.
147. H. Saito, Y. Iwanaga, R. Tabeta and T. Asakura, *Chem. Lett.*, **1983**, 427.
148. H. Saito, R. Tabeta, T. Asakura, Y. Iwanaga, A. Soji, T. Ozaki and I. Ando, *Macromolecules*, 1984, **17**, 1405.
149. T. Asakura, A. Kuzuhara, R. Tabeta and H. Saito, *Macromolecules*, 1985, **18**, 1841.
150. H. Saito, R. Tabeta, A. Kuzuhara and T. Asakura, *Bull. Chem. Soc. Jpn*, 1986, **59**, 3383.
151. H. Saito, M. Ishida, M. Yokoi and T. Asakura, *Macromolecules*, 1990, **23**, 83.
152. M. Ishida, T. Asakura, M. Yokoi and H. Saito, *Macromolecules*, 1990, **23**, 88.
153. T. Asakura, M. Demura, Y. Watanabe and K. Sato, *J. Polym. Sci., Polym. Phys.*, 1992, **30**, 693.
154. T. Asakura, T. Konakazawa, M. Demura, K. Komatsu and T. Itoh, *31st Meeting on NMR*, Himeji, Hyogo, 1992, 285.
155. L. K. Nicholson, *Biopolymers*, submitted.
156. X. Han, J. Guo, J. Hu, T. Ji, X. Zhang, J. Hu and J. Qui, *Bopuxue Zazhi*, 1990, **8**, 245.
157. R. D. Fraser and T. P. MacRae, *Conformation in Fibrous Proteins*. Academic Press, New York, 1973.
158. T. Asakura and T. Yamaguchi, *J. Seric. Sci. Jpn*, 1987, **56**, 300.
159. W. Traub and K. A. Piez, *Adv. Protein Chem.*, 1971, **25**, 243.
160. D. A. Torchia and D. L. VanderHart, *J. Mol. Biol.*, 1976, **104**, 315.
161. L. W. Jelinski and D. A. Torchia, *J. Mol. Biol.*, 1979, **133**, 45.
162. L. W. Jelinski and D. A. Torchia, *J. Mol. Biol.*, 1980, **138**, 255.
163. L. W. Jelinski and D. A. Torchia, *Frontiers in Protein Chemistry*, p. 89. Elsevier-North Holland, Amsterdam, 1990.
164. L. W. Jelinski, C. E. Sullivan, L. S. Batchelder and D. A. Torchia, *Biophys. J.*, 1980, **32**, 515.
165. L. S. Barchelder, C. E. Sullivan, W. Jelinski and D. A. Torchia, *Proc. Natl Acad. Sci. USA*, 1982, **79**, 386.
166. D. A. Torchia, *Methods Enzymol.*, 1983, **82**, 174.
167. S. K. Sarkar, C. E. Sullivan and D. A. Torchia, *J. Biol. Chem.*, 1983, **258**, 9762.
168. S. K. Sarkar, D. A. Torchia, K. D. Kopple and D. L. VanderHart, *J. Am. Chem. Soc.*, 1984, **106**, 3328.
169. D. A. Torchia, *Annu. Rev. Biophys. Bioeng.*, 1984, **13**, 125.
170. S. K. Sarkar, C. E. Sullivan and D. A. Torchia, *Biochemistry*, 1985, **24**, 2348.
171. D. A. Torchia, Y. Hiyama, S. K. Sarkar, C. E. Sullivan and P. E. Young, *Biopolymers*, 1985, **24**, 65.
172. S. K. Sarkar, P. E. Young and D. A. Torchia, *J. Am. Chem. Soc.*, 1986, **108**, 6459.

173. Y. Hiyama, J. V. Silverton, D. A. Torchia, J. T. Gerig and S. J. Hammond, *J. Am. Chem. Soc.*, 1986, **108**, 2715.
174. S. K. Sarkar, Y. Hiyama, C. H. Niu, P. E. Young, J. T. Gerig and D. A. Torchia, *Biochemistry*, 1987, **26**, 6793.
175. Y. Hiyama and D. A. Torchia, *Basic Life Sci.*, 1990, **56**, 273.
176. R. Fujiwara and Y. Kuboi, *Biochem. Biophys. Res. Commun.*, 1990, **167**, 761.
177. H. Saito, R. Tabeta, A. Shoji, T. Ozaki, I. Ando and T. Miyata, *Biopolymers*, 1984, **23**, 2279.
178. H. Saito and M. Yokoi, *J. Biochem.*, 1992, **111**, 376.
179. M. Bennet, L. Foucat, J. Dupuis and J. P. Renou, *J. Chim. Phys. Phys.-Chim. Biol.*, 1992, **89**, 227.
180. S. Tuzi and I. Ando, *J. Mol. Struct.*, 1989, **196**, 317.
181. S. Tuzi, S. Sakamaki and I. Ando, *J. Mol. Struct.*, 1990, **221**, 289.
182. S. Tuzi, PhD Thesis, Tokyo Institute of Technology, 1990.
183. P. L. Privalov, *Adv. Protein Chem.*, 1982, **35**, 1.
184. C. Cohn and K. C. Holes, *J. Mol. Biol.*, 1963, **6**, 423.
185. H. Yoshimizu and I. Ando, *Macromolecules*, 1990, **23**, 2908.
186. H. Yoshimizu, H. Mimura and I. Ando, *Macromolecules*, 1991, **24**, 862.
187. H. Yoshimizu, H. Mimura and I. Ando, *J. Mol. Struct.*, 1991, **246**, 367.
188. H. Yoshimizu, PhD Thesis, Tokyo Institute of Technology, 1991.
189. H. Mimura, H. Yoshimizu and I. Ando, *30th Meeting on NMR*, Tokyo, 1991, p. 291.
190. For example, (a) R. D. Fraser, T. P. MacRae and G. E. Rogers, *Keratins: Their Composition, Structure and Biosynthesis*. Charles C. Thomas, Springfield, IL, 1972; (b) J. H. Bradbury, *Adv. Protein Chem.*, 1973, **27**, 111; (c) R. D. Fraser and T. P. MacRae, *Conformation in Fibrous Proteins*, Ch. 16. Academic Press, New York, 1973.
191. I. J. O'Donnel and E. O. P. Thompson, *Aust. J. Biol. Sci.*, 1964, **17**, 973.
192. L. M. Dowling and W. G. Crewther, *Prep. Biochem.*, 1974, **4**, 203.
193. H. Sakabe, T. Miyamoto and H. Inagaki, *Sen-i Gakkaishi*, 1981, **37**, 273.
194. H. R. Kricheldorf and D. Muller, *Colloid Polym. Sci.*, 1984, **262**, 856.
195. J. W. Mack, D. A. Torchia and M. Steinert, *Biochemistry*, 1988, **27**, 5418.
196. H. Tournois, J. L. Bijvelt, C. W. M. Haest, J. Ier and B. Kruijff, *Biochemistry*, 1987, **26**, 6613.
197. T. Odahara, H. Akutsu and Y. Kyogoku, *Biochemistry*, 1990, **29**, 5968.
198. R. Sages and B. Witkop, *Biochemistry*, 1965, **4**, 2491.
199. D. W. Urry, *Proc. Natl Acad. Sci., USA*, 1971, **68**, 672.
200. R. Smith and B. A. Cornell, *Biophys. J.*, 1986, **49**, 117.
201. B. A. Cornell, F. Separovic, A. J. Baldassi and R. Smith, *Biophys. J.*, 1988, **53**, 67.
202. R. Smith, D. E. Thomas, F. Separovic, A. R. Atkins and B. A. Cornell, *Biophys. J.*, 1989, **56**, 307.
203. F. Separovic, K. Hayamizu, R. Smith and B. A. Cornell, *Chem. Phys. Lett.*, 1991, **181**, 157.
204. L. K. Nicholson, F. Moll, T. E. Mixon, P. V. LoGrasso, J. C. Lay and T. A. Cross, *Biochemistry*, 1987, **26**, 6621.
205. L. K. Nicholson. P. V. LoGrasso and T. A. Cross, *J. Am. Chem. Soc.*, 1989, **111**, 400.
206. P. V. LoGrasso, L. K. Nicholson and T. A. Cross, *J. Am. Chem. Soc.*, 1989, **111**, 1910.
207. L. K. Nicholson and T. A. Cross, *Biochemistry*, 1989, **28**, 9379.
208. Q. Teng, L. K. Nicholson and T. A. Cross, *J. Mol. Biol.*, 1991, **218**, 607.
209. L. K. Nicholson, Q. Teng and T. A. Cross, *J. Mol. Biol.*, 1991, **218**, 621.
210. S. W. Chiu, L. K. Nicholson, M. T. Brenneman, S. Subramaniam, Q. Teng, J. A. McCammon, T. A. Cross and E. Jakobsson, *Biophys. J.*, 1991, **60**, 974.
211. J. H. Davis, *Biochemistry*, 1988, **27**, 428.
212. R. S. Prosser, J. H. Davis, F. W. Dahlquist and M. A. Lindorfer, *Biochemistry*, 1991, **30**, 4687.

213. D. W. Urry, J. T. Walker and T. L. Trapane, *J. Membr. Biol.*, 1982, **69**, 225.
214. (a) M. Kleman, C. E. Williams, M. J. Costello and T. Gulik-Krywicki, *Philos. Mag.*, 1977, **35**, 33; (b) C. S. Rosenblantt, R. Pindak, N. A. Clark and R. B. Meyer, *J. Phys..*, 1977, **38**, 1105; (c) S. A. Asher and P. S. Pershan, *Biophys. J.*, 1979, **27**, 393.
215. G. S. Harbison, J. Herzfeld and R. G. Griffin, *Biochemistry*, 1983, **22**, 1.
216. G. S. Harbison, S. O. Smith, J. A. Pardoen, P. P. J. Mulder, J. Lugtenburg, J. Herzfeld and R. G. Griffin, *Biochemistry*, 1984, **23**, 2662.
217. G. S. Harbison, S. O. Smith, J. A. Pardoen, C. Winkel, J. Lugtenburg, J. Herzfeld, R. A. Mathies and R. G. Griffin, *Proc. Natl Acad. Sci. USA*, 1984, **81**, 1706.
218. G. S. Harbison, S. O. Smith, J. A. Pardoen, J. M. L. Courtin, J. Lugtenburg, J. Herzfeld, R. A. Mathies and R. G. Griffin, *Biochemistry*, 1985, **24**, 6955.
219. G. S. Harbison, P. P. J. Mulder, J. A. Pardoen, J. A. Lugtenburg, J. Herzfeld and R. G. Griffin, *J. Am. Chem. Soc.*, 1985, **107**, 4809.
220. A. Schmidt, S. O. Smith, D. P. Raleigh, J. E. Roberts, R. G. Griffin and S. Vega, *J. Chem. Phys.*, 1986, **85**, 4248.
221. S. O. Smith, I. Palings, V. Copie, D. P. Raleigh, J. Courtin, J. A. Pardoen, J. Lugtenburg, R. A. Mathies and R. G. Griffin, *Biochemistry*, 1987, **26**, 1606.
222. H. J. M. De Groot, V. Copie, S. O. Smith, P. J. Allen, C. Winkel, J. Lugtenburg, J. Hertzfeld and R. G. Griffin, *J. Magn. Reson.*, 1988, **77**, 251.
223. S. O. Smith, J. Couritin, E. van den Berg, C. Winkel, J. Lugtenburg, J. Herzfeld and R. G. Griffin, *Biochemistry*, 1989, **27**, 237.
224. S. O. Smith, H. J. M. De Groot, R. Gebhard, J. M. L. Courtin, J. Lugtenburg, J. Herzfeld and R. G. Griffin, *Biochemistry*, 1989, **28**, 8897.
225. L. P. J. Mollevanger, A. M. Kentgens, J. Pardoen, J. L. Courtin, W. Veeman, J. Lugtenburg and W. J. de Grip, *Eur. J. Biochem.*, 1987, **163**, 9.
226. S. Tuzi, A. Naito and H. Saito, *31st Meeting on NMR*, Himeji, Hyogo, 1992, p. 51.
227. V. D. Fedotov, N. P. Obuchov, J. Spevacek and J. Straka, *Makromol. Chem. Macromol. Symp.*, 1990, **34**, 249.
228. M. A. Hemminga, P. A. deJager, J. Kruse and R. M. J. N. Lamerichs, *J. Magn. Reson.*, 1987, **71**, 446.
229. R. S. Honkonen and P. D. Ellis, *J. Am. Chem. Soc.*, 1984, **106**, 5488.
230. P. S. Marchetti, P. D. Ellis and R. G. Bryant, *J. Am. Chem. Soc.*, 1985, **107**, 8191.
231. R. S. Honkonen, P. S. Marchetti and P. D. Ellis, *J. Am. Chem. Soc.*, 1986, **108**, 912.
232. P. S. Marchetti, R. S. Honkonen and P. D. Ellis, *J. Magn. Reson.*, 1987, **71**, 294.
233. P. S. Marchetti, L. Bhattacharyya, P. D. Ellis and C. F. Brewer, *J. Magn. Reson.*, 1988, **80**, 417.
234. R. A. Santos, E. S. Gruff, S. A. Koch and G. S. Harbison, *J. Am. Chem. Soc.*, 1990, **112**, 9257.
235. R. A. Santos, E. S. Gruff, S. A. Koch and G. S. Harbison, *J. Am. Chem. Soc.*, 1991, **113**, 469.
236. J. R. Garbow, H. Fujiwara, C. R. Sharp and E. W. Logusch, *Biochemistry*, 1991, **30**, 7057.
237. C. M. Dobson and L. Y. Lian, *FEBS Lett.*, 1987, **225**, 183.
238. A. I. Scott, *J. Mol. Catal.*, 1988, **47**, 139.
239. J. Schaefer, K. J. Kramer, J. R. Garbow, G. S. Jacob, E. O. Stejskal, T. L. Hopkins and R. D. Speirs, *Science*, 1987, **235**, 1200.
240. C. F. Morgan, R. Scheich, H. Caines and N. Farnsworth, *Biochemistry*, 1989, **28**, 5065.
241. J. R. Garbow and R. E. Stark, *Macromolecules*, 1990, **23**, 2814.
242. P. S. Belton, S. Duce and A. S. Tatham, *Int. J. Biol. Macromol.*, 1987, **9**, 357.